Measurement of Magnitude and Direction of Hot Gas Flow in a Fire Compartment with a Five-Hole Probe

---

by

J. K. Schulz

Supervised by Dr. Charley Fleischmann

Fire Engineering Research Report 2002

February 2002

This report was presented as a project report as part of the M.E. Fire degree at the University of Canterbury

---

School of Engineering
University of Canterbury
Private Bag 4800
Christchurch, New Zealand
Ph: +64 3 364 2250
Fax: +64 3 364 2758

Abstract

This report investigates the adaptation of a five-hole probe for measuring the magnitude and direction of hot gas flow in a fire environment. The probe was calibrated and tested in a boundary layer wind tunnel in ambient conditions; it measured the yaw angle to three degrees and pitch to two degrees accuracy over a range of +/- 25 degrees and gave velocity readings within 6%.

The probe was then used in a series of 22 full scale fire experiments with the aim of measuring the magnitude and direction of the plume of hot gases spilling out under the soffit of a doorway between two ISO rooms. The measurements were taken at ten positions along a 45-degree line perpendicularly to the plume. It was exposed to temperatures up to 365°C and velocities up to 3.5 m/s.
The four variables during the experiments were the fire size, the location of the burner in the fire compartment, the angle of the door in the doorway between the compartments and the size of the front opening of the adjacent compartment.

The results allowed a qualitative and quantitative description of the characteristics of the spill plume depending on the aforementioned variables.

The probe reached its limitations with the door 40 degrees open due to severe misalignment of the probe with the flow. The scatter of the collected data increased when the front opening was constructed as a doorway and the probe was fully submerged the deep upper hot layer.

It is concluded that the five-hole probe can be used in a fire environment to measure the magnitude and direction of hot gases provided it is roughly aligned with the flow. In more complex flow patterns the scatter of the data increases.

Acknowledgements

I would like to take the opportunity and thank those who have in many different ways contributed to my research project:

Dr. Charley Fleischmann, my supervisor.
Dr. Ian Huntsman from the Department of Mechanical Engineering for allowing me to use his programs, for his readiness to rewrite parts of it, his open ear and many quick solutions for the problems that came up along the way.
Dr. Roger Nokes and Dr. *Mark Davidson* for their enthusiasm and immense help.
Blair Liddell, without whom this project never would have left the infant stages.
The *staff of the Engineering Library* for finding reference material.
The technicians *Grant Dunlop, Graeme Harris, Kevin Wines* and *Michel Weavers*
Tony Parks, Luke Rutherford and Leigh Clark for their company during endless hours of testing.
The *University Masters Scholarship Program* and the *New Zealand Fire Service Commission* for their financial support throughout the year.
My Rowing Buddies for getting my mind of the deadline for a few hours every day.
And finally to *Ioane Ma'auga* for his cheerful grin when everything looked grim and his endless patience when between university and rowing there was not much time left in the day.

Contents

List of Figures

List of Tables

List of Photos

Nomenclature

Latin Symbols

Symbol	Units	Name
B	°, m/s	Bias
BC	-	Below the ceiling
C_{yaw}	-	Yaw coefficient
C_{pitch}	-	Pitch coefficient
C_{total}	-	Total pressure coefficient
$C_{dynamic}$	-	Dynamic pressure coefficient
D, d	m	Diameter
g	m/s^2	Gravity constant
L, l	m	Length
M	kg/kg.mol	Average molecular weight of air
ΔP	Pa	Pressure difference
P	Pa, mmH_2O	Pressure (1 mmH_2O = 9.81 Pa)
Q	kW	Fire size
Re	-	Reynolds number
R	J/mol.kg.K	Universal gas constant
R	-	Average coefficient of determination
t	sec	Time
T	K or °C	Temperature
U	°, m/s	Uncertainty
V	m/s	Velocity or speed

Greek Symbols

ρ	kg/m^3	Density
σ		Standard deviation

1 Introduction

Measurement of vent flows during a full scale fire experiment is essential to determine the amount of ambient air flowing into the compartment to supply oxygen to the fire and the amount of hot gases flowing out of the compartment into adjacent areas.
For more than 25 years the bi-directional probe was employed to serve this purpose. It has many advantages, as it is very sturdy, simple to use and does not require a great deal of alignment with the flow. However the disadvantage is that it cannot give any clues about the direction of the flow, information that is required to understand the flow pattern of hot gases through vents and compartments, especially when doors or other obstructions like smoke detectors are diverting the flow. Furthermore the viability of sophisticated computer models needs to be checked against full scale tests in order to ensure their accuracy and appropriate use in research and consultant work. It has not been possible up to date to validate the prediction of flow speed and direction through vents from programs like Fire Dynamic Simulator (FDS). To be able to do this, a more sophisticated probe is needed.

The four main aspects of this research project are:

- Find an appropriate probe to measure the magnitude as well as the direction of gas flows.
- Build the chosen probe and adapt it so it can be used in a full scale fire experiment.
- Conduct a series of full scale experiments in a two-compartment ISO room set-up and measure the hot gas spill plume characteristics from under a doorsill.
- Analyse the results gathered in the experiments and assess the quality of information collected by the probe.

Mechanical and hydraulic engineers use a large range of different probes to measure fluid flows ranging from very low to supersonic speeds, the flow patterns inside turbines and around obstacles like aeroplane wings, motorbikes and the like.
The section following the introduction will outline some of these methods of measuring fluid flow and reasons why they are appropriate or inappropriate for use in a fire compartment.

The third section will describe the construction, theory and calibration of the five-hole probe. It also covers the precision of the probe and assesses the sensitivity of the program p5hproc_Judith.exe used to convert pressure readings into yaw, pitch and velocity.

Section four explains the experimental set-up of the full scale experiments and the methodology employed to measure the speed and direction of a hot air plume spilling from under a door sill out of the fire compartment.

The results of ten experiments will be evaluated in section five. It also assesses the quality of information provided and the influence of fire size and location, front opening and door opening on the hot air flow from under the doorsill.

In the conclusion, some aspects are addressed that may improve the performance of the probe.

2 Flow Measurement Methods

The measurement of speed and direction of airflow in a fire compartment help to understand and verify theories of the movement of hot gases through a room. There are many methods available to do this in ambient conditions, however due to the hazardous conditions in a fire compartment, most of the numerous measuring techniques are not appropriate or give only limited information about the flow. This section will discuss six relatively common measuring techniques and assess their advantages and disadvantages in a fire environment.

The probe is required to resist temperatures of up to 365°C, measure very low speeds of 0.5 to 4.0 m/s. Its performance should not be hindered excessively by the presence of soot particles. The measurements should be fast enough to be able to handle the often encountered pulsing of air pockets in a fire enclosure.

The probe should be able to measure speed within 10 % and angles within five degrees accuracy.

2.1 Thermal Anemometer

Thermal anemometers are generally used to measure turbulence, i.e. velocity components. They consist of a sensor, usually a very thin wire, which is connected to a circuit that measures the change in resistance in the wire.

The method is based on the fact that airflow of sufficient speed induces a heat flux due to forced convection losses or gains in a submerged object, i.e. a piece of wire. The heat flux from or to the wire is proportional to the speed of the flow and can be measured by recording the change in resistance of the wire.

As velocity increases, the wire cools due to increased convection losses to air stream; the resistance of the wire reduces linearly for a constant current supply and can be recorded (Cheremisinoff, 1988). Alternatively the temperature of the wire is held constant (= constant resistance of the wire) and the change in current is monitored (DeCarlo, 1984).

Photo 1: Typical thermal anemometer (Cambridge website, Hot wire anemometer, 2002)

Typical hot wire anemometers have a wire made of tungsten, with d = 4 μm and l = 1.25 mm. The wire is part of a fast responding electric circuit, so that the probe is able to give very detailed information on dynamic flows.

Table 1 gives a short overview of the advantages and disadvantages of thermal anemometry.

Advantages	**Disadvantages**
Fast measurements	Conduction losses
Works in turbulent environment	Very fragile sensors
Good for low speed, incompressible flow	Need several probes to measure 3D flows
Low noise levels	Calibration shifts due to contamination likely
	Requires constant fluid properties for accurate measurements (i.e. density, temperature, pressure and composition)

Table 1: Advantages and disadvantages of thermal anemometry

Soot deposits would quickly contaminate the wire and render the probe inoperative.

2.2 Vane Anemometer

Vane anemometers consist of a set of blades similar to a windmill that is lined up perpendicular to the flow. If the direction of flow is unknown, the blades are generally replaced by three cups. They are often used to measure the air speed in shafts or wind speed in meteorology (Bradshaw, 1970). Their size varies between 7.6 – 38 cm outside diameter. They can measure speed in the range of 0.15 – 45 m/second (DeCarlo, 1984) in an environment from –10°C to + 50°C to +/- 3% accuracy (from Technical Information for Lowne Leda 1000 Vane Anemometer).

The vane anemometer shown in Photo 2 was used to determine the speed of the wind tunnel in the calibration procedures of the chosen probe.

Photo 2: Vane anemometer

There are many reasons why vane anemometers are inappropriate for use in fire experiments:

- Low temperature range
- Density changes affect accuracy of low velocity readings (Ower and Pankhurst, 1977)
- Cannot measure direction easily
- Inappropriate for instantaneous sampling

2.3 Cross-Correlation of Random Thermal Fluctuations

This technique measures the transit time of naturally occurring thermal fluctuations in the flow between two thermocouple trees (G. Cox, 1977). In order to establish the transit time correctly the recorded signals from the thermocouples need to be averaged statistically in order to account for turbulence. The advantages and disadvantages are shown in Table 2.

Advantages	Disadvantages
Robust equipment (thermocouples)	Sophisticated statistical averaging necessary
Can be used in flame and smoke	Only gives mean flow speed in one direction
Does not require additional measurement of temperature	Only gives flow speed averaged over fairly long distance (between trees)
Potential to measure 3D flow by arranging several thermocouple trees in different directions	Incapable of measuring flow direction easily

Table 2: Advantages and disadvantages of cross-correlation of random thermal fluctuations

The cross-correlation method is not capable of providing a good resolution of the flow pattern.

2.4 Pitot-Static Tube

Pitot tubes are generally used to measure a velocity at a point. They are shaped like an 'L' where the short arm is aligned with the flow. The inner of two coaxial tubes measures the stagnation pressure at the tip of the probe; the outer tube usually has eight holes downstream from the tip that transmit the static pressure, see Figure 1. Pitot-static tubes are fairly easy and cheap to manufacture. The side holes are placed so that the disturbances caused by the tip and the stem are cancelling out. The differential pressure is equal to the dynamic pressure assuming the flow is incompressible and if the density of the fluid is known, the velocity can be determined from:

$$P_{total} = P_{static} + P_{dynamic} \qquad \text{Equation 1}$$

$$P_{dynamic} = \tfrac{1}{2} \rho V^2 \qquad \text{Equation 2}$$

$$P_{total} = \tfrac{1}{2} \rho V^2 + P_{static} \qquad \text{Equation 3}$$

Inserting equation [2] into [1] and solving for V gives:

$$V = \sqrt{\frac{2P_{dynamic}}{\rho}} = \sqrt{\frac{2(P_{total} - P_{static})}{\rho}} \qquad \text{Equation 4}$$

The assumption of incompressible flow is valid as the fluid density changes due to motion can be neglected in the fire environment. The expected velocities of 4 m/s are much smaller than the critical velocity of approximately 60 m/s (Ower and Pankhurst, 1966).

Pitot-static tubes can measure velocity to an accuracy of +/- 2 % (Miller, 1996), and because the pressure differences are generally quite large, even small velocities can be measured. However they are very sensitive to misalignment, stem blockage by particles in the flow and turbulence or transverse velocity gradients. The direction of flow can be found by ‚nulling' the probe, i.e. changing its orientation until the probe is reading a minimum (Ower and Pankhurst, 1966, pg 56). This however is impossible to do in a fire compartment as one cannot easily walk in and change the position of the probe during an experiment.

Their use in a fire environment is therefore very restricted. A further disadvantage is the necessity to measure the temperature of the flow close to the tip in order to determine the density of the airflow accurately, which in turn could affect the measurement of the static pressure downstream.

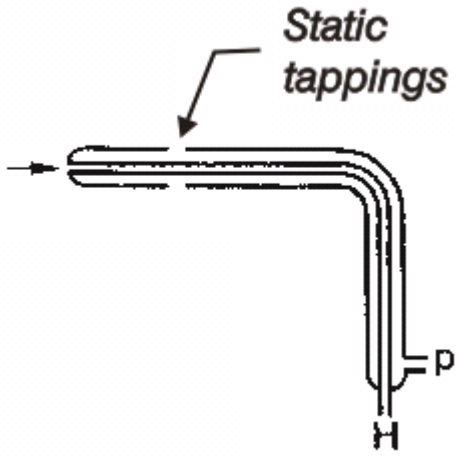

Figure 1: Pitot-static tube (Bryer, Pankhurst, 1971)

As the Pitot-static tube cannot measure the direction of flow and measures pressures at more than one point it is not practical for applications with steep velocity gradients and where alignment with the flow is potentially difficult.

2.5 Bi-Directional Probe

The bi-directional probe is the standard device to measure vent flow in fire experiments. It is also used where Pitot-static tubes are inappropriate due to its sensitivity to misalignment to fluid flow. Bi-directional probes allow the measurement of air speed up to 10% accuracy as long as the flow direction is within +/- 50 degrees of the probe axis (Emmons, 1995).

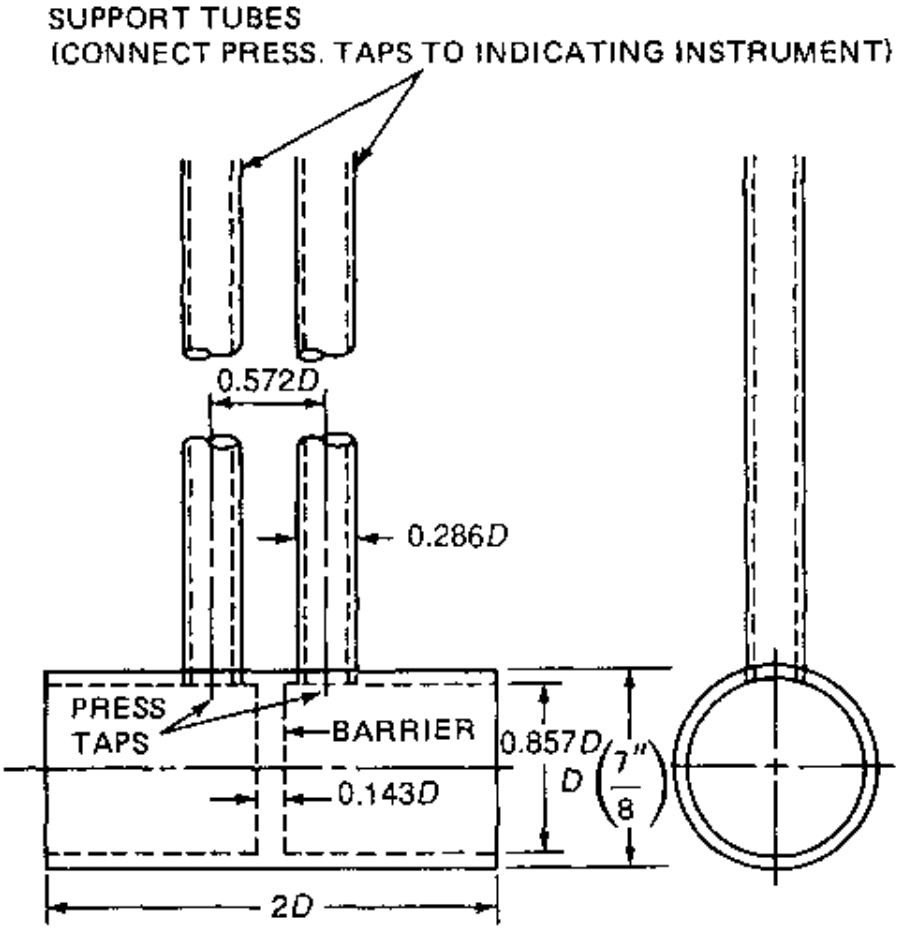

Figure 2: Principle of a bi-directional probe (Emmons, 1995)

It consists of a large diameter tube of diameter D and length 2D (see Figure 2) with a barrier in the centre. Pressures taps are located in front and behind the barrier; the differential pressure is measured with an indicating instrument.

The density of the airflow is determined by measuring the temperature as near as possible to the probe. The ideal gas law is applied assuming that the pressure differences have a negligible effect on gas density.

$$\rho = MP / RT \qquad \text{Equation 5}$$

Where

P = 101330	Standard atmospheric pressure	in Pa
M = 28.95	Average molecular weight of flowing gas	in kg/kg.mol
R = 8314	Universal gas constant	in J/kg.mol.K
T	Temperature of gas flow	in K

The speed is then (Emmons, 1995):

$$V = 0.93\sqrt{\frac{2|\Delta P|}{\rho}} \qquad \text{Equation 6}$$

where

ΔP	Pressure difference across bidirectional probe	in Pa
ρ	fluid density	in kg/m^3

Inserting Equation 5 in Equation 6:

$$V = sign(\Delta P) \cdot 0.070\sqrt{T|\Delta P|} \qquad \text{Equation 7}$$

The advantage of bi-directional probes is their robustness and insensitivity to misalignment to the fluid flow. However they cannot give any information on the direction of the flow. The following table summarizes pro and contra of the bi-directional probe.

Advantages	**Disadvantages**
Simple to make	Measurement not taken from one point
Low cost	Requires measurement of temperature
Robust	Does not read direction of flow
Can measure low velocities	
Insensitive to misalignment of up to 50°	

Table 3: Advantages and disadvantages of bi-directional probe

The bi-directional probe is a well-established instrument in fire experiments, however as it lacks the ability to measure the direction of the flow there is a need for a more precise measuring device.

2.6 Five-Hole Probe

The five-hole probe is just that. It measures five pressures instead of two and correlates pressure changes to the direction of the flow in the vertical and horizontal plane as well as the speed. It can give accurate readings within a 40 degrees incident angle of the flow to the probe and is capable of velocity readings ranging from approximately 1 m/s to supersonic velocities. Mechanical engineers often use five-hole probes to measure the flow pattern in turbomachines.

The shape of this probe is essentially the same as the pitot-static probe, however all five pressure tappings are facing forward. The holes are sited symmetrically in a cross pattern, so that the pressure readings are changing with the orientation of the probe to the flow. All measurements are taken close to one point.

Each probe requires a comprehensive calibration over the range of its intended use.

In order to use the probe in a fire environment, the density of the fluid at the point of sampling is required, which means that temperature should be measured as close to the probe tip as possible.

The advantages and disadvantages of the use of a five-hole probe in a fire compartment are listed in Table 4.

Advantages	**Disadvantages**
Simple to make	Requires measurement of temperature
Low cost to manufacture	Application at low end of velocity range not ideal
Robust	Tip of probe must not be scratched or damaged
Can measure low velocities	Requires five pressure transducers
Can measure direction of flow	
Pressure readings taken from one point	

Table 4: Advantages and disadvantages of five-hole probe

Clearly this method is favourable in the aim to measure both speed and direction of gas flow in a fire compartment. The following chapter will develop the concept further and describe the construction, calibration, testing and sensitivity to input parameters of the five-hole probe software.

The calibration of the probe for this research project is based on a method developed at the University of Cambridge for work in complex 3D flows and brought to the University of Canterbury by Dr. Ian Huntsman.

3 Five-Hole Probe

This chapter describes the construction, calibration precision and sensitivity of a five-hole probe.

3.1 Definition of Angles and Coordinates

In order to use the data collected with the probe correctly it was essential to define a coordinate system that was to be used in the calibration and the application later on. In all cases the positive x direction was pointing in the direction of flow, z was pointing up and y was adjusted so the coordinate system was following the right hand rule.

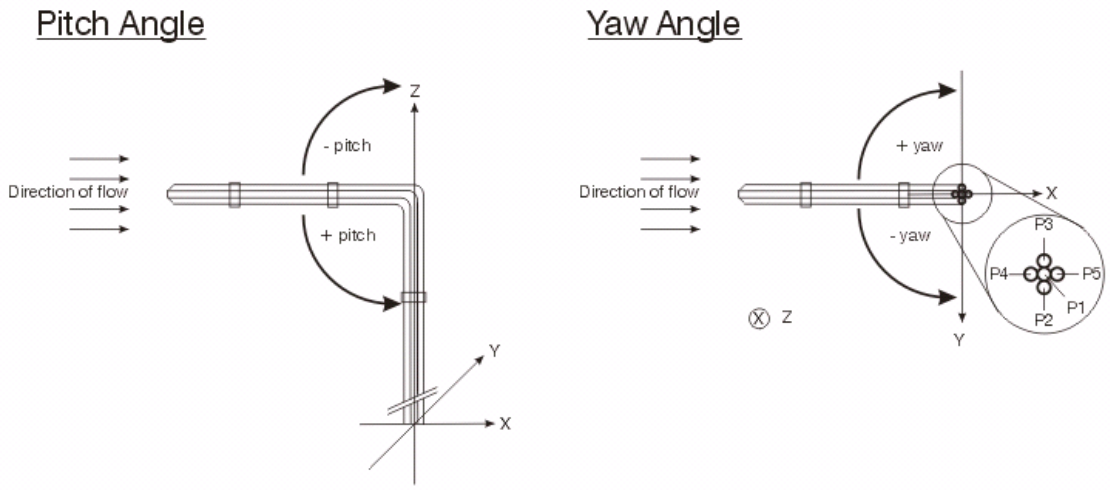

Figure 3: Definition of angles and coordinates of the five-hole probe for the calibration

The positive yaw angle was defined using the right hand rule with the right thumb pointing in the positive z direction; the positive pitch angle was defined with the right thumb pointing in the negative y direction.

Dr. Ian Huntsman wrote the programs needed for the calibration and processing of the pressure data to determine flow speed and direction for an orientation of the probe with the stem oriented vertically for an earlier research project at the Mechanical Department. In the full scale fire experiment the stem was horizontal, hence a simple angle conversion from the output of the program was required. This will be addressed later.

3.2 Construction of Five-Hole Probe

Due to the short time available for this project, the easiest method of construction was chosen, resulting in a forward-facing pyramid structure (as defined by Dominy and Hodson, 1993).

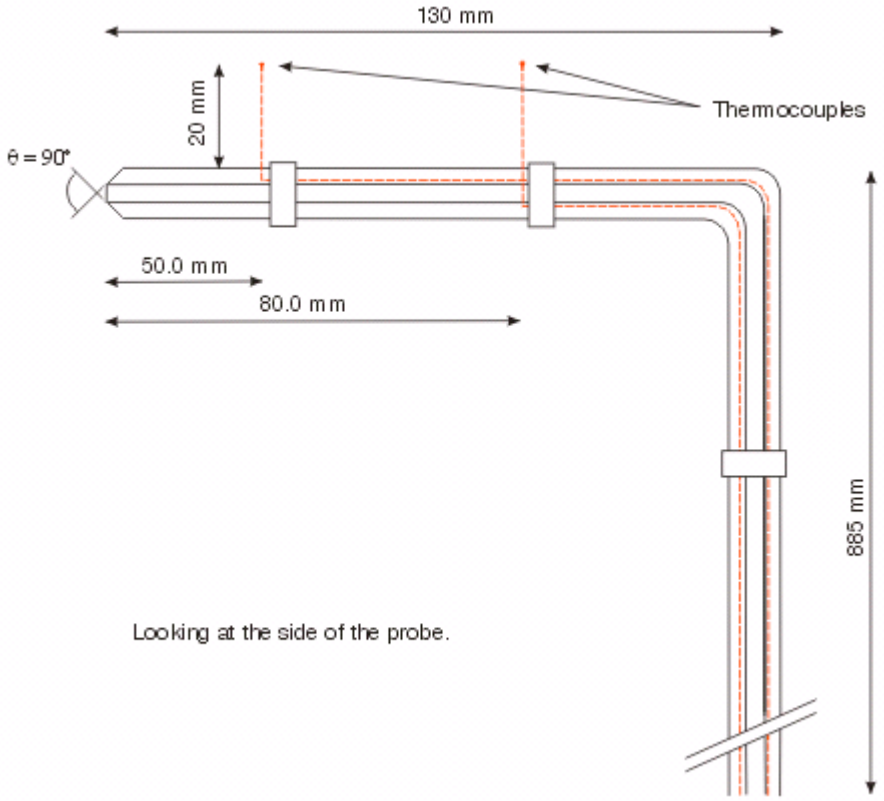

Figure 4: Dimensions of the five-hole probe

3.2.1 Forward-facing Pyramid Probe

The probe was shaped like an 'L', where the measuring tip was at the short arm. It made of five stainless steel tubes arranged in a cross pattern. All tubes had an outside diameter of 3.22 mm (1/8 inch) and inside diameter of 2.50 mm. Two tubes were positioned to the left and right and two above and below of the central tube, so that the probe was symmetrical about two axes. The outer tubes were cut on a 45-degree angle, so that the probe had the shape of a truncated pyramid when looking side on (see Figure 4).

The tip of the probe has a 90-degree apex angle, with all openings facing forward. The short arm of the 'L' was 130 mm long, which was sufficient to reduce the influence from the stem on the pressure tappings. The long arm of the 'L' was 885 mm long.

The tubes were welded together in order to resist the high temperatures in the hot layer. Photo 3 shows the short arm of the probe from the side and Photo 4 the tip of the probe looking face on.

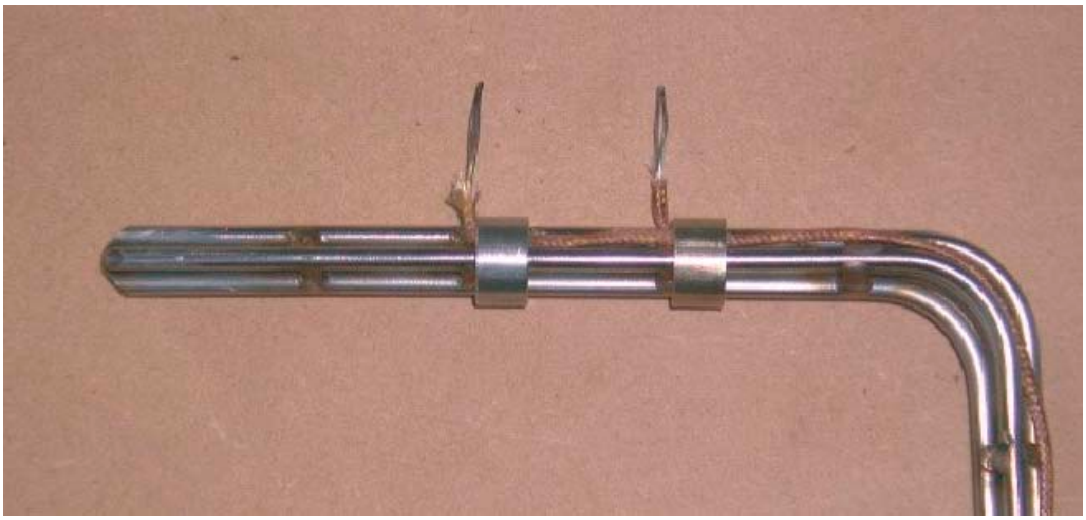

Photo 3: Side view of the tip of the five-hole probe with two thermocouples

Photo 4: Front view of the tip of five-hole probe with two thermocouples

3.2.2 Thermocouples

Two Type K thermocouples were located 20 mm above the short arm, 50 and 80 mm behind the probe tip. They were used to estimate the temperature and hence the density of the air flow at the tip of the probe. They were held in place using steel rings and high temperature RTV.

The temperature at the tip of the probe is found by linear extrapolation:

$$T_{tip} = T_1 - 50\text{ mm} / 30\text{ mm}\ (T_2 - T_1) \qquad \text{Equation 8}$$

Where T_1 is the thermocouple closest to the tip

T_2 is the thermocouple farthest from the tip

3.3 Theory

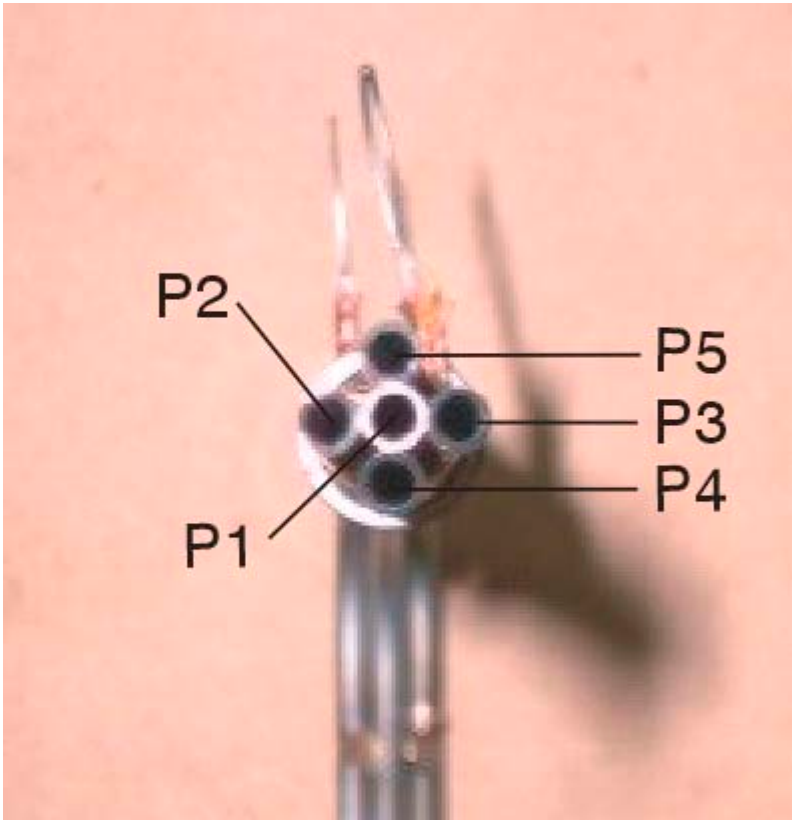

Figure 5: Looking at five pressure tappings on the face of the probe with stem oriented downwards.

The central tube P1 measures a reference pressure, which is the stagnation pressure when the probe is at 0 degrees yaw 0 degrees pitch. The change in pressures across the two horizontal tubes marked P2 and P3 is used to calculate the flow direction in the horizontal plane, the yaw angle, while the pressure changes across the two vertical tubes P4 and P5

are related to a change in pitch angle. The pressure on the central tube is generally the largest of the five pressures.

The principle is easiest to understand when looking at the individual changes in orientation, i.e. only horizontal change (yaw only) or only vertical change (pitch only). In order to limit the length of this section, only the pressure variations for a decreasing yaw angle and zero pitch will be described. The pressure changes for other orientations are shown in Table 5 and should be easily derived from the example. Changes of pressures for both yaw and pitch angles cannot be derived by superimposing the results shown below.

If the yaw angle is changed, i.e. decreased by rotating the probe of Figure 5 in the horizontal plane to the left, resulting in a plan view shown in Figure 6, ideally the pressures in the vertical tappings P4 and P5 should change equally, so the pressure difference $|P5 - P4|$ is zero. In reality this is not always the case due to defects in symmetry and surface finishing from manufacture and misalignment with the flow.

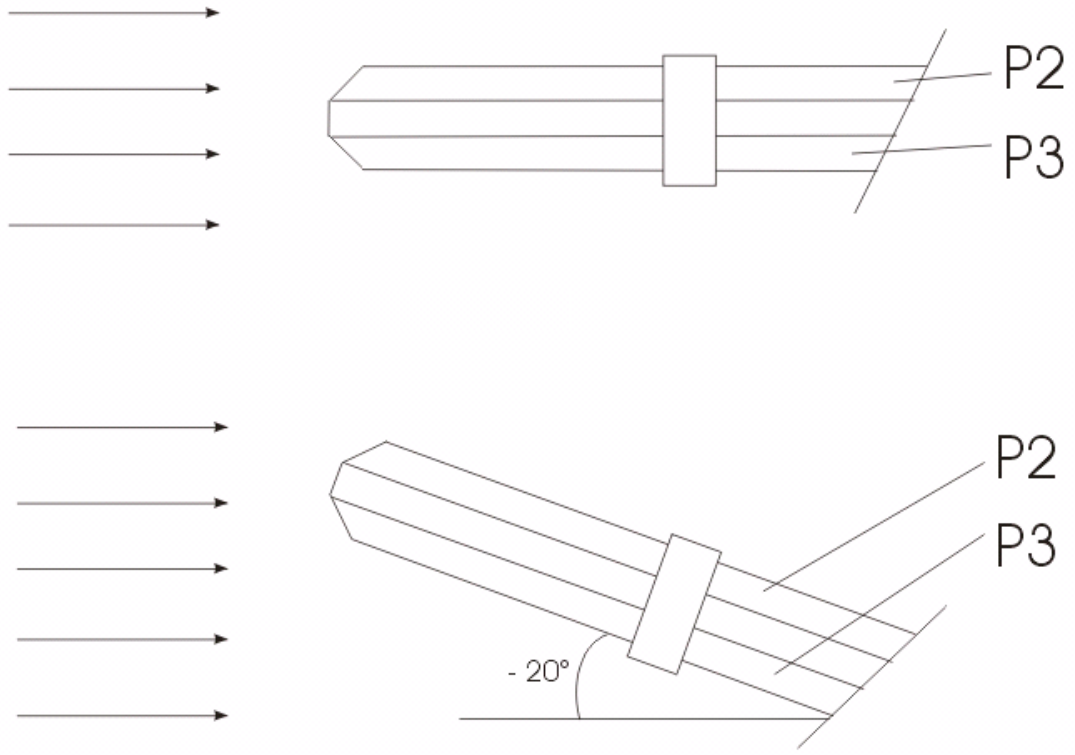

Figure 6: Plan view of the rotation of the probe in the horizontal plane (yaw = 0° and -20°)

If the probe is rotated to –20 degrees yaw as shown in Figure 6 then P3 is oriented more perpendicularly to the flow and therefore is a larger obstacle in the flow. This results in a lower velocity across the face and a higher the pressure on the face P3. The velocity of the flow over P2 is higher hence the pressure drops in P2. As a result the pressure difference across $|P2 - P3|$ increases.

If the yaw angle between the flow direction and the probe were increased even further to –45 degrees yaw, as shown in Figure 7, P3 would read stagnation pressure, while P2 would read static pressure. However if separation of the flow occurs at the edge, a separation bubble can occur which leads to highly fluctuating pressure readings in P2.

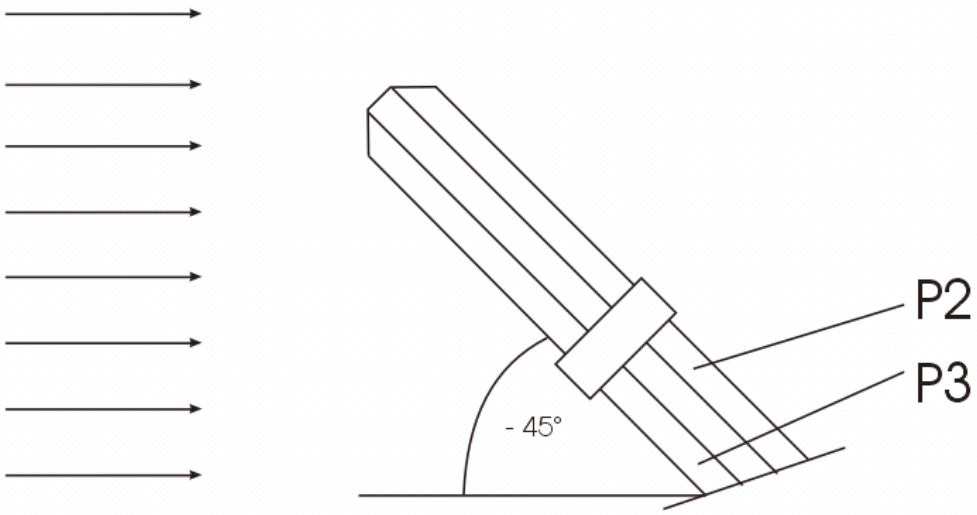

Figure 7: Rotation of the probe in the horizontal plane to the left (yaw = - 45°)

The following table summarizes the perfect pressure changes in either yaw or pitch angle:

Orientation	Horizontal pressure taps P2 and P3	Vertical pressure taps P4 and P5
zero yaw / zero pitch	Equal	Equal
+ve yaw / zero pitch	P2 ↑ P3 ↓	Δp equal
-ve yaw / zero pitch	P2 ↓ P3 ↑	Δp equal
zero yaw / +ve pitch	Δp equal	P4 ↓ P5 ↑
zero yaw / -ve pitch	Δp equal	P4 ↑ P5 ↓

Table 5: Ideal correlations between changes in orientation and pressure readings

3.4 Explanation of the Program p5hproc_judith.exe

This section will set out the mathematics behind the program p5hproc_judith.exe, which was used to convert the pressure readings to the magnitude and direction of the airflow. One data sample taken from the test series in the wind tunnel will be followed through. An example of an input file is attached in Appendix A - Input File for p5hproc_Judith.exe.

3.4.1 Pressure Coefficients

Four dimensionless pressure coefficients are used to determine the direction and speed of the airflow. Each coefficient is plotted on a map with the pitch and yaw angles as variables, as shown in Figure 8.

The two angle coefficients are defined as follows:

$$C_{yzw} = \frac{P_2 - P_3}{P_1 - P_{ave}}$$ Yaw coefficient Equation 9

$$C_{pitch} = \frac{P_4 - P_5}{P_1 - P_{ave}}$$ Pitch coefficient Equation 10

Where P_{ave} = ½ (sum of smallest two pressures) Equation 11

The two pressure coefficients are:

$$C_{total} = \frac{P_{total} - P_1}{P_1 - P_{ave}}$$ Total pressure coefficient Equation 12

$$C_{dynamic} = \frac{P_{total} - P_{static}}{P_1 - P_{ave}}$$ Dynamic pressure coefficient Equation 13

During the calibration all pressures P_1 to P_5 from the five-hole probe as well as P_{total} and $P_{dynamic}$ from the Pitot-static tube are known, so that the pressure coefficient maps can be created. Ideally the maps for the angle and pressure coefficients should show straight lines and concentric circles respectively. The maps are useful devices to check the quality of the calibration.

3.4.2 Data Input

One test orientation for the probe was –15 degrees yaw, +15 degrees pitch at a wind speed of 1.41m/s.

The pressure readings were:

P_1 = 1.0872 Pa

P_2 = 0.1216 Pa

P_3 = 0.9448 Pa

P_4 = 0.3176 Pa

P_5 = 0.8623 Pa.

The ambient temperature and atmospheric pressure were:

T = 291.2 K

P_{atm} = 99495.0 Pa.

3.4.3 Computation Procedures

The principles behind the computer program p5hproc_Judith.exe are described shortly in the following section.

Direction of Flow

The denominator of the pressure coefficients using the pressure values from above is

$$P_1 - P_{ave} = P_1 - ½ (P_2 + P_4) = 1.0872 – ½ (0.1216 + 0.3176) = 0.8676$$

The angle coefficients are:

C_{yaw} = (0.1216 – 0.9448) / 0.8676 = - 0.9488

C_{pitch} = (0.3176 – 0.9623) / 0.8676 = - 0.6278

The program now accesses both yaw and pitch coefficient maps and determines the yaw and pitch angle where both coefficients match at the same time. This is an iterative process. In the maps shown below, the closest matching line to the calculated values was chosen.

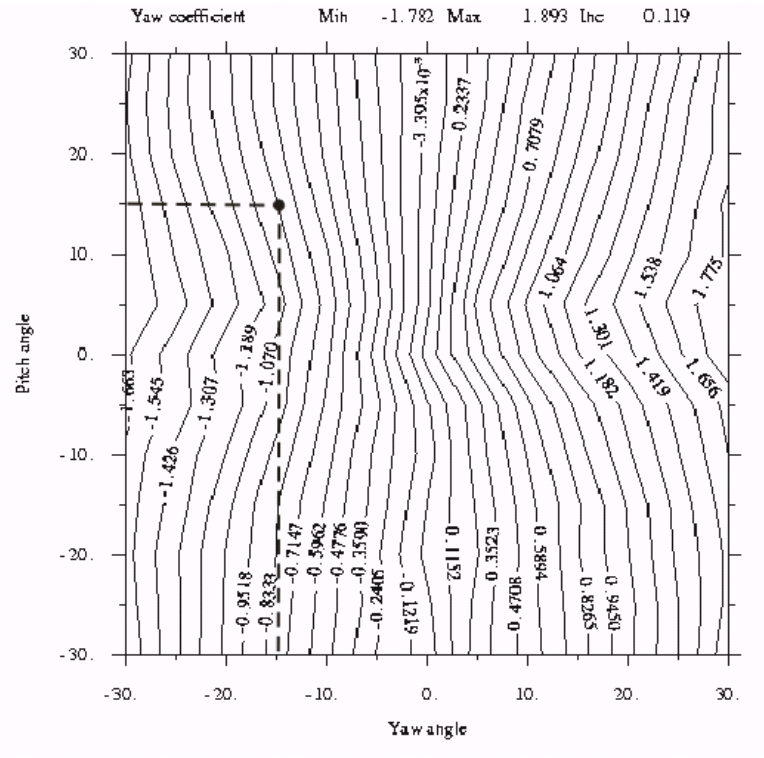

Figure 8: Yaw coefficient map with sample point at C_{yaw} =- 0.9488

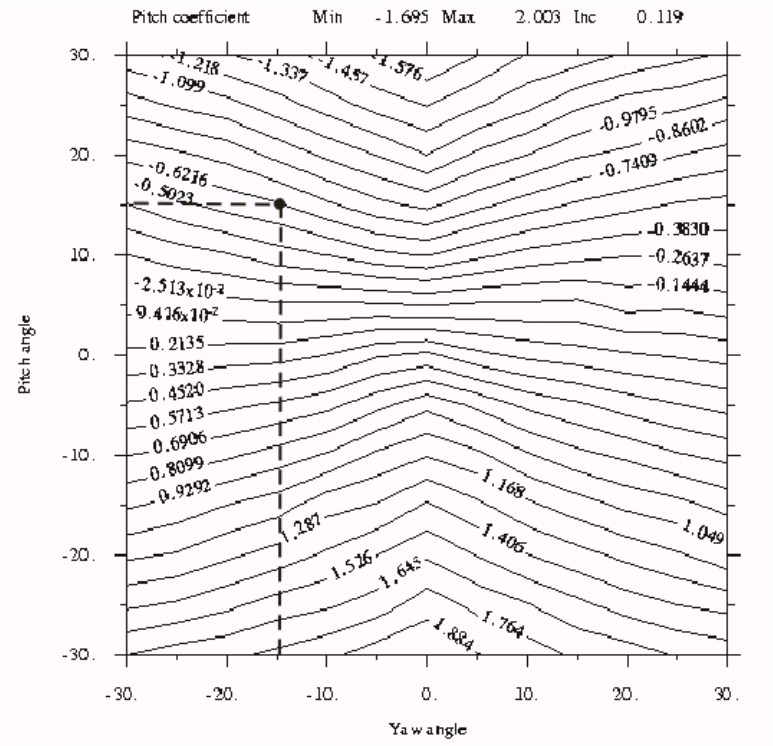

Figure 9: Pitch angle coefficient map with sample point at C_{pitch} = - 0.6278

The resulting angle combination is:

Yaw = -15°

Pitch = +15°

The program calculates the angles to several decimal places, an accuracy that is misleading.

Speed of Flow

Knowing the orientation of the probe, yaw and pitch angle, one can now proceed to find the speed of the flow. The next step is to determine the total and dynamic pressure coefficients from the maps shown in Figure 10 and Figure 11.

C_{total} = from map in Figure 10 = 0.1012

$C_{dynamic}$ = from map in Figure 11 = ½ (1.350 + 1.391) = 1.3705

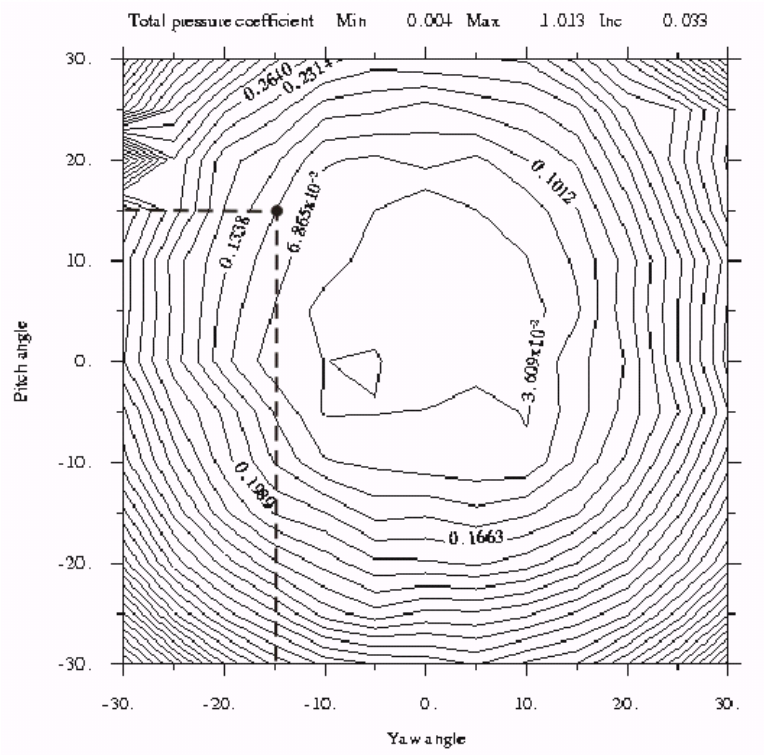

Figure 10: Total pressure coefficient map with sample point at C_{total} = 0.1012

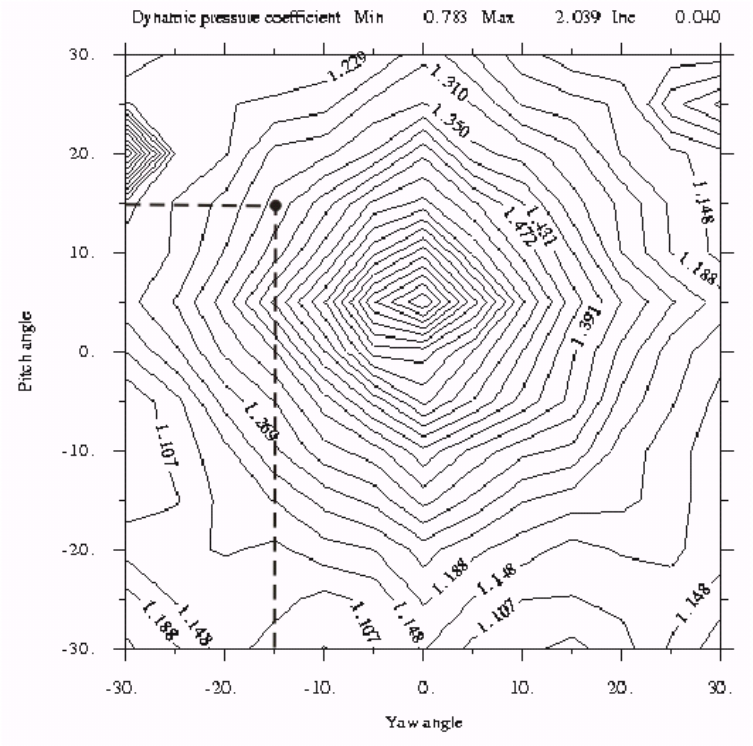

Figure 11: Dynamic pressure coefficient map with sample point at $C_{dynamic} = 1.3705$

The only unknown in C_{total} is P_{total}, so by rearranging Equation 12 we find:

$$P_{total} = C_{total} (P_{max} – P_{ave}) + P_1$$
$$= 0.1012 * 0.8676 + 1.0872$$
$$= 1.1750 \text{ Pa}$$

The only unknown in Equation 13 is now P_{static}:

$$P_{static} = P_{total} - C_{dynamic}(P_{max} – P_{ave})$$
$$= 1.1750 - 1.3705 * 0.8676 = -0.0146 \text{ Pa}$$

The total pressure, being the sum of dynamic and static pressures, in an incompressible flow is constant:

$$P_{total} = P_{dynamic} + P_{static} = \text{constant.} \qquad \text{Equation 1}$$

The dynamic pressure is proportional to the square of the velocity of the flow as follows:

$$P_{dynamic} = ½ \rho V^2 \qquad \text{Equation 2}$$

Where ρ = density of the fluid (air), determined using the ideal gas law.

$$\rho = MP / RT = M(P_{atm} + P_{static}) / RT. \qquad \text{Equation 5}$$

$$\rho = 28.95 \text{ kg/kg.mol x } (99459 - 0.0146 \text{ Pa}) / 8314 \text{ J/kg.mol.K x } 291.2 \text{ K}$$

$$\rho = 1.190 \text{ kg/m}^3$$

Due to the very low sensitivity of the density to changes in pressures at low speed, equation [4] could be simplified to (Karlsson and Quintiere, 2000, pg 89):

$$\rho = 353 \text{ kg/m}^3\text{.K} / T \qquad \text{Equation 14}$$

Solving the total pressure equation for the only unknown V:

$$V = \sqrt{\frac{2P_{dynamic}}{\rho}} = \sqrt{\frac{2(P_{total} - P_{static})}{\rho}} \qquad \text{Equation 4}$$

$$V = \sqrt{\frac{2 \cdot (1.1750 + 0.0146) Pa}{1.190 kg/m^3}} = 1.41 m/s$$

This result matches extremely well with the known orientation and speed of the flow.

3.5 Calibration

This section will describe the calibration procedures for the pressure transducers and the five-hole probe. The program p5hplt.exe, written by Dr. Ian Huntsman, converts the pressure readings of the calibration file (example attached in Appendix B – Calibration File Excerpt) into pressure coefficient maps. They allow the assessment of the quality of the calibration.

3.5.1 Set-up of Five-Hole Probe Calibration

The five-hole probe was calibrated in a boundary layer wind tunnel located in the Industrial Aeronautics Laboratory of the University of Canterbury. It was fixed at the end of the tunnel, so the tip of the probe was in the centre of the opening, just inside the tunnel. The stem was clamped in a rotary jig that allowed precise rotation about yaw and pitch angles in 5-degree intervals. Special care was taken that the tip of the probe did not come too close to the walls of the tunnel in order to ensure uniform wind speed across the required range. The velocity of the flow was measured with a vane anemometer several times at different points across the opening before and after the calibration to ensure stable and uniform conditions.

In addition a small Pitot-static tube was located near the five-hole probe to measure the total and static pressures and hence the velocity of the airflow in the wind tunnel. These were required to generate calibration maps for total and dynamic pressures. The Pitot-static tube was only needed during the calibration of the probe.

All seven pressures were converted to a voltage output using high sensitivity, unidirectional pressure transducers that were run off a 24V DC power source. The signals were recorded using 'datalogger boxes' and the program 'Universal Data Logger' (UDL).

A picture of the set-up is shown below.

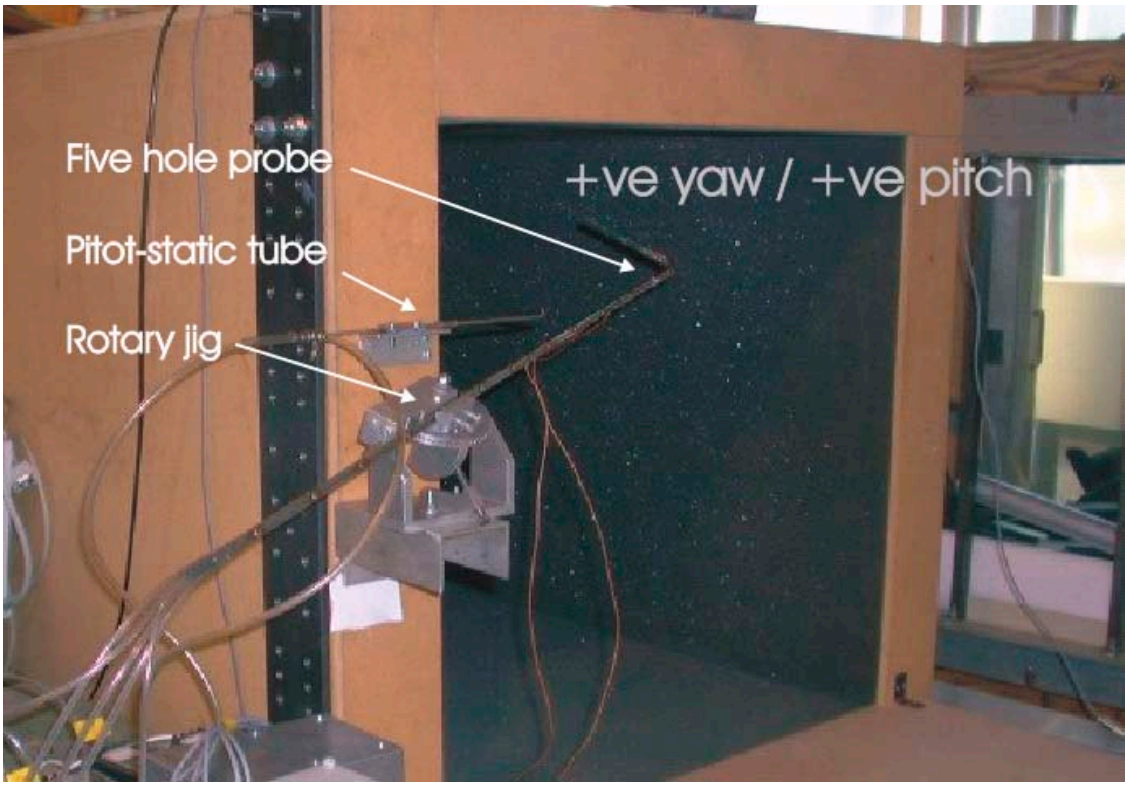

Photo 5: Set-up of the five-hole probe calibration

3.5.2 Calibration Procedure of Pressure Transducers

The seven pressure transducers used in this experiment were made by Setra, Model 264, with a unidirectional output range 0-5V, measuring +/- 2.5 mm H_2O. The transducers were warmed up for a minimum of two hours prior to the calibration; each transducer was earthed separately to avoid potential problems with the data logging boxes.

A manometer was used to determine the pressure changes, ranging from + 2.0 to – 2.0 mmH_2O in 0.5 mmH_2O intervals. They were induced with a small syringe. The voltage output was recorded with the software UDL mentioned above.

The results are shown in Table 6. All transducers exhibited a very good linear behaviour in the tested range with an average coefficient of determination R of 0.9993.

Transducer #	**# 1**	**# 2**	**# 3**	**# 4**	**# 5**	**# 6**	**# 7**
Serial #	614399	614400	614404	614402	614397	614396	614403
Calibration Constant (V to mmH_2O)	1.0075	1.0328	1.0138	1.1165	1.0221	0.9916	1.0303
R	0.9999	0.9991	0.9992	0.9994	0.9985	0.9996	0.9995

Table 6: Calibration constants for pressure transducers

3.5.3 Calibration Procedure of Five-Hole Probe

A calibration consisted of the following steps:

- Warm up transducers for at least two hours.
- Take reference reading for zero yaw and zero pitch in still ambient conditions.
- Align the five-hole probe with the flow for zero pitch and yaw.
- Note ambient pressure.
- Measure the velocity of the air flow in the wind tunnel at several points across the opening with a digital vane anemometer to assure uniform wind speed across the opening.
- Vary the orientation of the five-hole probe in 5-degree intervals between –25 and +25 degrees yaw and –25 to +25 degrees pitch, resulting in a 11 x 11 = 121 grid of measurement points (or +/- 30 degrees, 13 x 13 = 169 grid).
- Take reference reading in quiescent ambient conditions after the calibration is completed to make sure they have not changed significantly.
- Create a calibration file (see Appendix B – Calibration File Excerpt), read into the program 5hplt.exe and create calibration maps for yaw, pitch, total and dynamic pressure coefficients.

The calibration coefficient maps for the probe can be found independently from the wind speed, because the coefficients are non-dimensional. In order to assure accurate readings at low speeds and to investigate Reynolds number effects, the probe was calibrated at two different speeds (1.25 m/s and 2.24 m/s) over +/-25 degree range and at 2.24 m/s over +/- 30 degrees. The calibration files were tested against each other in a series of three tests.

3.6 Precision of Five-Hole Probe - Tests in the Wind Tunnel

In order to assess the accuracy of measurements that can be achieved using the five-hole probe and chose the best calibration file, three tests comprising of a total of 61 measurements were run in the boundary layer wind tunnel in the Industrial Aeronautics Laboratory.

The probe should be able to read velocities with 10 % accuracy and angles within 5 degrees accuracy to be useful for data collection in a fire environment. Higher precision is not required due to the fluctuation and unstable nature of fires.

3.6.1 Definitions of Precision

The precision of the probe will be assessed following the guidelines of Baker outlined in his book 'An Introductory Guide to Flow Measurement', 1989.

$\sigma = \left\{ \frac{1}{n-1} \sum_{n=1}^{n} (x_i - \bar{x})^2 \right\}^{1/2}$	Standard Deviation	Equation 15
$P = 2 \times \sigma$	Precision	Equation 16
$B = \text{mean}$	Bias	Equation 17
$U = B + 2 \times \sigma$	Uncertainty	Equation 18

3.6.2 Testing Procedure

The procedure was identical to the calibration procedure, except the number of measurement points was reduced and the wind speed was varied during the tests. The data was analysed in two steps:

- Run program p5hproc_Judith.exe using a calibration file *'JcalX.txt'* and a data file *'testX.txt'*. The output file contains the yaw and pitch angle, static and total pressure and velocity for each data line.
- Read output file *'testX.out'* into excel.

Three concepts were adopted for the testing of the probe. Tables with the exact orientation of the probe and the velocity of the air flow are attached in Appendix C – Test Combinations. The concepts were:

- Variation of locations with three different velocities with emphasis on the 25° combinations.
- Emphasis on large angle combinations and negative pitch at high velocity
- Emphasis on medium and small angle combinations at lower velocity

Three different calibration files were used to analyse the results. They varied in wind speed and range of angle variation:

- *Jcal2.txt*: wind tunnel velocity V = 1.25 m/s, angle variation +/- 25 degrees
- *Jcal3.txt*: wind tunnel velocity V = 2.16 m/s, angle variation +/- 25 degrees
- *Jcal5.txt*: wind tunnel velocity V = 2.24 m/s, angle variation +/- 30 degrees

3.6.3 Results

All 61 points were analysed using all three calibration files. The precision was evaluated more closely once the best file was determined.

Range of Errors

- *Jcal2.txt* and *Jcal3.txt* based on +/- 25-degree grid erred significantly for the large angle readings as the program p5hproc_Judith.exe does not converge well at the edges of the calibration maps and were discarded. This problem could be rectified using the file Jcal5.txt with a +/- 30-degree angle variation. The calibration at higher speed seemed lead to slightly smaller errors.
- *Jcal5.txt* gave good results for angles up to 25 degrees. It erred on the yaw angles between –3.31 and +2.89 degrees and on the pitch angles between –2.55 and +0.65 degrees. The velocity readings erred by a maximum of 7 %.

The calibration file *Jcal5.txt* was the only one capable of giving reasonable results up to +/- 25 degrees and was used for the analysis of the airflow in the fire compartment.

Error Distribution

All 61 measurements were analysed more closely using the calibration file '*Jcal5.txt*' in order to achieve a more detailed picture of the quality of the results.

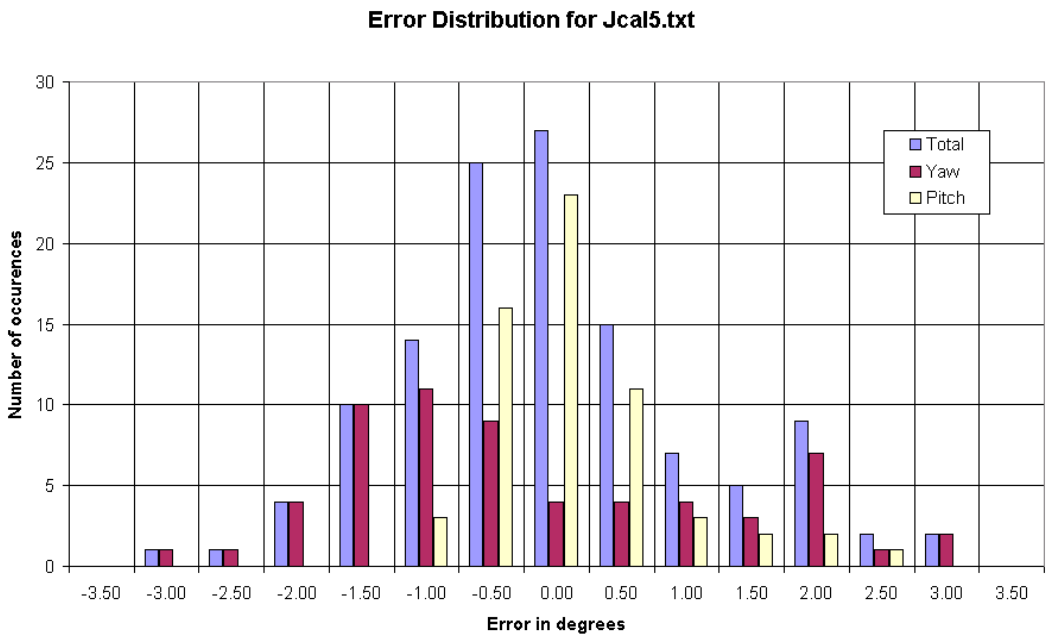

Figure 12: Distribution of yaw and pitch errors for the calibration file *Jcal5.txt* using all three test runs.

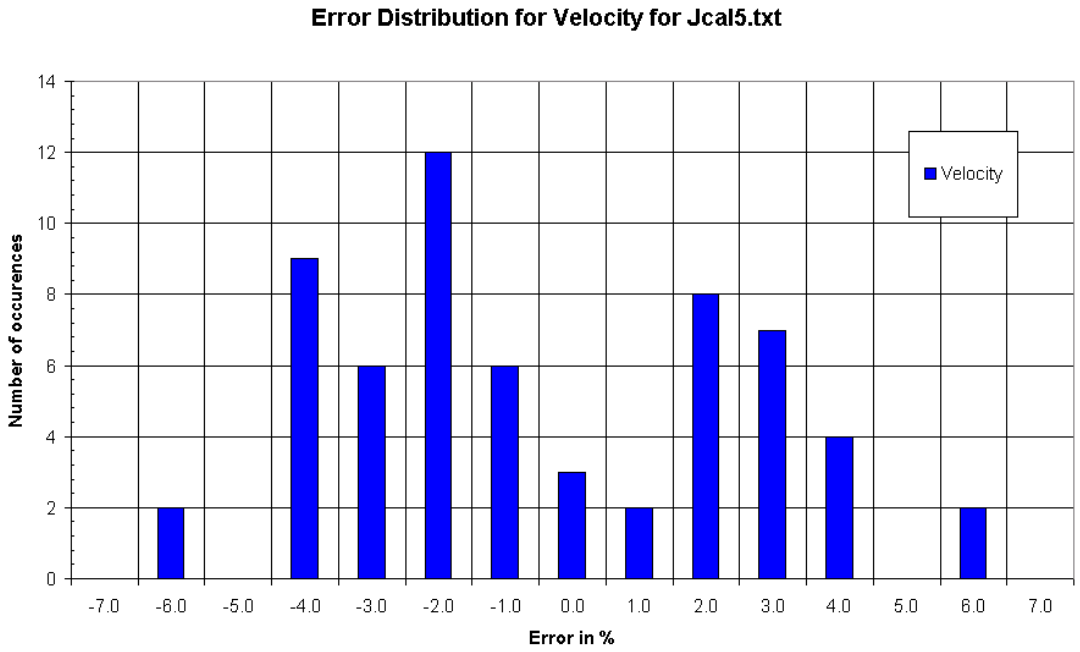

Figure 13: Distribution of velocity errors for the calibration file *Jcal5.txt* using all three test runs.

Figure 12 and Figure 13 show the distribution of errors in the angle measurements in 0.5 degree - intervals ranging from –3.00 to +3.00 degrees and in the velocity measurement ranging from –7.0 to +7.0 percent. The x-axis in Figure 12 is chosen so that the column at

–2.0 includes the number of samples with an error ranging between –2.00 and –1.50 degrees. The same holds for Figure 13 respectively.

The statistical analysis of the test results using the calibration file *Jcal5.txt* illustrated that:

- The error in yaw angle measurements does not demonstrate a normal distribution, but rather two plateaus, one between –1.50 and 0.00 degrees and the other at 0.00 to 2.00 degrees. The standard deviation of the error is fairly large (1.47 degrees); however the probe is not biased, as the average of all errors is close to zero (0.04 degrees). The achievable precision is 2 x σ = +/- 3 degrees for 95 % confidence. The uncertainty in the yaw measurements is equal to the precision, as the bias is zero.
- The error in the pitch angles follows a normal distribution, with the maximum number of measurements having an error between 0.00 and 0.50 degrees. The graph is slightly skewed to the right, which indicates a bias of the probe to overestimate the yaw angle. The deviation from the mean is very good (0.66 degrees). The precision of the probe for pitch measurements is 1.32 degrees for 95% confidence. The uncertainty is with 1.72 degrees slightly larger due to the bias of 0.40 degrees.
- The errors in the velocity readings seem fairly random varying mainly between -4 % and +4 %. They are unbiased and have an uncertainty of 6 %. This is of sufficient accuracy for the full scale fire experiments. It is important to note that the reference velocities were measured with a vane anemometer over a time step of 15 seconds, which smoothes out any minor fluctuations that might occur.

All results are summarized in Table 7 below.

Statistics for Jcal5.txt				
Error in test readings	**Yaw [°]**	**Pitch [°]**	**V [m/s]**	**V [%]**
Std Deviation σ	1.47	0.66	0.05	2.95
Average	-0.04	-0.40	0.01	-0.04
Precision P	2.94	1.32	0.10	5.91
Bias B	0	0.40	0	0
Uncertainty U	2.94	1.72	0.10	5.91

Table 7: Statistical analysis of Jcal5.txt for 95 % confidence

Dependency on Reynolds Number

The test results were also analysed with regards to the Reynolds number in order to determine a possible relationship between the error and the Reynolds number.

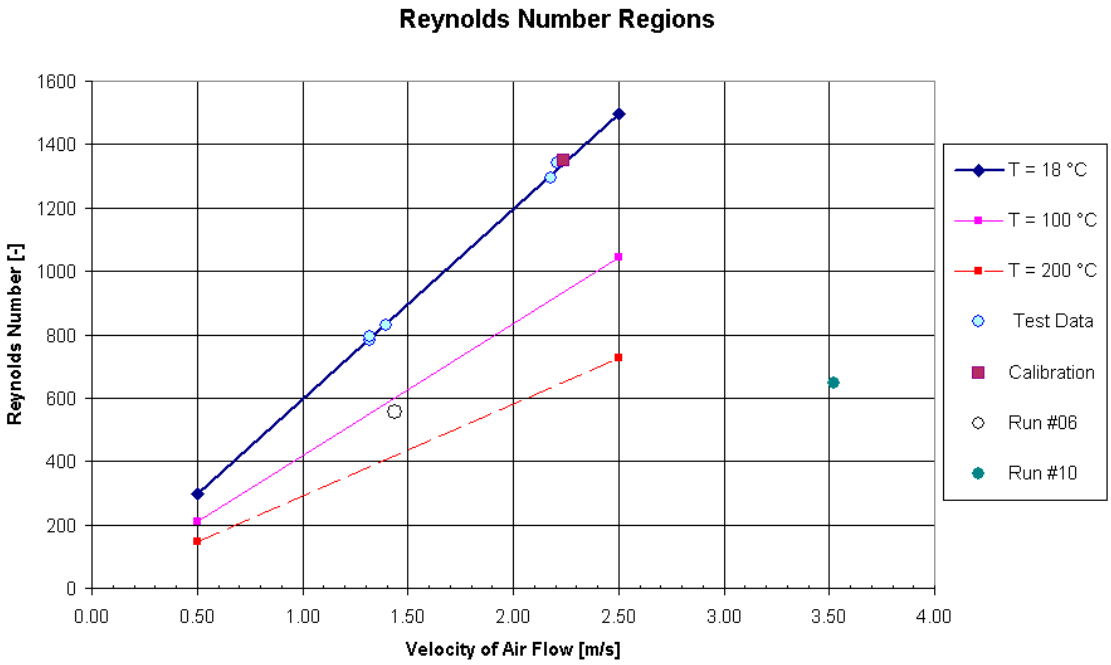

Figure 14: Reynolds number regions of calibration and experiments

The calibration was done in an airflow of 2.24 m/s at ambient temperatures, which is equivalent to Re ~ 1350.

The tests runs in the wind tunnel at the Industrial Aeronautics Laboratory ranged from Re = 783 to 1340, which represents the higher end of the expected Reynolds number spectrum, shown in Figure 14. It was not possible to lower the Reynolds numbers further, as the probe is not expected to give very reliable results at flow speeds below 1.0 m/s. The alternative of raising the air temperatures was not feasible.

The experiments ranged from 125 °C and V ~ 1.44 m/s (Run #06, burner in centre, Q = 60 kW) to 365 °C and V ~ 3.52 m/s (Run #10, burner in corner, Q = 180 kW) which is equivalent to Re = 554 for Run #06 and Re = 646 for Run #10.

As seen in Table 8 there is no clear tendency for less accurate readings at lower Reynolds numbers. It shows the dependency of the standard deviation and the average error on the Reynolds number. It is important to note that the sample size for each Reynolds number is not very large.

Error distribution		Re				
		783	793	830	1293	1340
σ	yaw [°]	0.73	0.69	1.04	1.54	1.38
	pitch [°]	0.41	0.94	0.59	0.36	0.57
	velocity [%]	3.35	1.94	2.18	1.01	1.42
ave	yaw [°]	-0.62	-1.16	1.62	0.68	0.39
	pitch [°]	0.18	0.39	0.70	0.46	0.31
	velocity [%]	1.46	2.82	0.90	-1.66	-2.67
sample size		6	18	8	11	18

Table 8: Dependency of standard distribution and average error on Reynolds Number for Jcal5.txt

Summarizing the results shows that:

- The yaw angle errors show a slightly lower standard deviation for smaller Reynolds numbers, however the average errors do not converge to a predictable trend.
- The standard deviation and average error in the pitch angle is unpredictable for all Reynolds number regions tested.
- The velocity errors seem to worsen for lower Reynolds numbers as the standard deviation as well as the average percentage errors tend to increase.

From this analysis it is expected that the precision of the velocity output of the probe might decrease with decreasing Reynolds numbers. A trend in the behaviour of the angle measurements cannot be predicted.

The five-hole probe is capable of measuring the yaw direction within 3 degrees, pitch within 2 degrees and velocity of airflow within 6 % accuracy. The lower Reynolds numbers encountered during the experiments could affect the accuracy of the velocity readings. The effect on angle readings cannot be predicted from the tests.

3.7 Sensitivity Analysis of p5hproc_judith.exe

The program p5hproc_Judith.exe was not written for an application in fire environment. It is necessary to analyse the sensitivity of the output to all input parameters, ambient pressure, temperature, and the five pressure readings to be able to quantify the sensitivity to possible fluctuations or inaccuracies of the input parameters.

3.7.1 Ambient Pressure and Temperature Input

The ambient pressure was not measured at McLeans Island, the site of the full scale experiments, but provided by NIWA Climate Data Centre for the weather station at the Christchurch Airport, circa two kilometres away from the test location. The data is accurate to 20 Pascal. Plots of the atmospheric pressures during the tests are attached in Appendix E – Atmospheric Pressure for Christchurch Airport.

The thermocouples were capable of measuring temperature to approximately 5°C accuracy.

Density

The density of the gas is calculated using the ideal gas law:

$$\rho = MP / RT = M(P_{atm} + P_{static}) / RT. \qquad \text{Equation 5}$$

where

M	= 28.95 kg/kg.mol
P_{atm}	~ 10130 Pa >> P_{static} ~ +/- 2 Pa
R	= 8314 J/kg.mol.K
T	~ [20 – 350] °C = [293 – 523] K

The static pressure is negligible as it is much smaller than the atmospheric pressure reading.

The fluid density is directly proportional to the ambient pressure and indirectly proportional to the temperature. Variations in ambient pressures by +/- 20 Pascal are negligible, a temperature increase of 5 degrees results in a reduction of 0.021 kg/m^3 in density or 2 %, as shown in Figure 15 below.

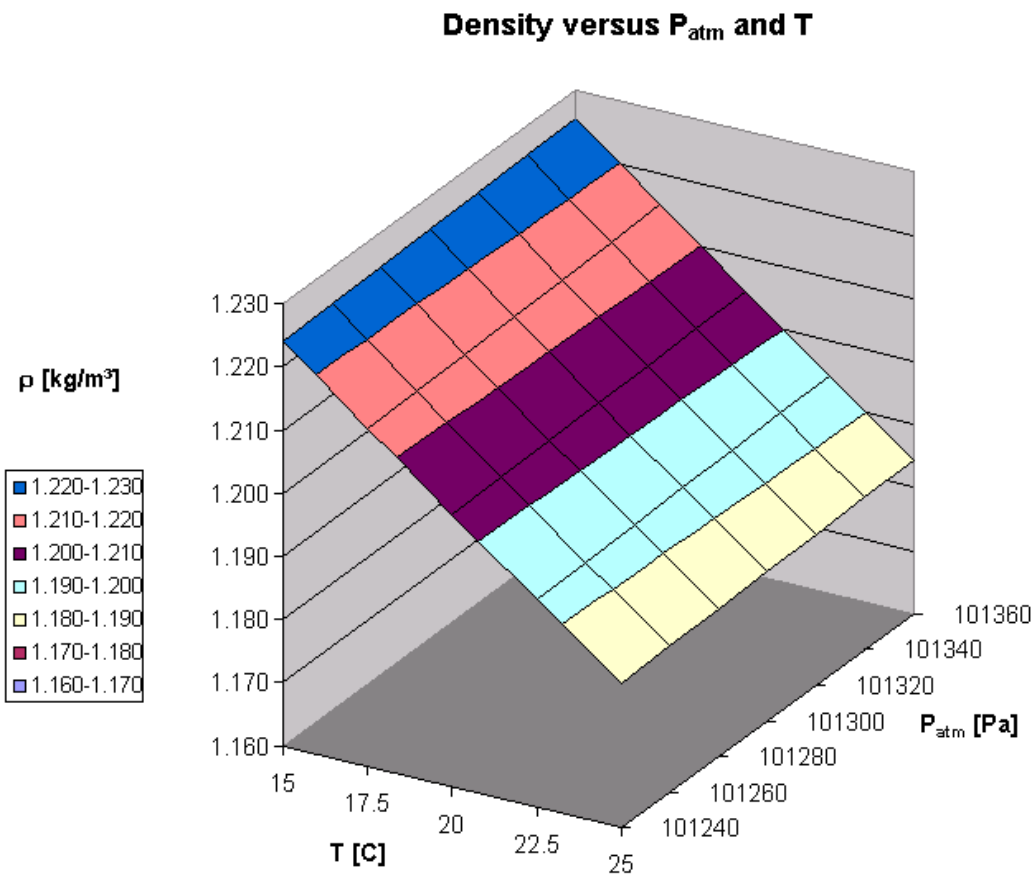

Figure 15: Dependency of fluid density on atmospheric pressure and temperature

Velocity

The velocity is calculated as follows:

$$V = \sqrt{\frac{2P_{dynamic}}{\rho}} = \sqrt{\frac{2P_{dynamic}RT}{MP}} = const\sqrt{\frac{P_{dynamic}T}{P_{atm}}} \qquad \text{Equation 4}$$

where P_{atm} ~ 10130 Pa >> $P_{dynamic}$ ~ +/- 4 Pa

Figure 16 shows that a change in atmospheric pressure has a negligible impact on the velocity, while an increase in temperature by 5 degrees leads to an increase in velocity by 0.01 m/s or 1 %.

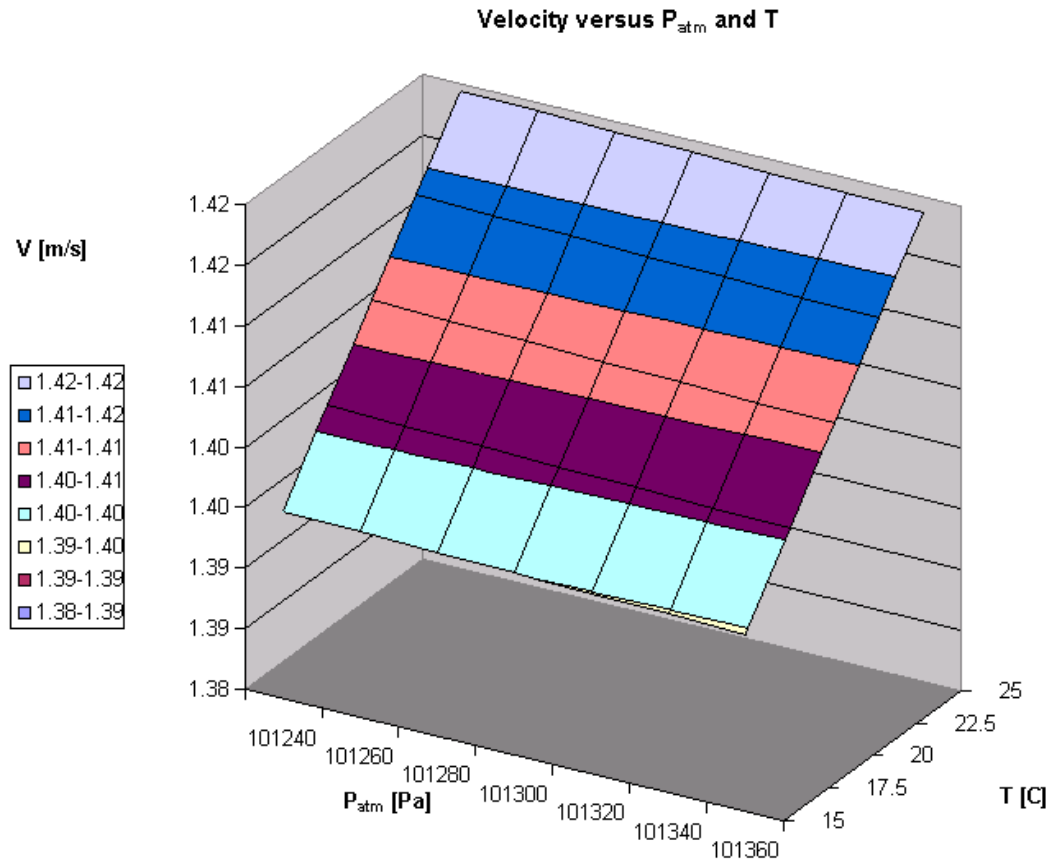

Figure 16: Dependency of velocity on atmospheric pressure and temperature

The accuracy of temperature and atmospheric pressure data is therefore sufficient and does not affect the results adversely.

3.7.2 Pressure Input

The voltage output of the SETRA pressure transducers were sampled every second as a snapshot to three decimal places accuracy. The noise at ambient conditions was 0.003 V, which is equivalent to approximately 0.003 V x 10 Pa / V = 0.030 Pa.
The voltage readings ranged from 2.130 V to 2.640 V, which is equal to a pressure range of 40 Pascal.

Two different pressure combinations were analysed in order to assess the sensitivity of the program p5hproc_Judith.exe to fluctuations in the five pressure inputs. The first was taken from the tests in the wind tunnel and the second from the full scale experiment run #06, at t = 2250 seconds. In both cases the pressures were increased in 0.010 Pascal increments, first all five pressures together and then each port separately with the other

four ports held constant. The original pressure readings are shown in Table 9. The atmospheric pressure was set at 10,000 Pa for all runs.

Wind tunnel data:

P1 [Pa]	P2 [Pa]	P3 [Pa]	P4 [Pa]	P5 [Pa]	T [K]
1.087	0.122	0.945	0.318	0.862	291.20

McLeans Island data:

P1 [Pa]	P2 [Pa]	P3 [Pa]	P4 [Pa]	P5 [Pa]	T [K]
1.691	0.660	0.675	0.600	0.598	394.93

Table 9: Input pressures for sensitivity analysis of p5hproc_Judith.exe

Yaw Angle

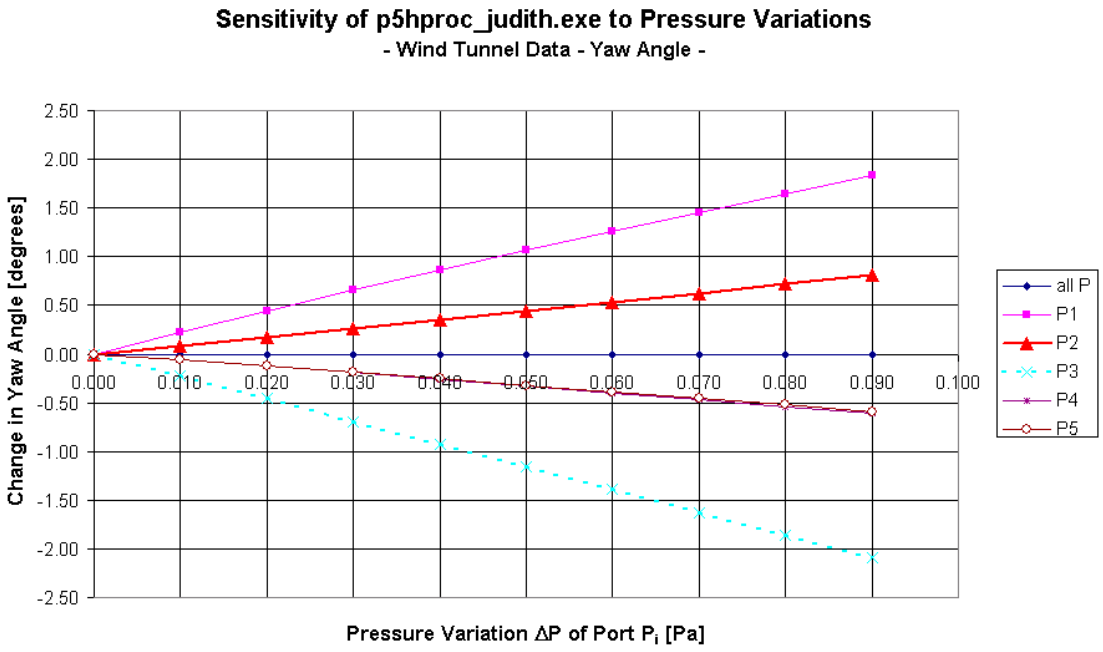

Figure 17: Sensitivity of yaw calculations in p5hproc_Judith.exe to pressure fluctuations, data taken from wind tunnel tests

The yaw angle measurements of the wind tunnel data were most influenced by changes in port #1, # 2 and #3, which was to be expected according to the definition of the yaw coefficient:

$$C_{yzw} = \frac{P_2 - P_3}{P_1 - P_{ave}} \qquad \text{Yaw coefficient} \qquad \text{Equation 9}$$

A change in all ports simultaneously does not affect the angles as the yaw and pitch coefficients do not change. A change of 0.090 Pascal of port #1 resulted in an increase of

1.8 degrees, shown in Figure 17. This is acceptable given the intended accuracy of the probe of 5 degrees. Increasing port #2 by 0.090 Pascal lead to an increase of 0.8 degrees; increasing port #3 reduced the yaw output by 2.1 degrees.

The small effect of port #5 on the yaw angle stems from the strong influence of port #5 on the pitch coefficient. Due to the fact that the calibration maps for yaw and pitch coefficients are not perfectly parallel lines this can result in a change of both angles during the interpolation between the two charts.

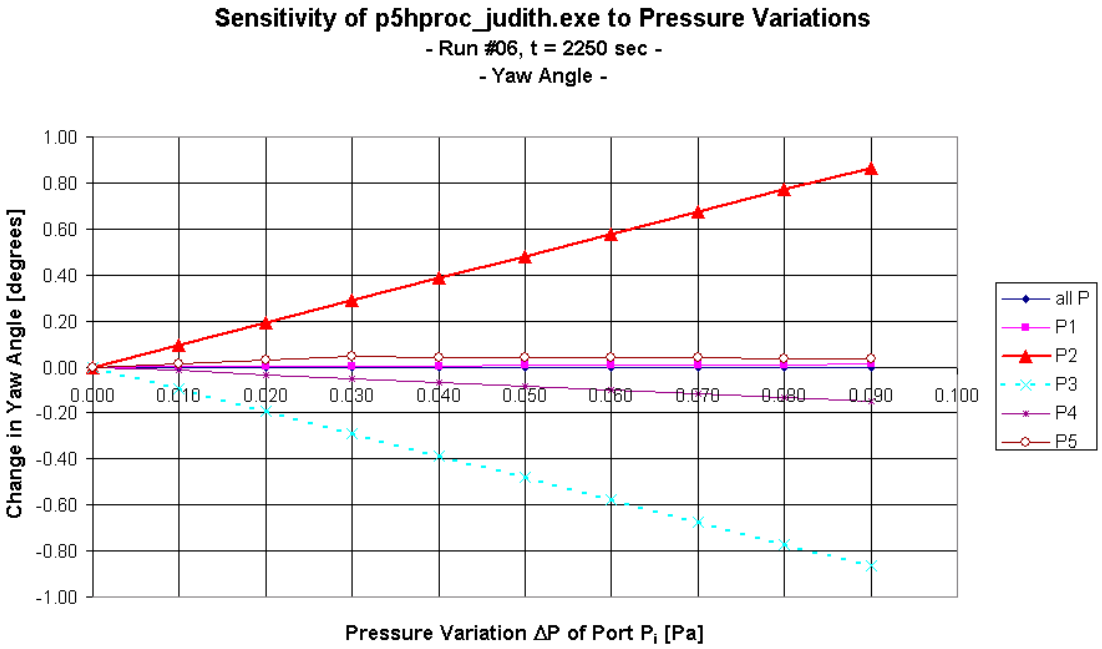

Figure 18: Sensitivity of yaw calculations in p5hproc_Judith.exe to pressure fluctuations, data taken from McLeans Island experiment

Changes in the McLeans Island data are very similar, as again port #2 and #3 are dominating. A 0.090 Pascal increase in port #2 or #3 leads to a diversion of +/- 0.9 degrees from the original reading, which is negligible.

Pitch Angle

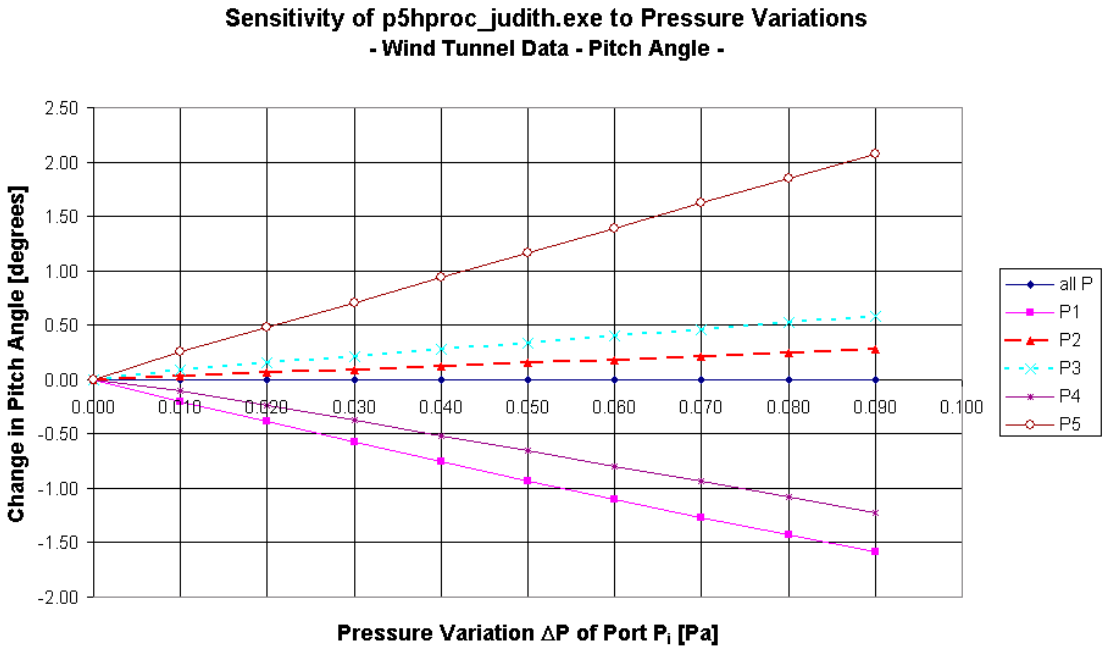

Figure 19: Sensitivity of pitch calculations in p5hproc_Judith.exe to pressure fluctuations, data taken from wind tunnel test

The pitch angle measurements of the wind tunnel data were most influenced by changes in ports #1, #4 and #5, which was anticipated in relation to the definition of the pitch coefficient:

$$C_{pitch} = \frac{P_4 - P_5}{P_1 - P_{ave}} \qquad \text{Pitch coefficient} \qquad \text{Equation 10}$$

A change in all ports does not affect the pitch angle. A change of 0.090 Pascal of port #1 resulted in a decrease of 1.6 degrees. This is acceptable given the intended accuracy of the probe of 5 degrees. Increasing port #4 by 0.090 Pascal leads to a decrease of 1.2 degrees while #5 leads to an increase of 2.1 degrees.

The small effects of port #2 and #3 stem from the strong influence of this port on the yaw coefficient, which again affects the interpolation process.

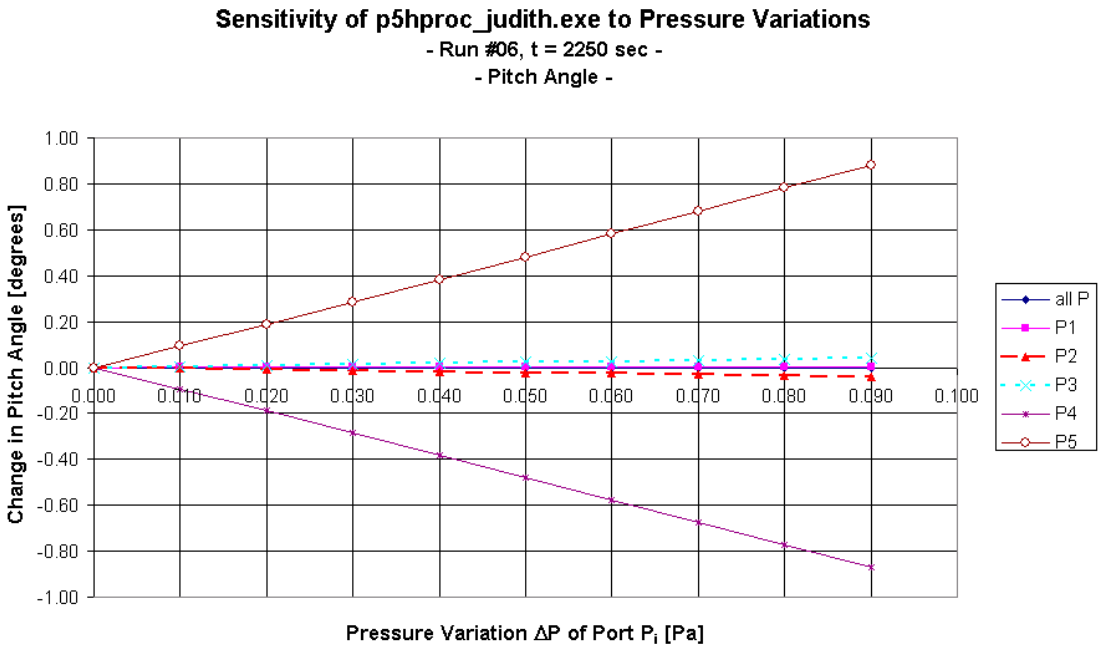

Figure 20: Sensitivity of pitch calculations in p5hproc_Judith.exe to pressure fluctuations, data taken from McLeans Island experiment

A 0.090 Pascal increase in port #4 or #5 leads to a diversion of +/- 0.9 degrees from the original reading, which is negligible. The changes of other ports have almost no effect.

Velocity

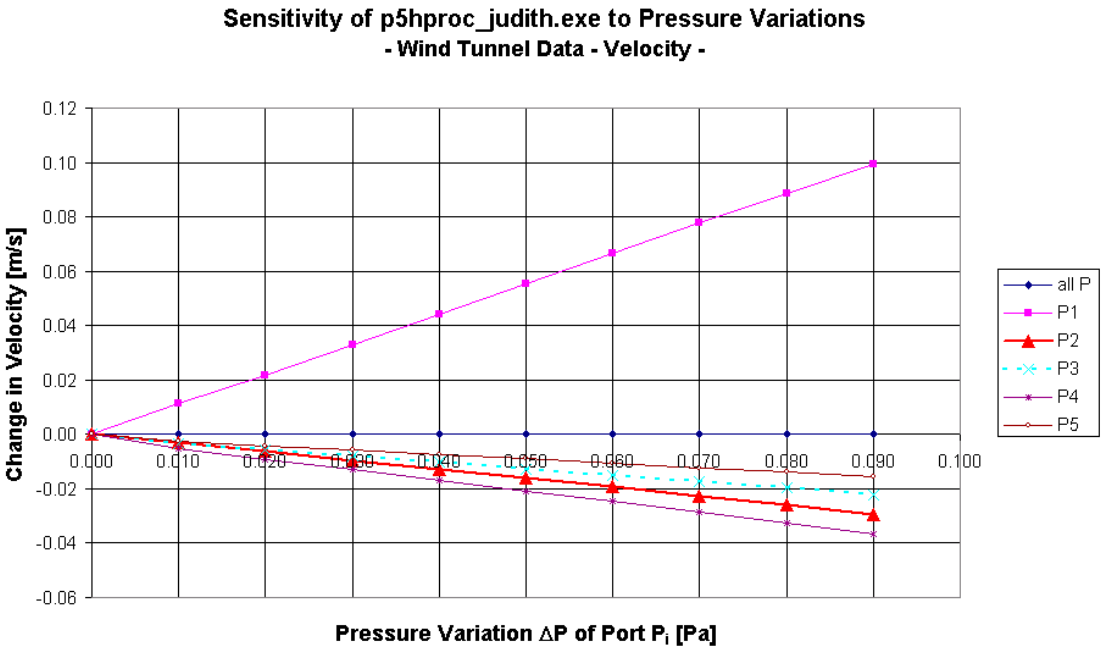

Figure 21: Sensitivity of velocity calculations in p5hproc_Judith.exe to pressure fluctuations, data taken from wind tunnel test

The velocity for the wind tunnel data is reasonably insensitive to changes in pressures as it increases only 0.10 m/s for a 0.090 Pa increase in port #1, for fluctuations of 0.030 Pascal the velocity varies 0.03 m/s. Changes in ports #2 to #5 lead to a slight reduction in velocity.

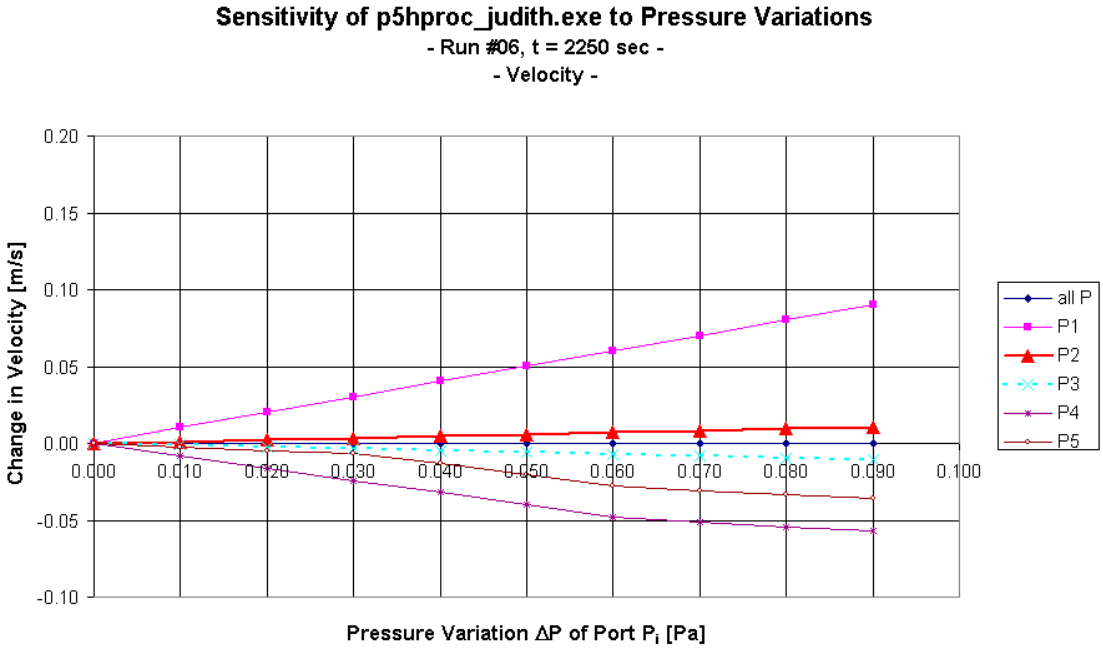

Figure 22: Sensitivity of velocity calculations in p5hproc_Judith.exe to pressure fluctuations, data taken McLeans Island experiment

The second case is even less sensitive to port #1 as shown in Figure 22, as an increase of 0.090 Pa lead to an increase of 0.09 m/s. Increasing port #4 by 0.06 Pascal decreased the velocity by 0.06 m/s. The kinks in port #4 series at 0.06 Pascal and #5 at 0.03 and 0.06 Pascal are probably due to a change in slope in the total or dynamic calibration map.

The accuracy of the atmospheric pressure and the temperature input does not affect the calculation of velocity significantly. The expected pressure fluctuations of 0.030 Pascal have no significant effect on the output of the program p5hproc_Judith.exe.

4 Experiments / Methodology

The five-hole probe was used in a series of 22 full scale fire experiments which were undertaken at McLeans Island near the Christchurch Airport. The tests took place on the 18/12/01 and during the period 21/01/02 – 29/01/02. Up to three tests were run each day with at least 1.5 hours between runs to allow the compartment to cool down. The aim of the tests for this project was to measure the direction and speed of hot gases flowing out of an ISO-room through a doorway into an adjacent ISO room. The measurements were taken above the door along the line of symmetry. The samples were crossing the spill out under the soffit as shown in Figure 23 at a 45 degree angle, so the probe moved perpendicular across the plume.

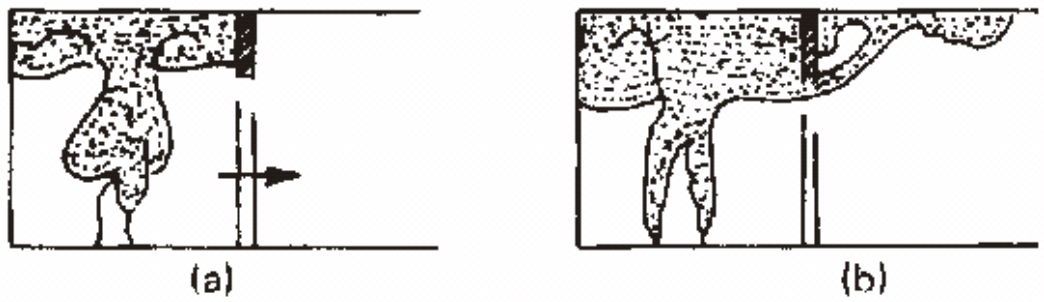

Figure 23: Spill out under the soffit of the doorway into an adjacent room (Evans, 1995)

The flow of hot air under the soffit is essentially the same as water spilling over a weir only upside down. The driving force in the fire experiment is the buoyancy of the hot gases while in a weir it is gravity.

4.1 General Description

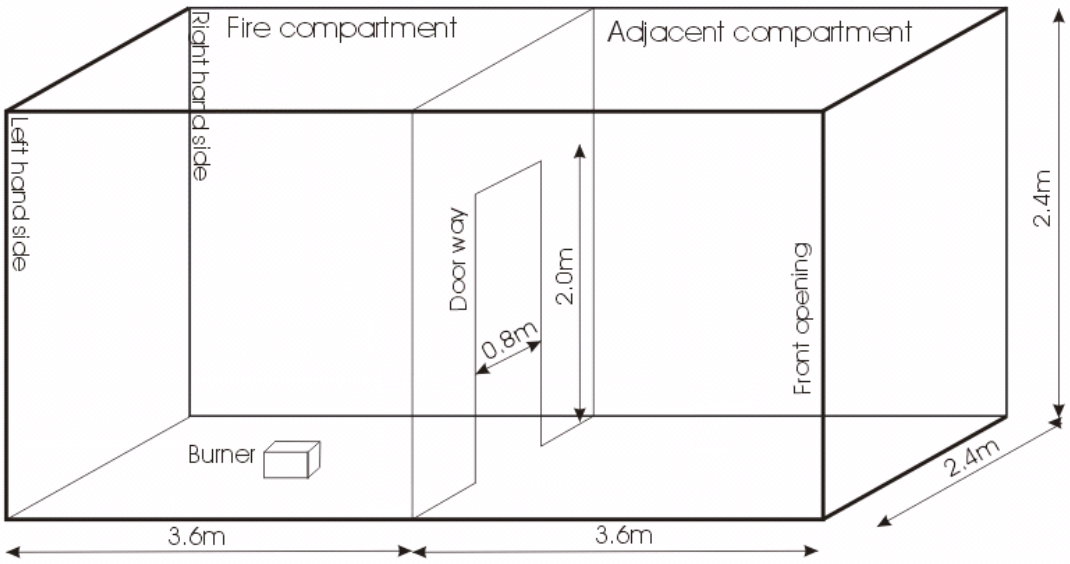

Figure 24: Dimensions of the two ISO rooms (L. Rutherford, 2002)

The ISO rooms are 3.6 m long, 2.4 m high and 2.4 m wide as shown in Figure 24. They were located inside a large shed at McLeans Island near the Christchurch airport.

The two rooms were separated by a 0.10 m thick wall, which contained a 2.0 m by 0.80 m door opening in the centre. One end of the adjacent compartment, called the 'front opening', was completely open. For seven experiments a door was fitted in the doorway wall which opened to the back compartment. The set-up is shown in Photo 25. The 300 mm x 300 mm LPG (liquid petroleum gas) burner was located in the centre of the fire compartment for 16 runs, in the far corner for three runs and at the centre of the back wall for three runs.

The notations 'left hand side' and 'right hand side' refer to a position viewing the front opening of the compartment.

The photo below is showing the burner in the corner, with no door in the door opening and the front opening unrestricted. Most of the instrumentation is located on the right side.

Photo 25: ISO room set-up with burner in the corner

4.2 ISO-room Construction

The main frame of the ISO rooms was made of rectangular steel sections. All internal surfaces were made of 12.5 mm thick fire rated gypsum plasterboard. The boards of floor and ceiling were screwed to wooden joists; the wallboards were screwed to steel studs. The floor was reinforced with wooden boards under the gypsum boards. All internal surfaces including the door were lined with 10 mm thick ceramic fibreboard (properties are attached in Appendix D – Triton Kaowool Ceramic Fibre Board Properties). All holes in the gypsum from previous experiments were sealed with high temperature RTV.
A 260 mm x 260 mm window was installed in the fire compartment in the centre of the right wall so that the behaviour of the fire could be seen when the door to the fire compartment was closed.

Due to the symmetry of the set-up the spill plume is expected to flow along the centreline of the compartment, provided there is no door installed in the doorway and the burner is located on the centreline of the fire compartment. Minor deviations from the centreline

could originate from irregularities of the soffit, rough edges and the fluctuating character of the fire.

4.3 Instrumentation

This project was part of a larger series of experiments. Apart from the five-hole probe, there were six thermocouple trees spaced equally along the centre line of the room, three in each compartment. Oxygen sample probes were located in the fire compartment, the doorway and the adjacent compartment in the upper and lower.

Eight bi-directional probes, six aspirated thermocouples and eight oxygen sample probes were located in the doorway as part of L. Clark's research project.

The instrumentation that was not relevant to this project will not be covered in more detail here. Please refer to the project reports 'The Effect of Door Angle on Fire Induced Flow Through A Doorway' by L. R. Clark and 'Experimental Results for Pre-Flashover Fire Experiments in Two Adjacent ISO Compartments' by L. Rutherford for more information on the location and type of other instrumentation used.

4.3.1 Five-hole Probe

The five-hole probe was installed so its measuring tip moved along a 45-degee plane along the centre line of the room. The probe could not be positioned perfectly horizontally, which resulted in a bias error in the angle measurements in the vertical plane of approximately 2 degrees (pitch measurements biased by approximately +2 degrees).

The measurements were taken in 50 mm intervals starting at 150 mm from the ceiling down to 600 mm below the ceiling. A sketch of the sample points is shown in Figure 26, the locations are stated in Table 10.

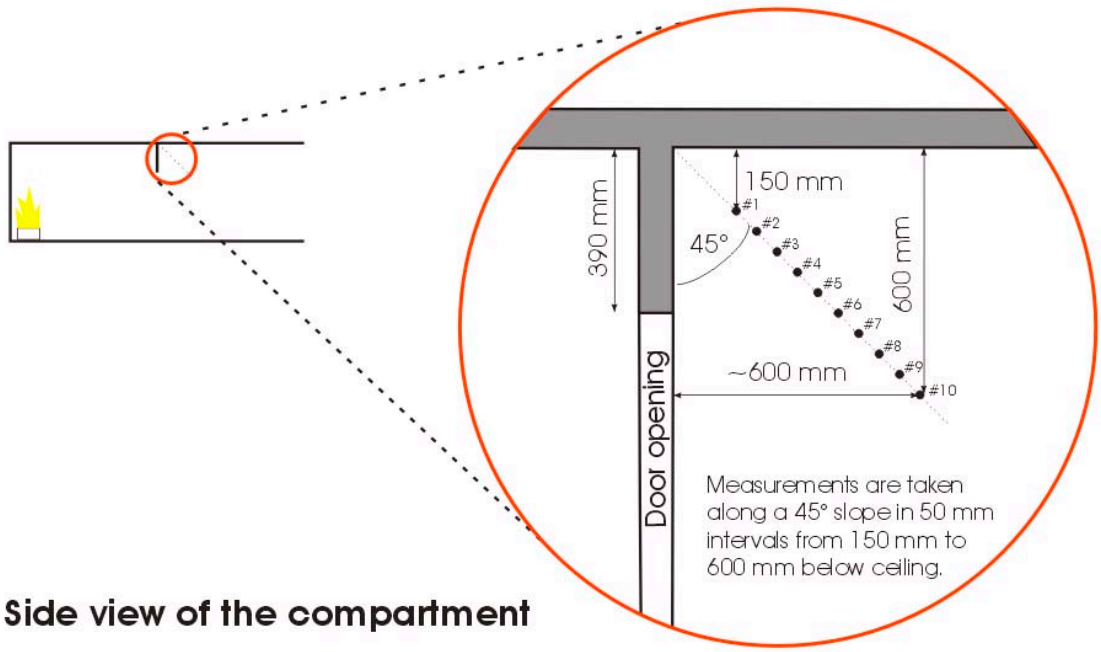

Figure 26: Location of measurements of five-hole probe

The positions of the probe were checked and adjusted prior to every run. The accuracy was within +/- 5 mm.

Position	Distance from ceiling [mm]	Distance from wall [mm]	Duration [min]	Duration [sec]
baseline	150	160	00:00 – 3:00	0 – 180
#01	150	160	03:00 – 20:00	180 – 1200
#02	200	210	20:00 – 25:00	1200 – 1500
#03	250	260	25:00 – 30:00	1500 – 1800
#04	300	308	30:00 – 35:00	1800 – 2100
#05	350	355	35:00 – 40:00	2100 – 2400
#06	400	405	40:00 – 45:00	2400 – 2700
#07	450	460	45:00 – 50:00	2700 - 3000
#08	500	510	50:00 – 48:00	3000 - 3300
#09	550	560	55:00 – 60:00	3300 – 3600
#10	600	610	60:00 – 65:00	3600 – 3900
#04	300	308	65:00 – 70:00	3900 - 4200
#05	350	355	70:00 – 75:00	4200 - 4500
baseline	350	355	75:00 – 80:00	4500 – 4800

Table 10: Overview of the positions of the five-hole probe during the tests

The probe was at position #1 for the first 20 minutes of the experiments and was then moved in 5-minute intervals down to position #10. It was pulled back up to position #4 after 65 minutes and after a further five minutes lowered to position #5, so the reproducibility of measurements could be checked.

4.3.2 Thermocouples

Two type K Chromel-Alumel 0.5 mm diameter thermocouples were used to measure the temperature near the tip of the probe. The bead was approximately 1 mm. They were located 50 mm and 80 mm behind the tip, 20 mm above the top steel tube.

4.3.3 Tubing to Pressure Transducers

The five stainless steel tubes of the probe were connected to 2.0 m copper tubing reaching down to the lower layer and then to 3.0 m plastic tubing leading out of the compartment to the pressure transducers. This allowed for sufficient flexibility in the pressure tubes for the movement of the probe during the tests.

4.3.4 Rail System for Movement of the Probe During Fire Tests

The probe had to be moved during the fire test so measurements could be taken across the spill plume.

This required a rail system that allowed movements perpendicular to the spill plume at set intervals without entering the room during the experiments. It also had to withstand high temperatures.

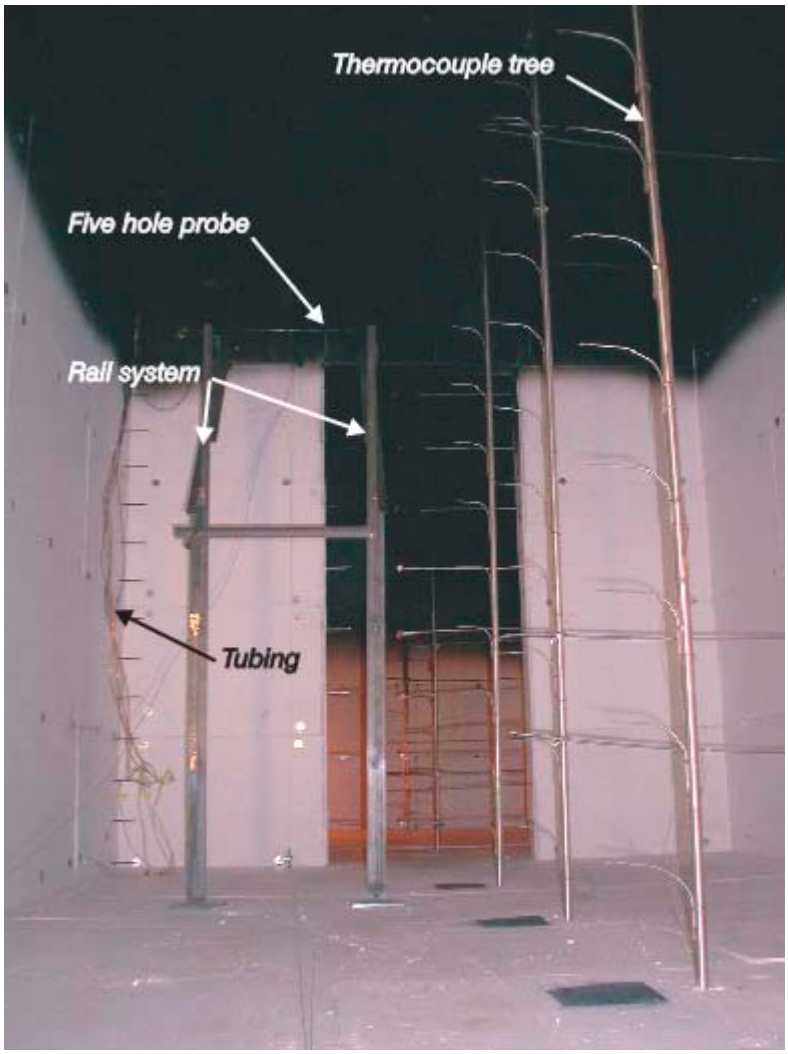

Photo 6: Rail system for the five-hole probe

Photo 6 shows the rail system left of the door opening. The probe was mounted on two carriers, 490 mm apart so that the tip of the probe was 200 mm clear of the rails in line with the centreline of the room. The probe was moved downwards using mild steel wire and a pulley system. The angle of the rails as well as the orientation of the probe on the carriers could be altered, which enabled good alignment of the probe with the flow for a symmetrical flow with a fully open doorway.

The entire system was made out of steel; all connections were either welded or bolted together. The carriers were running on wheels with a T-section as rails, as shown in Photo 7.

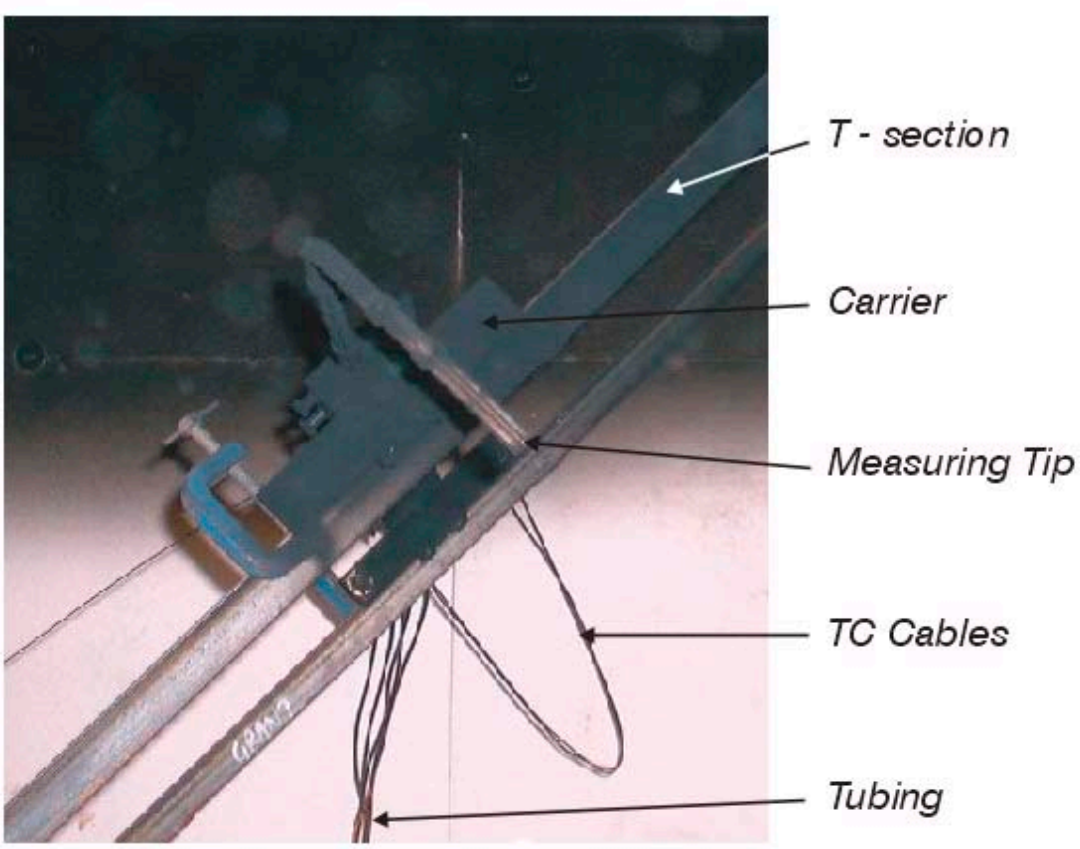

Photo 7: Five-hole probe clamped into the carriers

4.3.5 Pressure Transducers

Five pressure transducers made by Setra, Model 264 were used. The output range was 0-5 V, measuring +/- 2.5 mm H_2O.

The pressure transducers were mounted 0.3 m from the ceiling on the outside of the compartment, shown in Photo 8. The large gap between the adjacent compartment walls and protected the transducers from heating up.

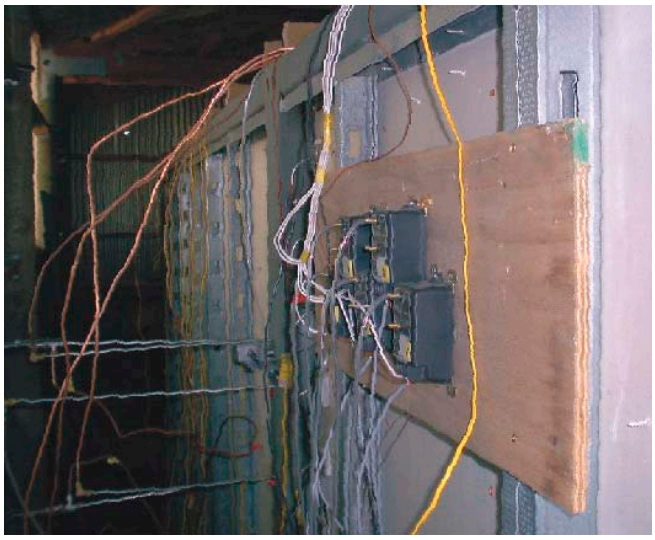

Photo 8: Location of the pressure transducers on the fire compartment

4.3.6 Data Acquisition Equipment

Data logging boxes and the software packet UDL were used to record the temperatures from the thermocouples and the voltage readings from the pressure transducers. Samples were taken every second.

4.3.7 Video Equipment

The experiments were filmed from approximately 5 m from the front of the adjacent compartment as well as through the window in the right hand side of the fire compartment.

4.3.8 Door

A 2.0 m by 0.80 m door was installed between the two rooms. It was made of fire rated gypsum plasterboard and was lined with ceramic fibreboard on both sides.

4.4 Overview of all Experiments

The following table gives an overview of all experiments and the main variables.

Run #	Date	Fire Size	Burner Location	Front	Door	T_{amb}	RH	Atmospheric
		[kW]			[°]	[°C]	[%]	[Pa] *
1	18/12/2001	120	centre	unrestricted	20	17	64	101010
2	21/01/2002	120	centre	unrestricted	60	16	73	101580
3	21/01/2002	120	centre	unrestricted	40	21	56	101530
4	21/01/2002	120	centre	unrestricted	30	24	51	101500
5	22/01/2002	120	centre	unrestricted	fully open	16	79	102030
6	22/01/2002	60	centre	unrestricted	fully open	21	58	102030
7	22/01/2002	180	centre	unrestricted	fully open	24	54	102120
8	23/01/2002	60	corner	unrestricted	fully open	19	74	102040
9	23/01/2002	120	corner	unrestricted	fully open	22	60	101870
10	23/01/2002	180	corner	unrestricted	fully open	25	54	101660
11	24/01/2002	60	wall	unrestricted	fully open	19	82	101220
12	24/01/2002	120	wall	unrestricted	fully open	24	64	101110
13	24/01/2002	180	wall	unrestricted	fully open	27	53	101160
14	25/01/2002	60	centre	soffit	fully open	16	76	102130
15	25/01/2002	120	centre	soffit	fully open	19	67	102080
16	25/01/2002	180	centre	soffit	fully open	19	64	102070
17	28/01/2002	60	centre	door opening	fully open	20	71	102020
18	28/01/2002	120	centre	door opening	fully open	22	65	101970
19	28/01/2002	180	centre	door opening	fully open	22	64	101900
20	29/01/2002	120	centre	door opening	40	20	76	101950
21	29/01/2002	120	centre	door opening	30	25	60	101810
22	29/01/2002	120	centre	door opening	20	28	53	101700

*Accuracy of atmospheric pressure readings to +/- 30 Pa. Data provided by NIWA.

Table 11: Overview of all experiments

The shaded runs were analysed in more detail.

4.5 Definition of Angles and Coordinates

The figures in earlier sections containing the definitions of angles referred to Dr. Huntsman's programs designed for a different probe orientation, while the figures below convert the output from the program to the actual fire experiment direction.

The yaw output of p5hproc_Judith.exe now refers to flow direction in the vertical plane, while pitch refers to the horizontal plane. A simple conversion chart for the program output is shown in Figure 27.

Angles in the vertical plane are measured relative to the 45 degree position of the probe, angles in the horizontal plane are measured from the centreline of the adjacent compartment.

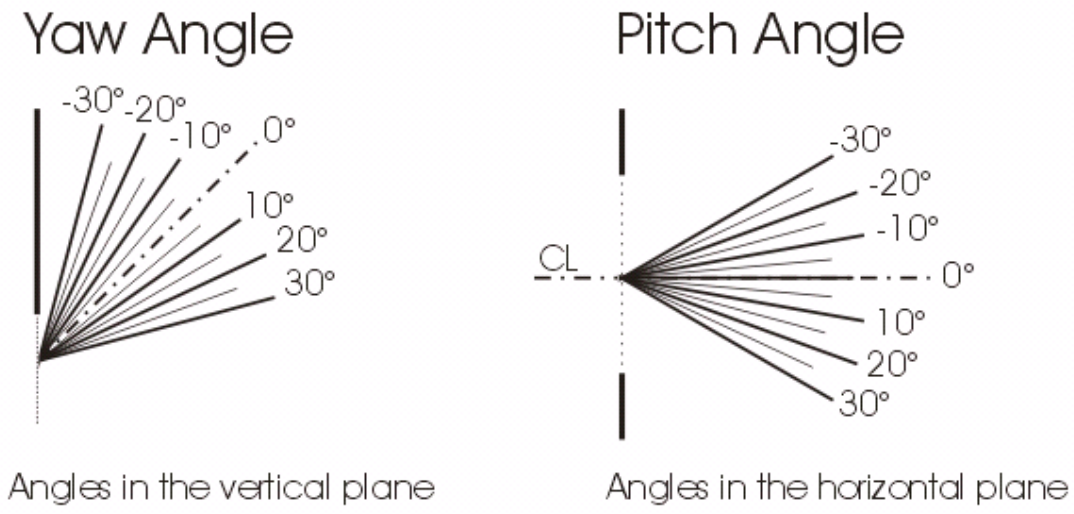

Figure 27: Conversion chart for the yaw and pitch output

4.6 Data Reduction

The data required some manipulation prior to converting the voltage output of the pressure transducers into yaw, pitch and velocity data of the flow, all of which will be described below.

4.6.1 Preparation of Input File for p5hproc_Judith.exe

The voltage output from the pressure transducers was converted to pressures following two steps:

- Calculate a baseline voltage for t = 1 sec to t = 130 seconds:

  V_{amb} = average ($V_{t=1s}$ to $V_{t=130s}$) Equation 19

- Convert Volts to Pascal at t = i seconds:

  P [Pa] = ($V_{t=i}$ – V_{amb}) x C_i Equation 20

  Where C_i is the calibration constant for each pressure transducer (~10 Pa/V)

The temperature at the tip of the probe was extrapolated linearly from the two thermocouples on the probe:

$T_{tip} = T_1 – 50\ mm / 30\ mm\ (T_2 – T_1)$ Equation 8

The denominator of the coefficients, $P_1 – P_{ave}$, had to be non-zero, or the program p5hproc_Judith.exe would crash. This problem can occur when the flow hits the probe on a very steep angle, so that the pressure in the centre is not the largest. Good alignment should eliminate this difficulty.

The five pressures and the temperature together with the atmospheric pressure during the time of the experiment were then saved into a text file ready to be read into p5hproc_Judith.exe. A short sample file is attached in Appendix A - Input File for p5hproc_Judith.exe.

4.6.2 Averaging Methods

Several different averaging methods were explored in order to smooth the pressure fluctuations that were observed during the experiments. Figure 28 shows the result of the original data and moving averages:

- a 60 second average of the input data prior to running the program p5hproc_Judith.exe.

In order to reduce the number of data points from several thousand to fifteen,

- a 120 second average of the last two minutes of each position and
- a 300 second average for each position were calculated.

The original data is denoted as series '1 sec'. The numbers at the top of the Excel plot show the position of the probe at that time. At the start the probe was at position #1, and then moved to down to position #10 in five-minute intervals. At 3900 seconds the probe was pulled back to position #4 and after five minutes moved to position #5. It stayed at position #5 during the baseline at the end unless stated otherwise. For exact locations please refer to Table 10.

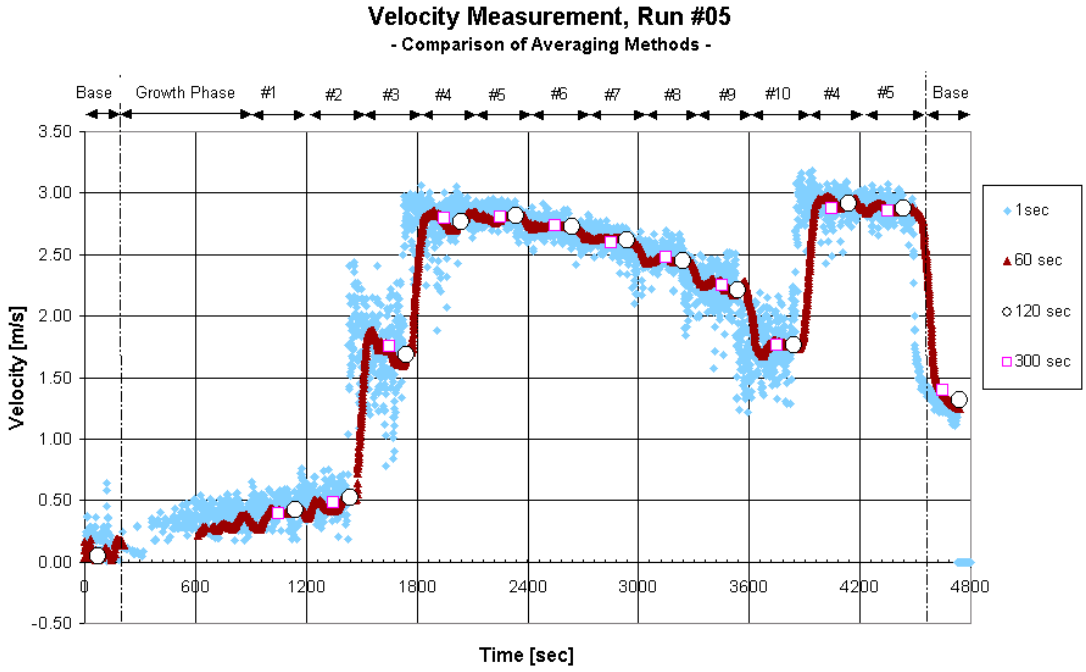

Figure 28: Comparison of averaging methods, run #05, velocity

The noise in the pure data varies depending on the location of the probe. At position #2, #9 and #10 the probe seems to be located at the outer edges of the spill plume and more exposed to turbulent flow than in the centre of the spill plume.

The series averaged over 60 seconds follows the pure data well, however it demonstrates a slight time lag towards the end of the experiment.

Both averages over 120 and 300 seconds match the unchanged and the 60-second interval series well.

The 120-second averaging method was used to compare the flow characteristics of different experiments because it is free of any influence of the movement of the probe on the pressure readings.

5 Results

Eleven out of the 22 runs were analysed in order to assess the effects of varying fire size, fire location, door angles and front opening on the flow characteristics of the spill plume under the soffit. The velocity data was also compared against the speed results from the top bi-directional probe in the doorway.

5.1 General Observations

5.1.1 Soot Accumulation

The soot deposition on the tip of the probe was minimal during the 60 kW and the 120 kW fires and did not affect the pressure readings. Tests with Q = 180 kW produced larger amounts of soot, especially with the door in the doorway, however this increased soot contamination did not affect the pressure readings noticeably. The tip was cleaned prior to every run to avoid excessive soot deposition.

5.1.2 Density Variations

The density variation between the upper hot layer (T_{max} = 365°C, ρ ~ 0.55 kg/m^3) and ambient conditions (T_{amb} = 18°C, ρ ~ 1.21 kg/m^3) is not expected to have significant effect on the pressure readings, as all five tubes were routed through the same temperature fields and therefore underwent the same temperature variation.

5.2 Run #05, Q = 120 kW, Burner in Centre, No Door, Front Opening Unrestricted

A set of plots from run #05 will be used to make general observations about the behaviour of the probe in the fire environment and its limitations.

The plots for the other ten experiments are attached in Appendix G – Yaw, Pitch and Velocity Plots.

Temperature

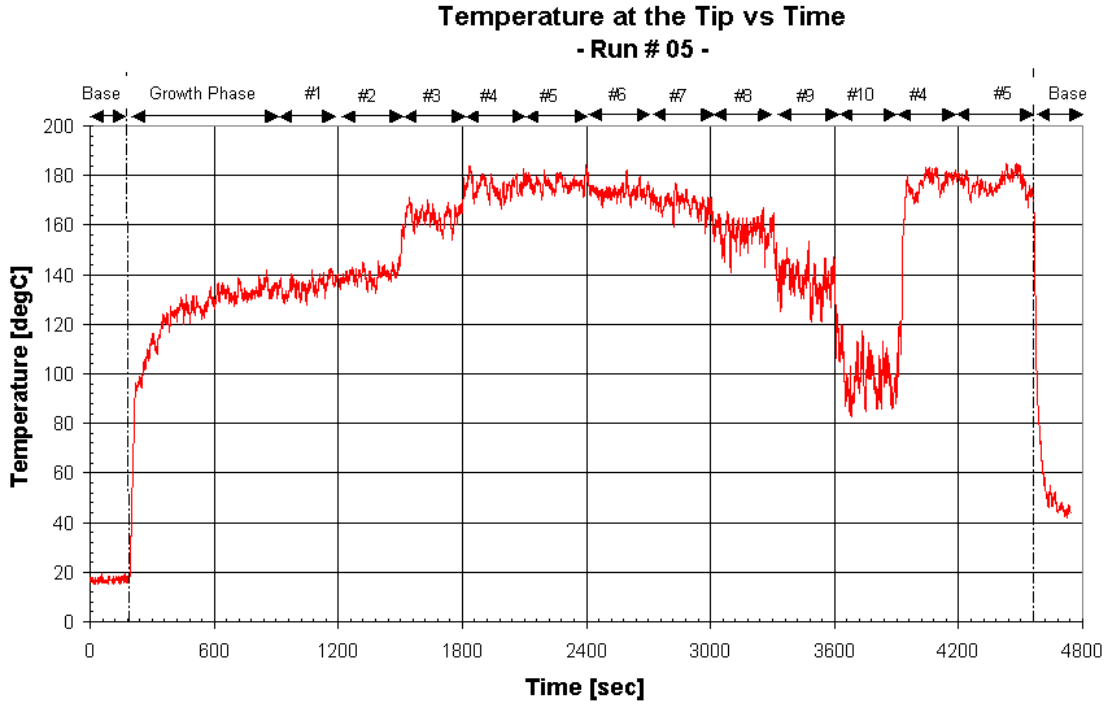

Figure 29: Temperature at the tip of the five-hole probe for run #05

Temperatures reach steady state after approximately 15 minutes (900 seconds). As the probe moves across the plume the temperatures rise until they reach a maximum of 180°C at positions #4 and #5 (300 mm and 350 mm BC). The fluctuations increase between position #8 and #9 as cooler ambient air is entrained into the edge of the plume. The temperature drops on average from 160°C to 100°C between position #8 and #10.

Yaw Angle

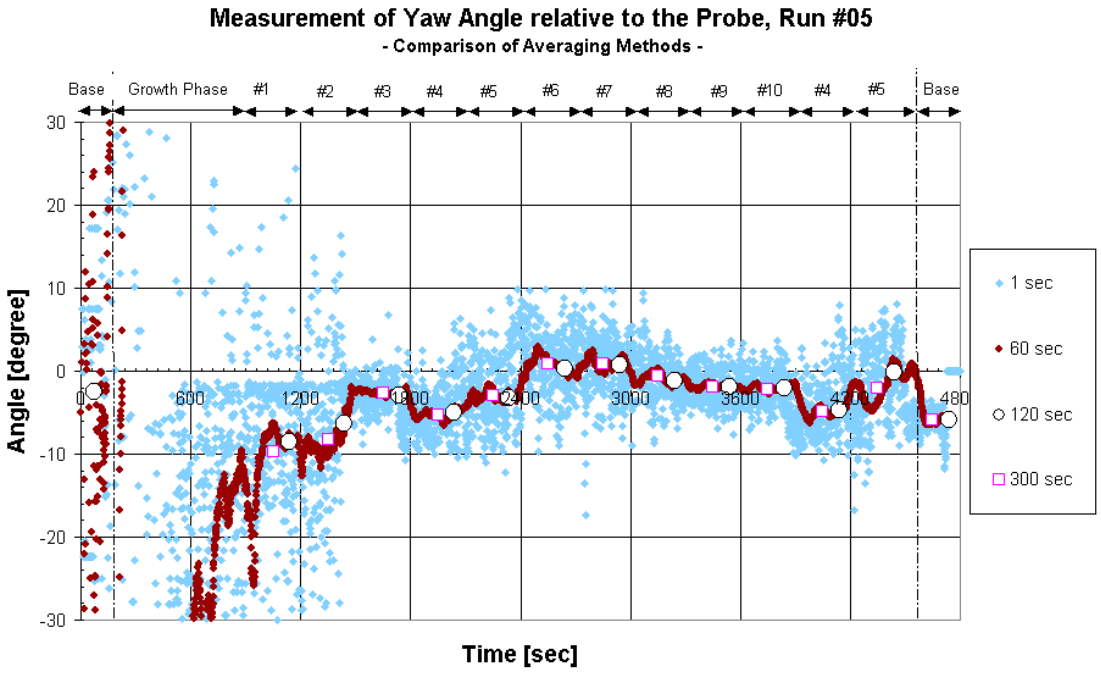

Figure 30: Yaw angle measurements for run #05

During the baseline (0 – 180 seconds) the angle measurements are extremely scattered as there is ambient air movement and hence no flow. During the following 15 minutes the fire grows and temperatures in the compartment stabilize.

Figure 30 shows that the scatter of yaw measurements for positions #1 and #2 is also very large, which is an indicator that the probe tip is located in a re-circulation region. During the following 50 minutes the yaw angle fluctuates between +/- 10 degrees, with the main trend lying close to zero degrees. Only position #4, 300 mm below the ceiling shows a slightly lower yaw of –5 degrees.

Figure 31 shows the results averaged over 180 seconds with the length of the flow vectors proportional to the velocity. It is easily visible that positions #1 and #2 are not inside the plume, but possibly in an eddy region. The velocity increases steeply to reach a maximum at position #5 and then reduces gradually.

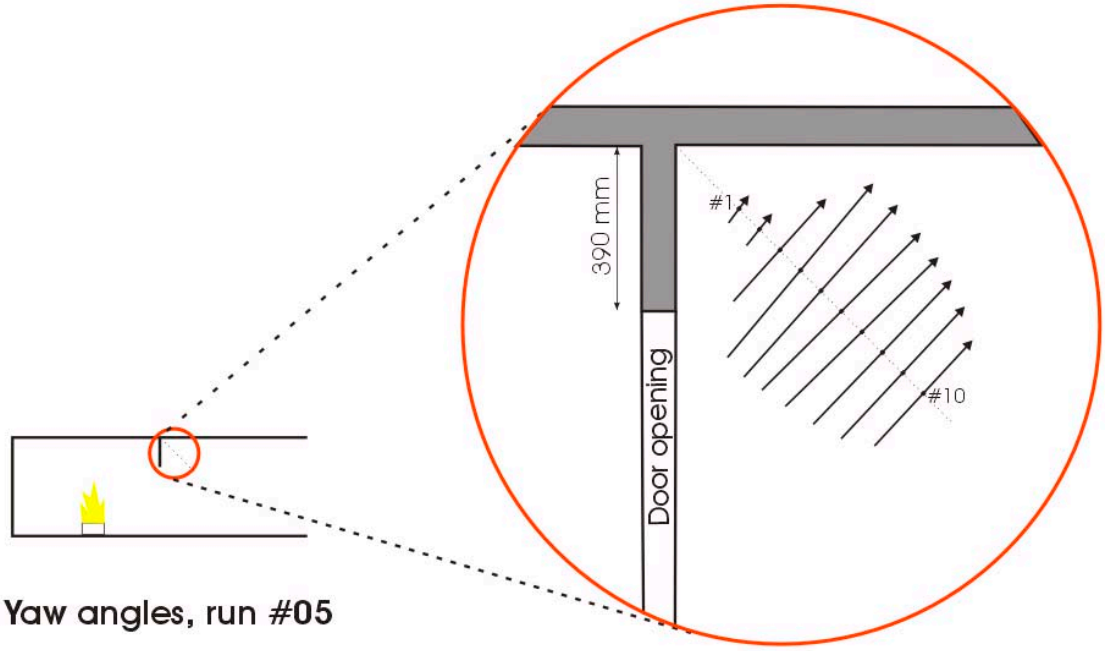

Figure 31: Flow pattern in the vertical plane of the spill plume for run #05

Pitch Angle

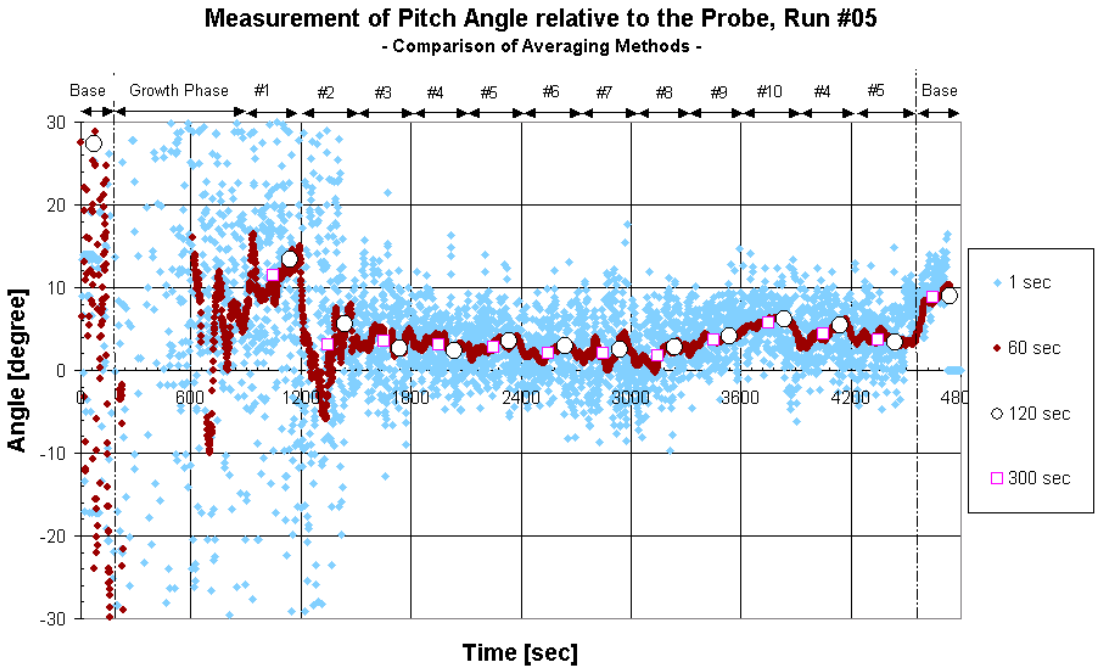

Figure 32: Pitch angle measurements for run #05

The pitch angle measurements seen in Figure 32 are also fluctuating strongly during the first 1500 seconds. The average lies between 2.4 degrees and 3.6 degrees for positions #3

to #9, which indicates – taking the bias of +2 degrees into account – that the actual pitch is very close to zero.
At position #10, the pitch increases slightly, probably because the probe tip is in the outer, more turbulent region of the spill plume.

The angle results greater than 30 degrees stem from linear extrapolation out of the calibration maps due to very large yaw and pitch coefficients. They must be ignored and were therefore not plotted.

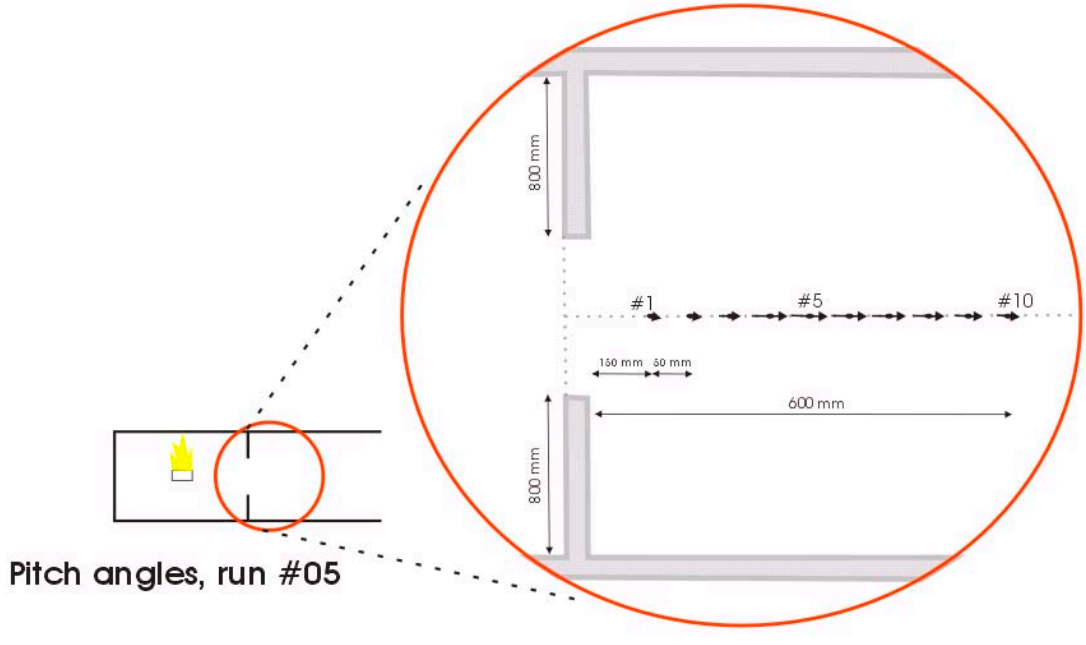

Figure 33: Flow pattern in the horizontal plane of the spill plume for run #05

Figure 33 illustrates the flow direction in the horizontal plane. The spill plume is well in line with the centreline of the compartment.

Velocity

The velocity measurements show a clear step character as the probe moves through the plume as seen in Figure 34.

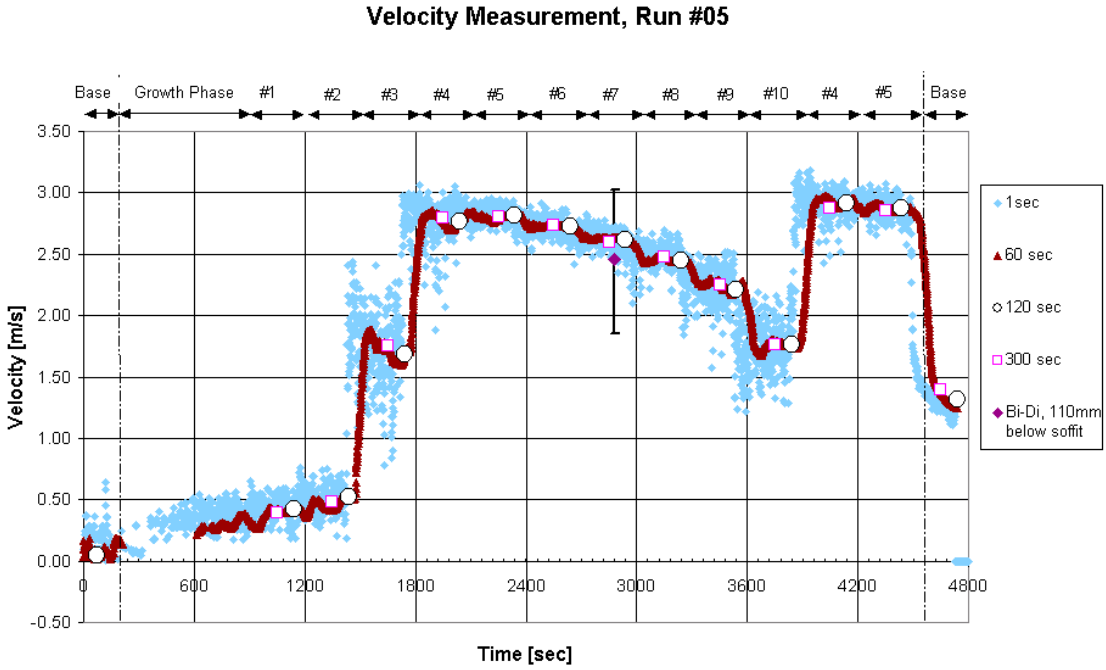

Figure 34: Velocity measurements for run #05

During the 180-second baseline the velocities are close to zero, just as expected. During the growth phase the pressures on the probe tip are very unsteady, resulting in cases where the pressure on the centre tube is smaller than on the surrounding tubes. This can lead to a mathematical error in the calculation process which again results in a default output of V = –99 m/s, ignored on the plots here.

The low velocities at positions #1 and #2 of around 0.5 m/s signal that the probe tip has not yet entered the plume, but is in a re-circulation region. The large fluctuations at position #3 (250 mm BC) ranging from 1.0 m/s to 2.25 m/s indicate the turbulences of the outer edge of the plume. At position #5 the tip has reached the point of maximum velocity, 2.82 m/s on average. This coincides with the point of maximum temperature T_{max} ~ 180°C, as shown in Figure 29. The velocity $V_{\#4}$ of 2.82 m/s (averaged over 120-seconds) is 13 % higher than the average speed measured with the top bi-directional probe in the door way, $V_{bi\text{-}di,\ ave}$ = 2.46 m/s. However the velocity readings all lie within the range of $V_{bi\text{-}di,\ min}$ = 1.85 m/s to $V_{bi\text{-}di,\ max}$ = 3.02 m/s.

The velocity gradually decreases to a minimum of 1.75 m/s at position #10 (600 mm BC). From position #8 to #10 the fluctuations increase again, marking the approach of the lower edge of the spill plume with higher turbulences.

At 3900 seconds the probe was pulled back to positions #4 and #5, in order to assess the reproducibility of measurements during an experiment. The velocities are with averages of 2.90 m/s and 2.85 m/s slightly higher than previously, but the error of 3.6% is within the expected range in a fire environment.

5.3 Run #10, Q = 180 kW, Burner in Corner, No Door, Front Opening Unrestricted

Run #10 produced the hottest upper layer temperatures with T_{max} = 365°C and greatest velocity of 3.53 m/s at position #4 (300 mm BC). The plume in the vertical plane generally flows in a 42 degree direction (Figure 35), measured from the vertical. The top two positions are outside the plume.

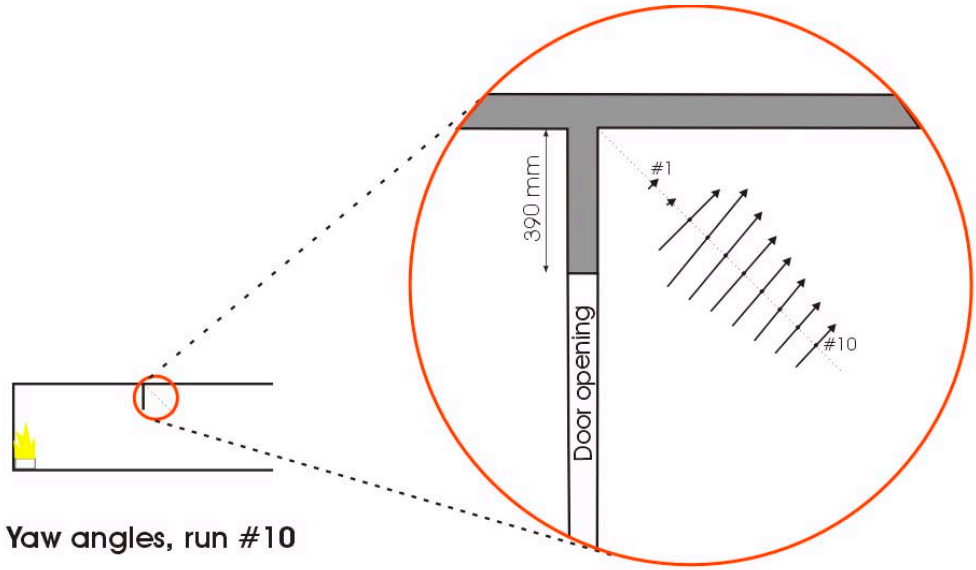

Figure 35: Flow pattern in the vertical plane of the spill plume for run #10

The plume in the horizontal plane flows along the centreline of the compartment except at position #5 (350 mm BC), where the flow is diverting by 10 degrees (Figure 36). This phenomenon was also found in run #09, with a smaller fire size of 120 kW.

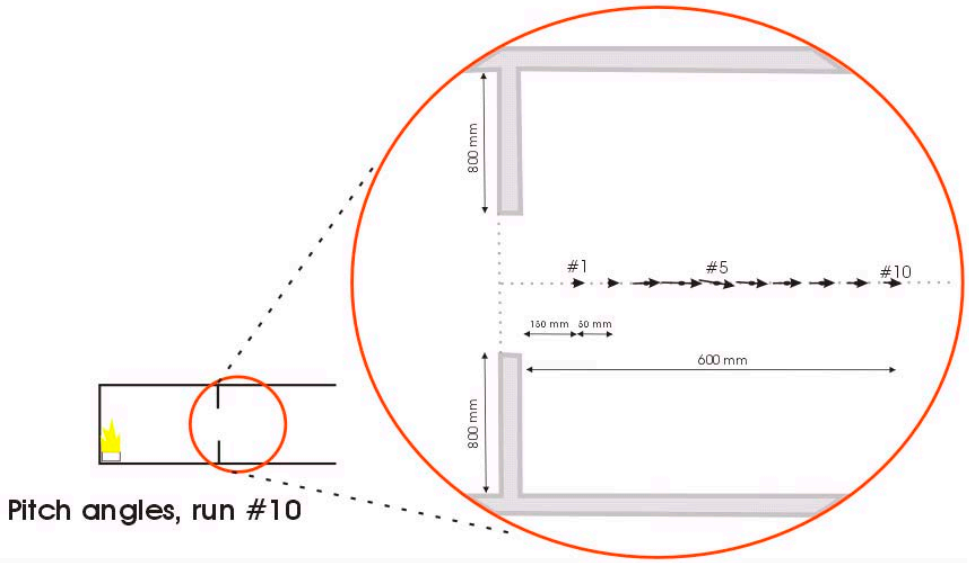

Figure 36: Flow pattern in the horizontal plane of the spill plume for run #10

5.4 Run #03, Q = 120 kW, Burner in Centre, Door at 40°, Front Opening Unrestricted

The door in the doorway caused the plume to deflect, so that the probe was no longer in alignment and the points of measurement were not perpendicular to the flow.

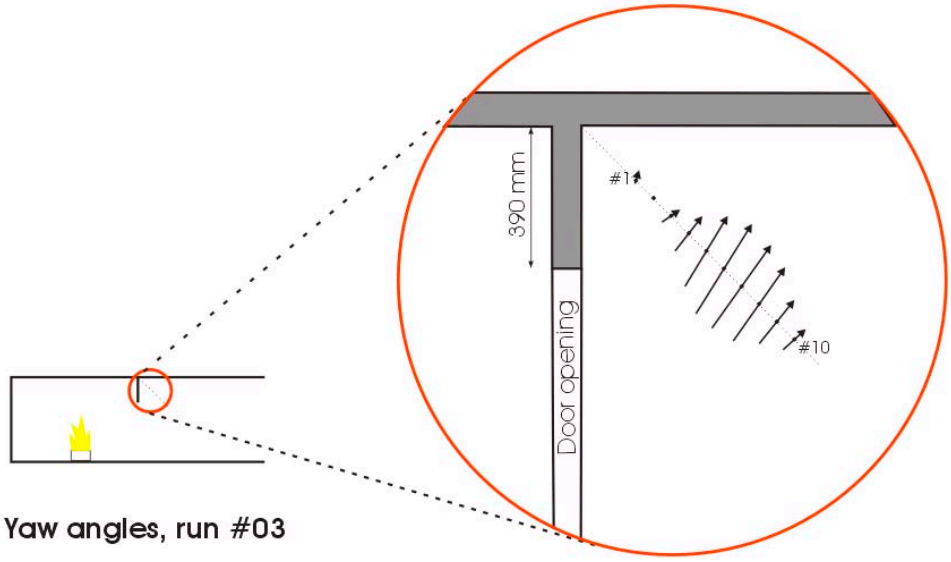

Figure 37: Flow pattern in the vertical plane of the spill plume for run #03

The point of maximum velocity now occurs at position #6 (400 mm BC), see Figure 37. The probe cannot measure the direction up to position #3, because of the misalignment, the very low velocity and eddies occurring in this area. The flow deflects between 11 and 16 degrees from the centreline between positions #4 to #10, as shown in Figure 38.

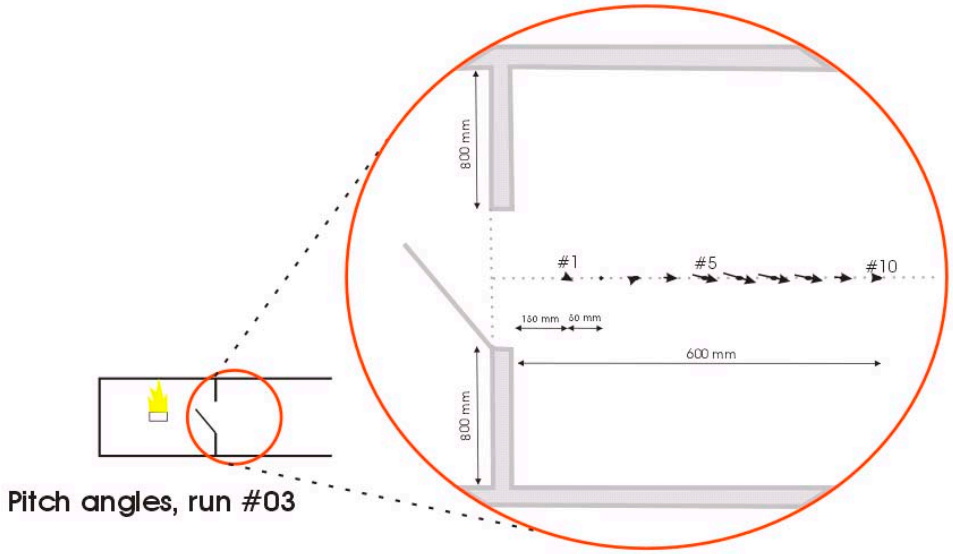

Figure 38: Flow pattern in the horizontal plane of the spill plume for run #03

5.5 Comparison with Speed Measurements from Bi-Directional Probe

Where possible the velocities were compared with speed data from the top bi-directional probe in the doorway, located approximately 110 mm under the soffit at the centre line of the room. The data was provided by L. Clark and includes the minimum, average and maximum speed of the air flow during a 10 minute interval starting at 43 minutes until 53 minutes of each experiment and is attached in Appendix F – Speed Measurements of Bi-directional Probe. The plot below compares the maximum velocity derived with 2-minute averaging method of the five-hole probe with the average speed measured by the bi-directional probe. Minimum and maximum speed of the bi-directional probe is shown as error bars. Clarks data is also included in the velocity plots in Appendix G – Yaw, Pitch and Velocity Plots as a single point $V_{bi\text{-}di,\ ave}$ at t = 2880 seconds (48 minutes) with the minimum and maximum range shown as error bars.

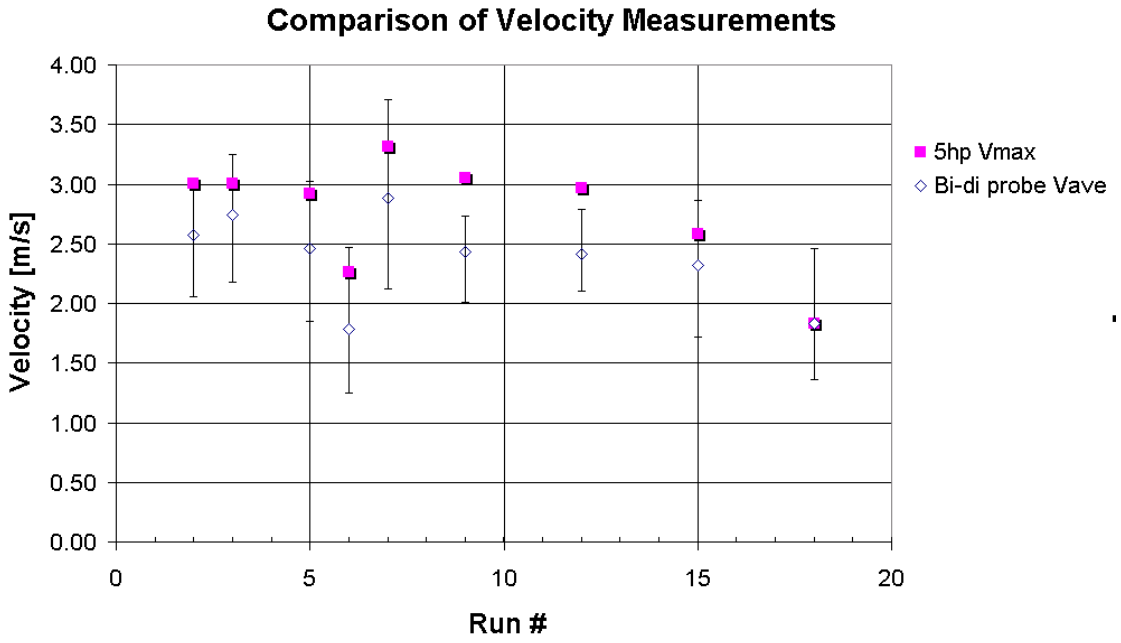

Figure 39: Comparison of velocity measurements of five-hole probe and bi-directional probe

The velocity of the five-hole probe is higher than the speed measured by the bi-directional probe, except in run #18, where they are identical. The difference varies between 0.0 m/s in run #18 and 0.26 m/s in runs #02 and #15.

These patters might arise from the door 40 degrees open in run #02 and the inclusion of the soffit and door opening at the front of the adjacent compartment in runs #15 and #18.

In all other runs the difference varies between 0.44 m/s and 0.62 m/s, which might occur due to the different sampling location.

5.6 Variation of Fire Size

In runs #05, #06 and #07 the burner was located in the centre of the fire compartment, there was no door in the doorway and the front opening of the adjacent compartment was unrestricted. The only variable was the fire size, ranging from 60 kW in #06, 120 kW in #05 to 180 kW in #07.

In run #07 the probe was located at position #6 from 3900 seconds until the end due to problems with the rail system; this is marked on the graphs.

Temperature

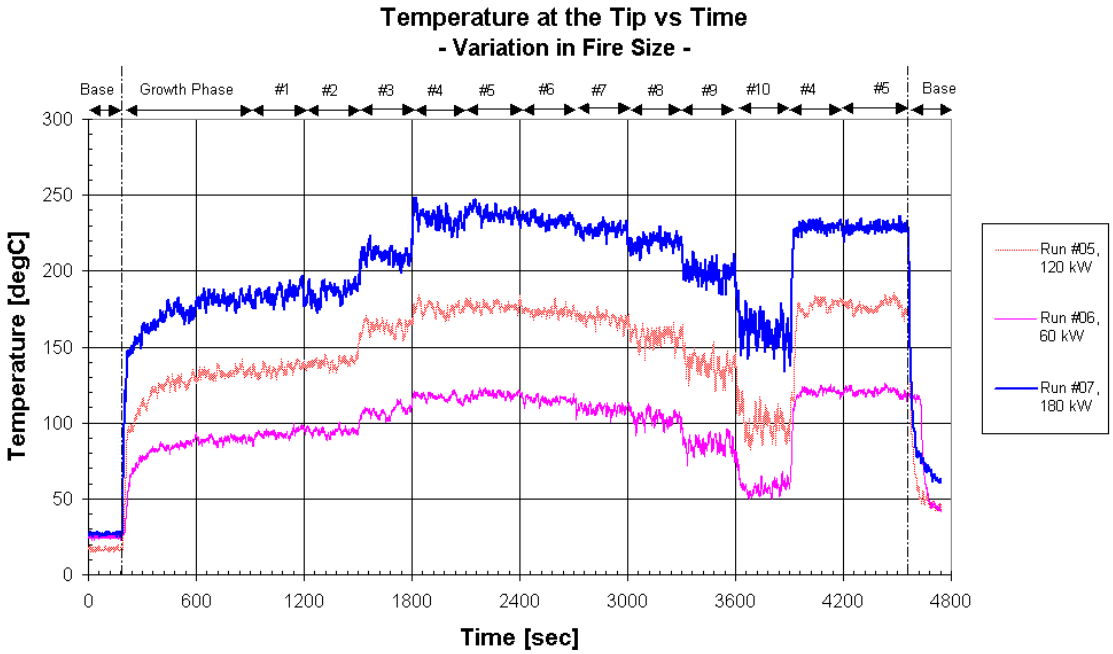

Figure 40: Temperature at the tip for runs #05, #06 and #07

The temperatures at the tip of the probe are directly proportional to the fire size, as shown in Figure 40. They reach a maximum at positions #4 and #5 (400 mm to 450 mm BC) and decrease from position #7 to #10. The noise in the signal increases from position #8 to #10, indicating a more turbulent region where more mixing with the cooler ambient layer may be taking place.

Yaw Angle

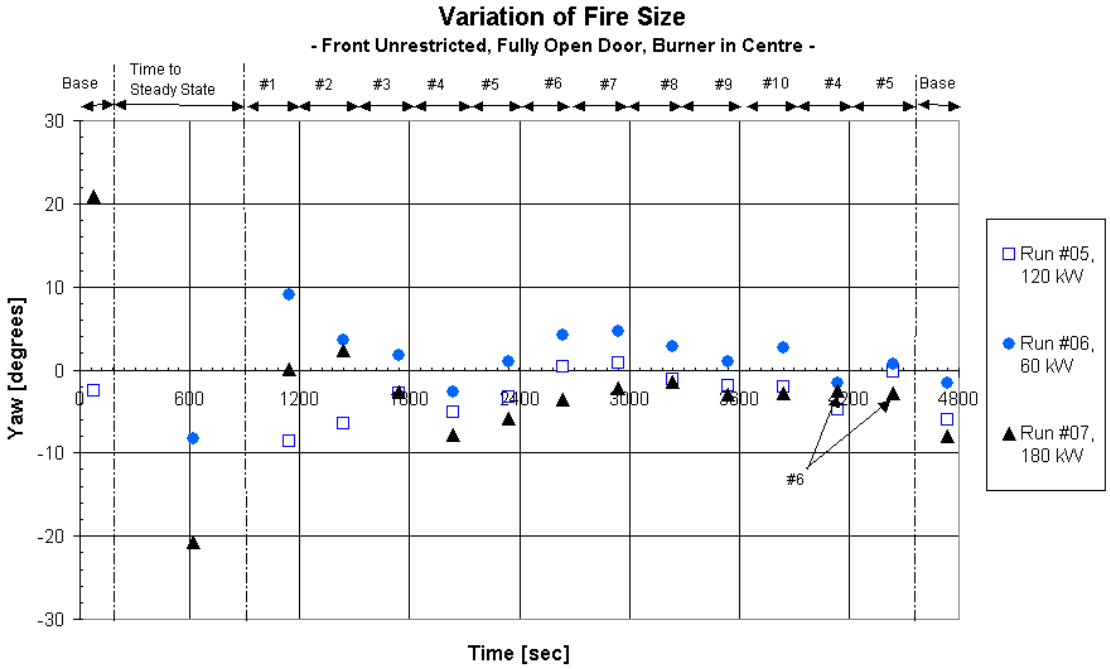

Figure 41: Influence of the fire size on the yaw angle

In positions #1 and #2 (150 mm and 200 mm BC) the probe is still in the more turbulent outer edge of the spill plume. The general trend is the smaller the fire the larger the yaw angle, or the flatter the spill plume (Figure 40). This is reasonable as the temperature of the hot air is much higher for the larger fire size, hence the density of the air is smaller and the upward acting buoyant force larger. When the probe moves further out of the spill plume, the yaw angle differences between run #05 and #07 become less distinct and the flow converges to 45 degrees.

The plume displays its steepest point at position #4 (300 mm BC), coinciding with the area of maximum temperature.

The 120 kW fire seems to produce a spill plume that aligns well along the 45 degree axis, while the plume of the 60 kW fire is slightly flatter and the plume of the 180 kW fire is slightly steeper.

Pitch Angle

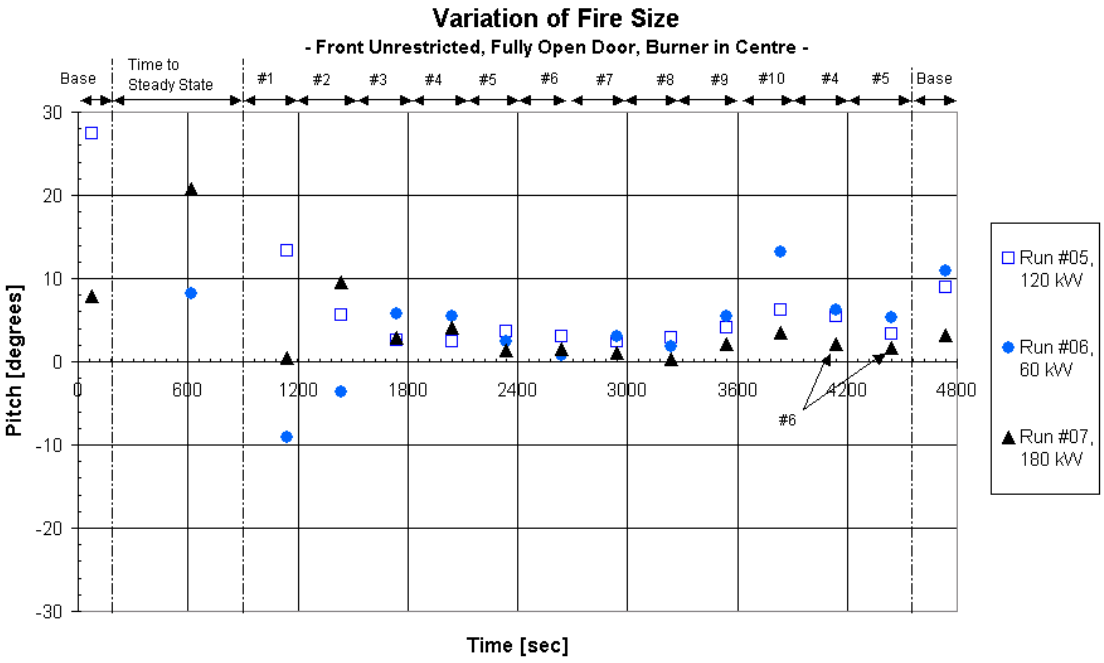

Figure 42: Influence of the fire size on the pitch angle

The pitch angles do not show a very clear dependency on the fire size. They are very close to 2 degrees for positions #5 to #8, so the air plume in the horizontal plane flows generally along the centreline of the compartment, again allowing for +2 degrees bias in the pitch measurements.

Figure 42 shows that for positions #9 and #10 the pitch angles tend to be more positive at position #10, indicating a slight change of direction towards the left hand side of the compartment. This effect seems to be extreme for the smaller 60 kW fire and is most likely due to the fact that the probe is exiting the spill plume and exposed to turbulences from mixing between the plume and the ambient air and reduced velocities.

Velocity

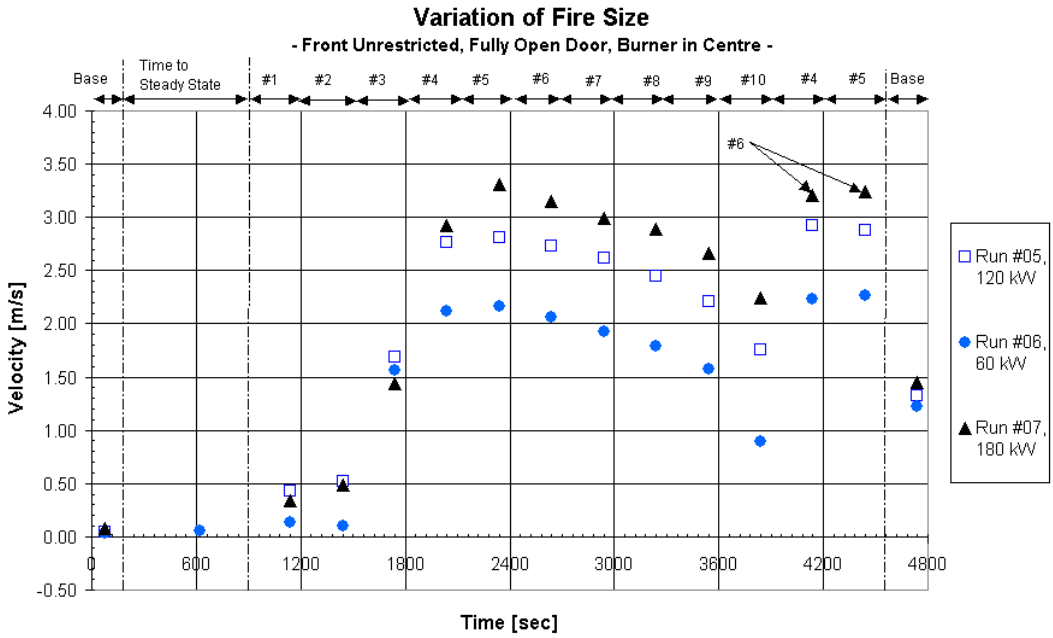

Figure 43: Influence of the fire size on the velocity

It comes to no surprise that the velocity across the plume is directly proportionally related to the fire size, the bigger the fire the faster the flow.

As seen in Figure 43 the velocity for positions #1 through #3 are almost identical for all three fire sizes. The 60 kW and 120 kW fires reach their maximum of V_{max} = 2.16 m/s and 2.82 m/s around positions #4 and #5 (see Appendix G – Yaw, Pitch and Velocity Plots for more continuous plots of the velocity), while the 180 kW fire shows a more distinct peak of V_{max} = 3.31 m/s at position #5. In all three fire sizes the velocity decreases gradually from position #5, 350 mm below the ceiling, down to position #10, 600 mm BC. In run #06 the velocity reaches a minimum of 0.90 m/s at position #10, which is getting near the limits of reliability of the probe.

The velocities measured at positions #4 and #5 in runs #05 and #06 and position #6 in run #07 after moving the probe back up are slightly higher than before, however the error of a maximum of 5.4 % is acceptable.

5.7 Variation of Burner Location

In runs #05, #09 and #12 the fire size was 120 kW, there was no door in the doorway and the front opening of the adjacent compartment was unrestricted. The only variable was the location of the burner, being in the centre in run #05, in the corner in run #09 and in the centre of the rear wall of the fire compartment in run #12, as shown in Figure 44.

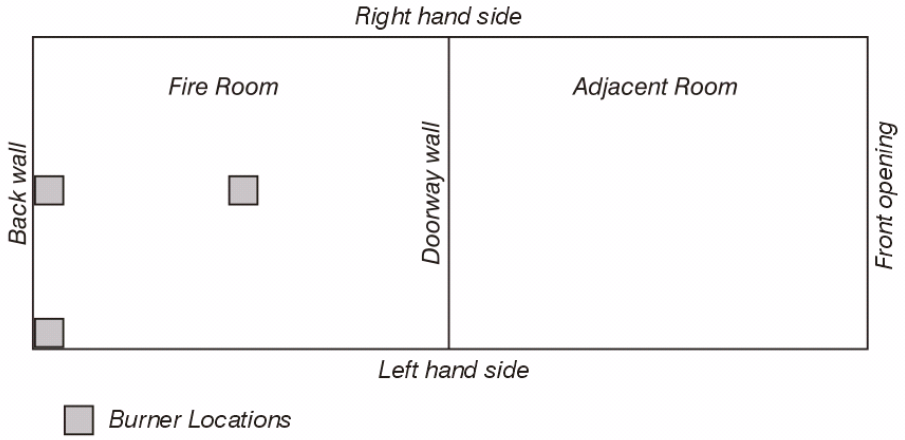

Figure 44: Burner Locations in runs #05, #09 and #12 (L. Rutherford, 2002)

Temperature

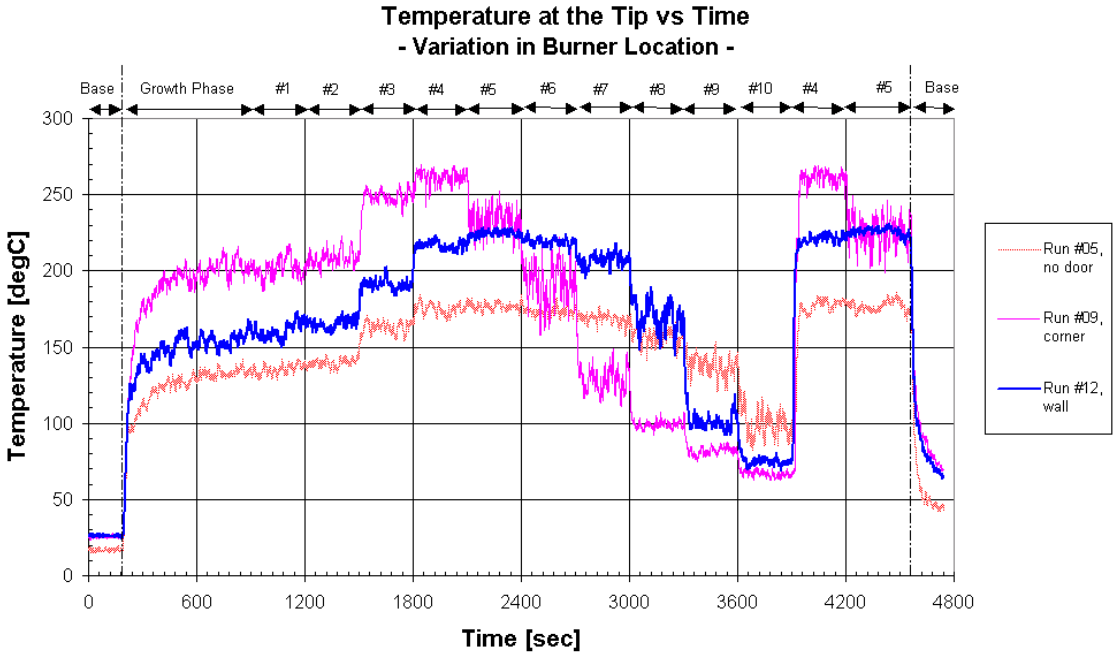

Figure 45: Temperature at the tip for runs #05, #09 and #12

The temperature at the tip of the probe shows a more defined step character the further the fire is away from the door. For run #09 (burner in the corner) the temperature reaches a clear maximum of T_{max} = 270°C. The readings for positions #5 - #7 are much noisier than in runs #05 and #12, an indicator that the flow might be more turbulent 450 mm to 550 mm below the ceiling.

Yaw Angle

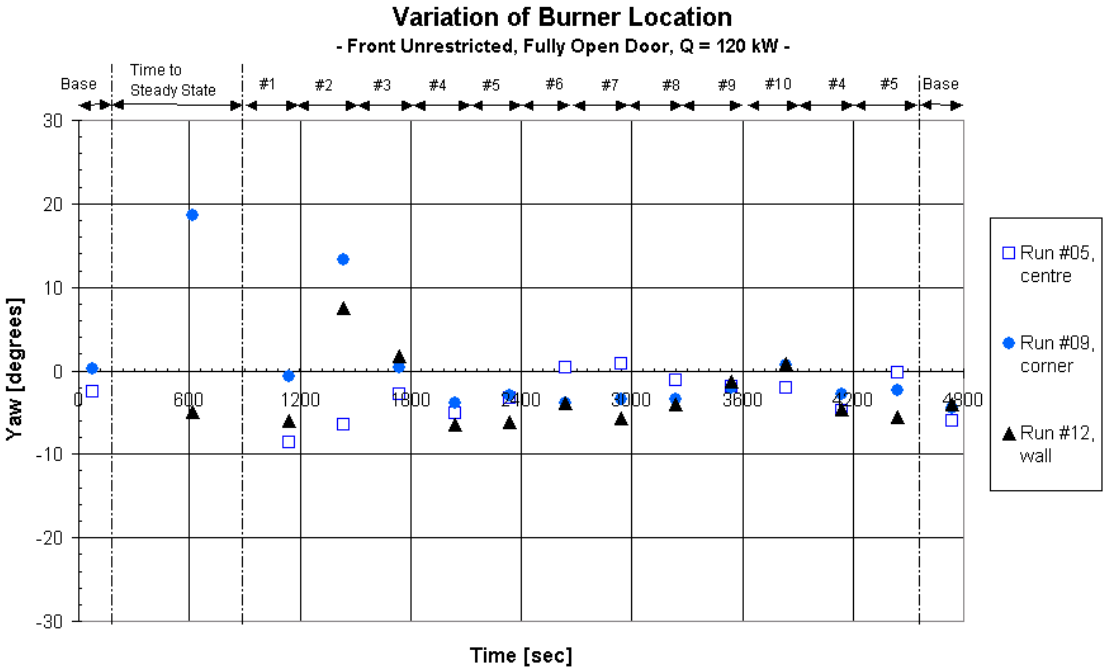

Figure 46: Influence of the burner location on the yaw angle

Positions #1 and #2 show the effects of the more turbulent outer edge of the spill plume as before. In general the yaw angles are in the range of 0.8 degrees to –6.5 degrees. They are smallest when the burner is at the back wall, and very steady for the burner in the corner.

At positions #4 and #5, 300 mm to 350 mm below the ceiling, the plume displays its steepest region (smallest yaw angle), coinciding with the area of maximum temperature (Figure 45).

Overall the spill plume in the vertical plane seems to flow in a 40 degree to 45 degree direction measured from the vertical.

Pitch Angle

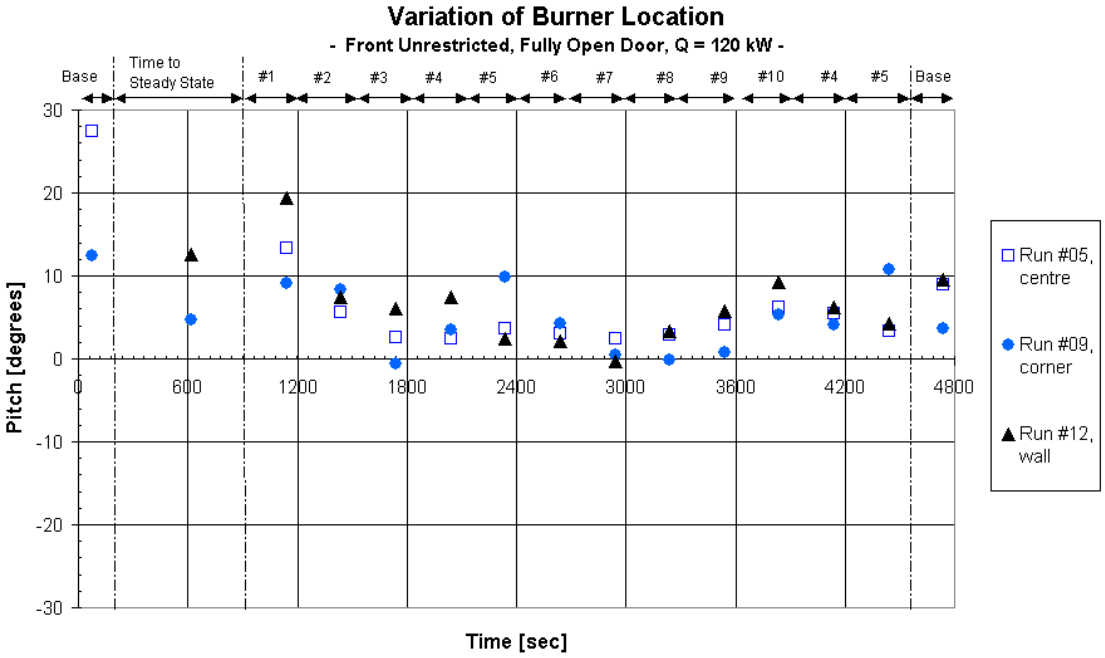

Figure 47: Influence of the burner location on the pitch angle

The flow in the horizontal plane seems to be turbulent up to position #2. The direction of flow for the burner in the centre is oriented along the centreline of the adjacent compartment, as previously described.

When the burner is located in the corner (run #09), the flow appears to follow a sinusoidal pattern between position #4 and #10 (300 mm to 600 mm BC). The yaw angle shows a clear peak at position #5 (350 mm BC), which is reproduced as the probe is moved back up at t =3900 seconds. A minimum occurs at position #8 (500 mm BC), indicating a wavelength of 600 mm; the amplitude is approximately 10 degrees.

A similar pattern can be found for the burner at the rear wall, however the peak is at position #10 and the trough at position #7. Wavelength and amplitude appear identical.

Velocity

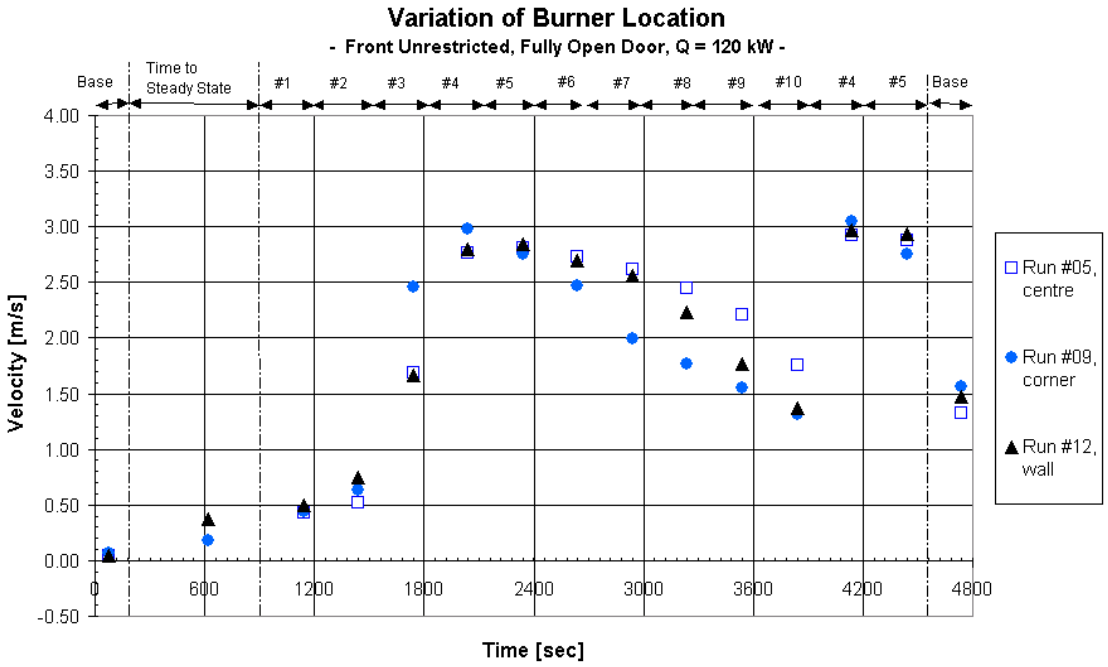

Figure 48: Influence of the burner location on the velocity

The velocity profiles for the burner in the centre in run #05 and at the rear wall in run #12 are very similar up to position #7 (450 mm BC), reaching a maximum of 2.82 m/s and 2.85 m/s respectively. The decrease from position #8 to #10 is steeper with the burner at the rear wall.

When the burner is in the corner (run #09) the velocity gradients are much steeper, reaching the maximum velocity at position #4 with 2.98 m/s and then dropping off faster than in both other cases.

At 3900 seconds, when the probe was moved back up to positions #4 and #5, the velocities are again slightly larger than before, with a maximum increase of 6.1 % in run #12 for position #4.

5.8 Variation of Front Opening

In runs #05, #15 and #18 the burner was located in the centre of the fire compartment, there was no door in the doorway and the fire size was 120 kW. The only variable was the front opening of the adjacent compartment, ranging from unrestricted during run #05, to a soffit in #15 and a door opening in #18, shown in Figure 49.

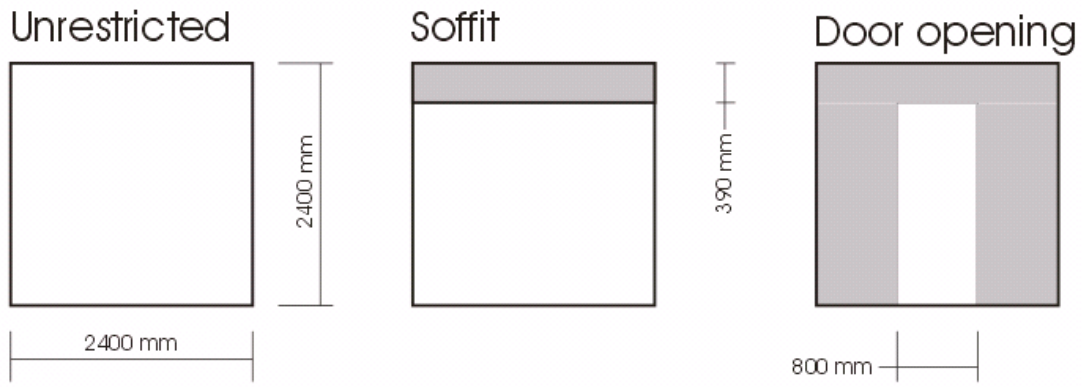

Figure 49: Variations of the front opening (adapted from L. Rutherford, 2002)

The soffit reached 390 mm down from the ceiling across the entire width of the opening. It was made of fire rated gypsum board and ceramic insulation board, identical to the rest of the compartment.

The door opening was a replica of the opening between the fire compartment and the adjacent compartment.

The sequential closing of the front opening increases the hot gas layer depth in the adjacent compartment. The probe is not just aligned with the spill plume but is becoming more and more submerged in a layer of hot gas as well. This complicates the flow pattern around the probe tip as some backflow occurs in addition to the spill plume.

Temperature

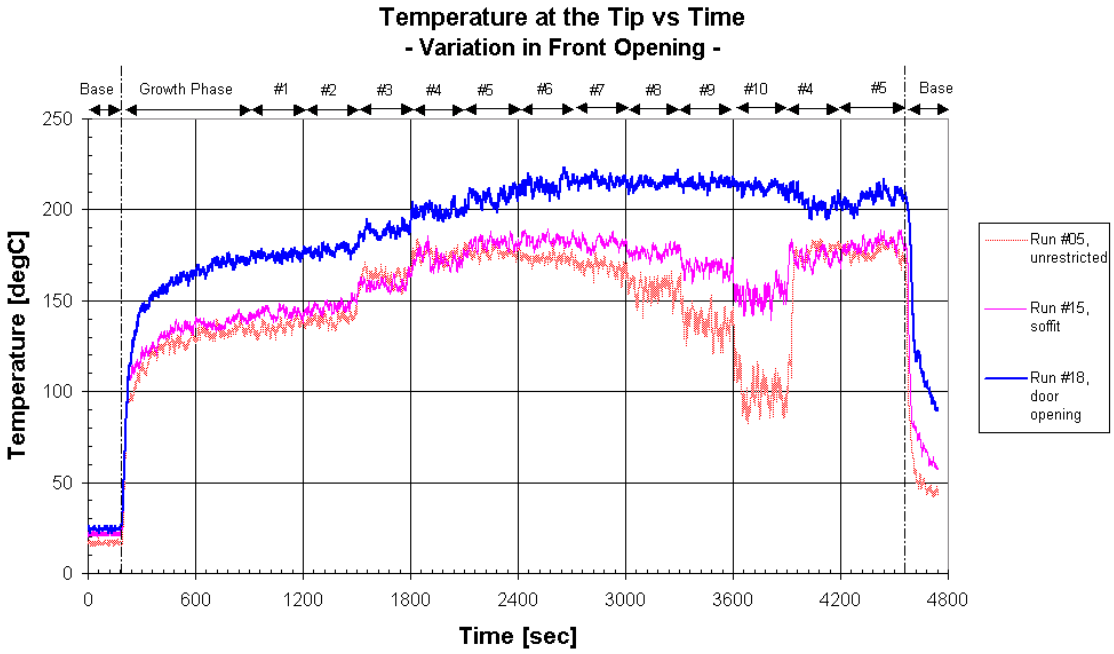

Figure 50: Temperature at the tip for runs #05, #15 and #18

The temperatures at the tip of the probe are increasing the more the front opening is closed off, as the upper layer gets deeper. They reach a maximum of 220°C with the door opening at the front, 185°C with the soffit and 180°C with the unrestricted opening.

The step character between positions #6 and #10 is less distinct in run #15 and disappears in run #18 as the spill plume becomes permanently submerged in the upper hot layer and the probe when moving through the plume is no longer reaching the cooler lower layer.

Yaw Angle

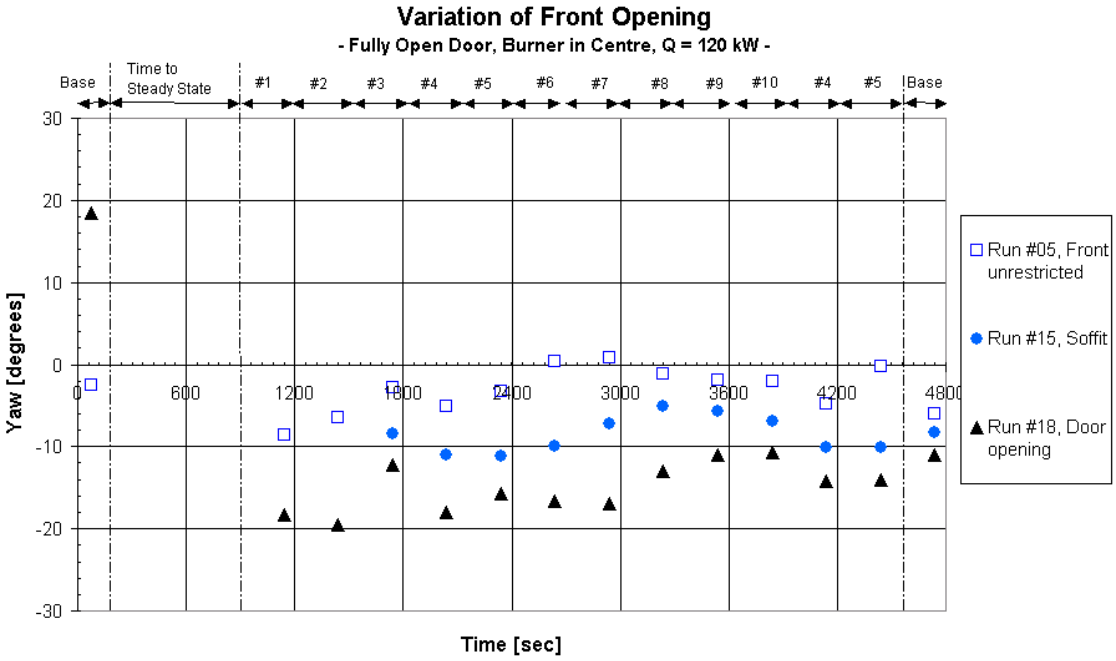

Figure 51: Influence of the front opening on the yaw angle

The general trend for the flow direction in the vertical plane is that the deeper the hot layer becomes the more negative the yaw readings are and hence the steeper the spill plume gets. The results suggest that the plume is angled from the vertical between 25 degrees (-20 degrees yaw) with the door opening and 35 degrees (-10 degrees) with the soffit. The steepest region is 300 mm to 450 mm below the ceiling.

With the soffit in place the plume is with –5 degrees yaw flattest at position #8 (500 mm BC), while with the door opening the flattest position is #10 with –11 degrees yaw.

The reproducibility of the yaw readings deteriorates as the front opening gets smaller. In run #15 the repeated readings at positions #4 and #5 are with only 1 degrees increase very good, while in run #18 the error is with a 4 degrees decrease relatively large.

It is difficult to know how much this steepening phenomenon is influenced by the backpressure of the hot layer acting on the tip of the five-hole probe. The unreduced data plots in Appendix G – Yaw, Pitch and Velocity Plots suggest that the turbulences are increasing significantly in positions #7 to #9 for the soffit and are fluctuating by 25 degrees with the door opening.

Pitch Angle

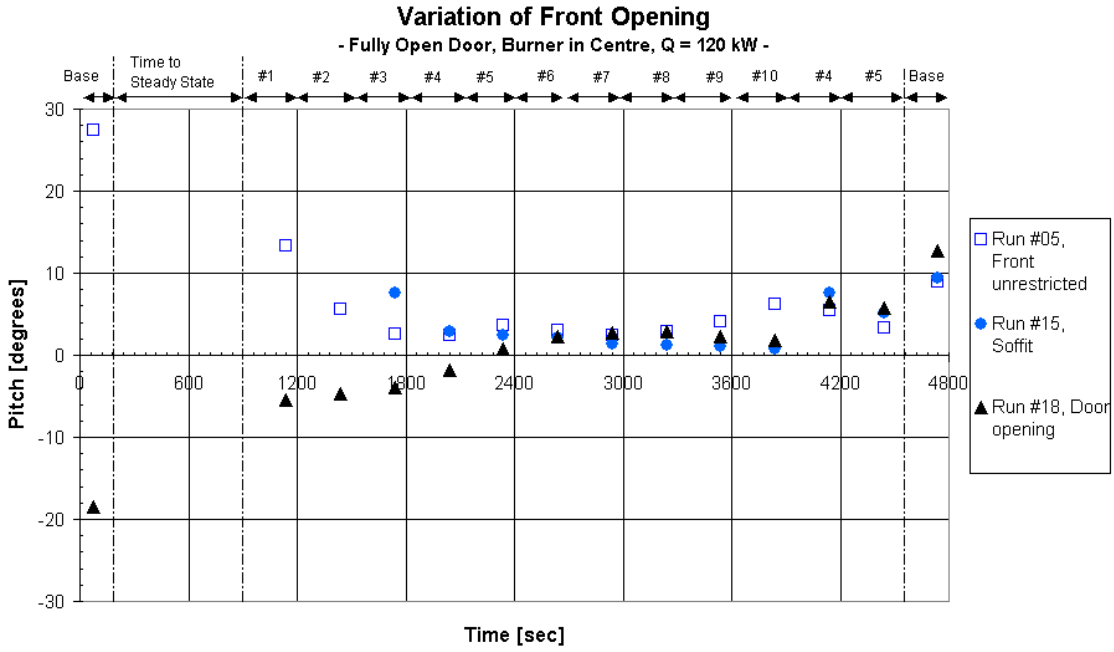

Figure 52: Influence of the front opening on the pitch angle

The orientation of the flow in the horizontal plane is less affected by the variation of the front opening; for positions #4 to #10 the plume seems well aligned with the centreline of the compartment as the pitch readings are close to 2 degrees (allowing for the +2 degrees bias).

However the readings at position #4 and #5 for all do not reproduce well, they change by up to 8.3 degrees in run #18.

Again the influence of the hot layer on the pressure at the probe tip seems to be significant and the fluctuations increase to 25 degrees for the entire duration of run #18 (front as door opening).

Velocity

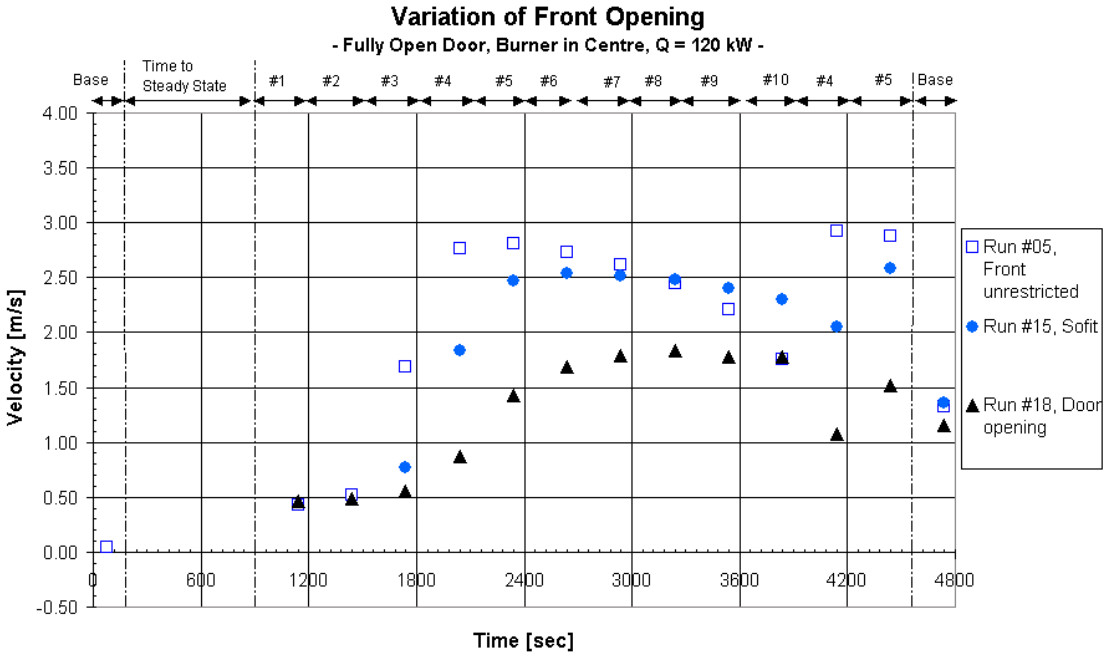

Figure 53: Influence of the front opening on the velocity

The velocity profile seems to flatten out the more the front opening is enclosed and the deeper the upper hot layer becomes. The location of the maximum velocity moves further across the plume.

The highest velocity of 2.82 m/s occurs at position #5 (350 mm BC) when the front opening is unrestricted and the hot gas can flow out of the adjacent compartment freely.

The soffit reduces the maximum velocity to 2.54 m/s and pushes the location down to position #6 (400 mm BC).

Enclosing the front further leads to a reduction of the maximum velocity to 1.83 m/s, located even lower at position #8 (500 mm BC).

The results of position #4 are not reproduced well with up to 24 % increase, however the velocity position #5 with a maximum of 6 % error was repeated well.

5.9 Variation of Door Opening

In runs #02, #03 and #05 the fire size was 120 kW, the burner was located in the centre of the fire compartment and the front opening of the adjacent compartment was unrestricted. The only variable was door opening, being 60 degrees open in run #02, 40 degrees in run #03 and fully open in run #05, shown in Figure 54.

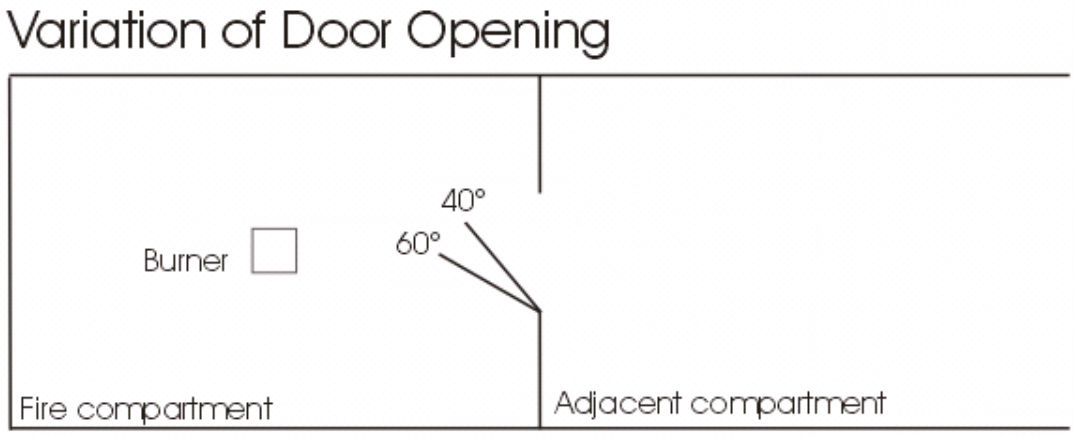

Figure 54: Variation of door opening

In run #02 the probe was moved after 15 minutes to position #2, while in runs #03 and #05 it was moved after 20 minutes. In the temperature plot the start of the series of run #02 was delayed by 300 seconds to be able to compare the temperatures at positions #1 to #10 with runs #03 and #05. In Figure 55 this occurs as if the experiment #02 was started five minutes later.

Yaw and pitch angle and velocity were plotted against the position and not against time. The growth phase and the repetition of positions #4 and #5 could not be included, however the data is available in Appendix G – Yaw, Pitch and Velocity Plots.

Temperature

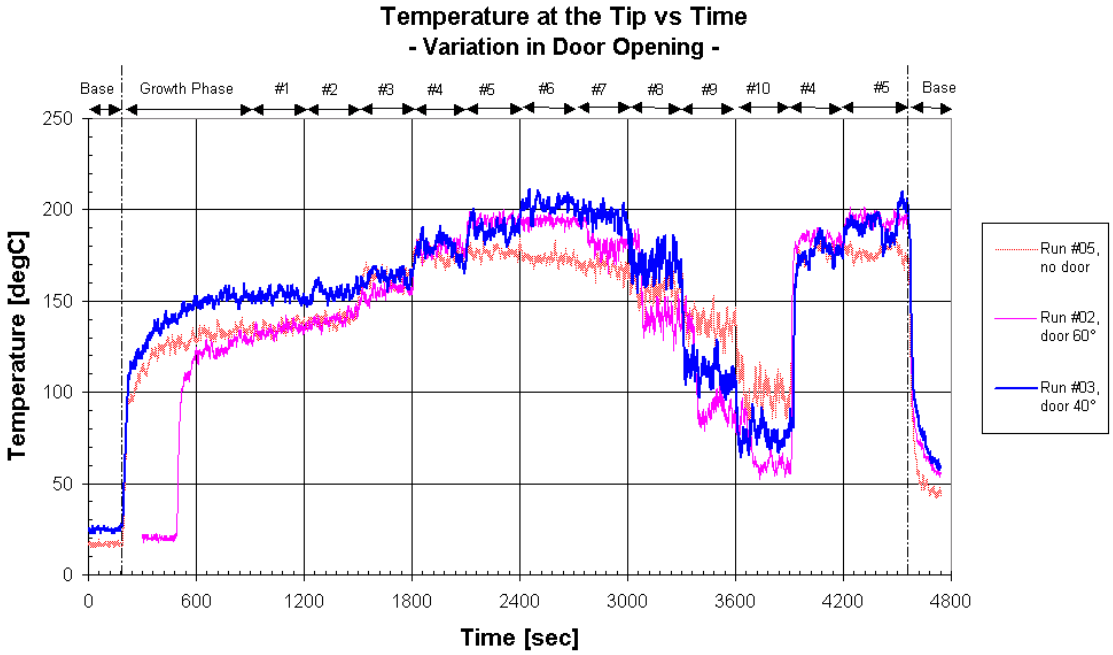

Figure 55: Temperature at tip for runs #02, #03 and #05

The temperatures at the tip of the probe are generally higher the more the door is closed, because the smaller effective opening to the adjacent compartment results in a deeper and hotter layer in the fire compartment and hence hotter gases exiting the compartment.

The profile across the plume is steeper for the 40 degree door opening, reaching a maximum of 210°C in position #6 (400 mm BC), and a minimum of 75°C at position #10 (600 mm BC).

When the door is 60 degrees open, the maximum temperature is slightly lower at 195°C at position #5. The minimum temperature is 65°C 600 mm below the ceiling.

Yaw Angle

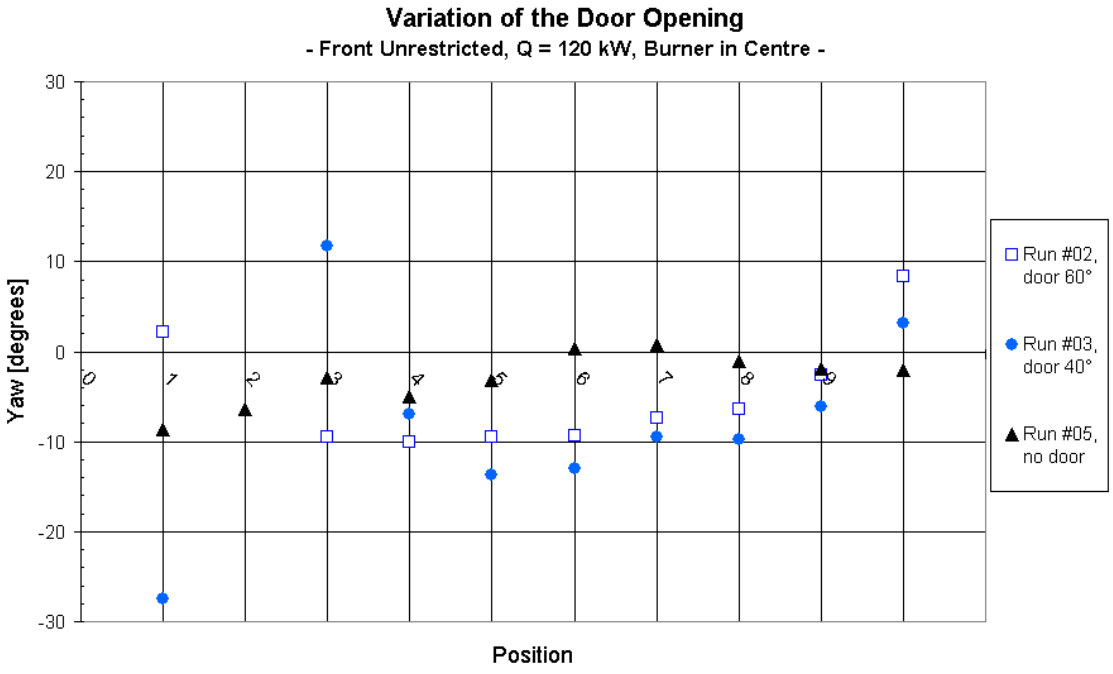

Figure 56: Influence of the door opening on the yaw angle

The plume seems to be steeper from positions #5 to #10 the more the door is shut. This agrees with the earlier finding that the hotter the gases get, the steeper the flow is in the vertical plane.

Between position #9 (550 mm BC) and #10 (600 mm BC), the flow flattens by 10.9 degrees sharply for the 40 degrees and 60 degrees cases from a fairly steep flow to a shallower flow. It remains close to the 45 degrees line for run #05.

This could indicate that the flow in the 550 mm to 600 mm region is hitting the probe at its limitations in the horizontal plane, causing error during the interpolation on the yaw and pitch coefficient maps, or that the probe has moved through the spill plume.

Pitch Angle

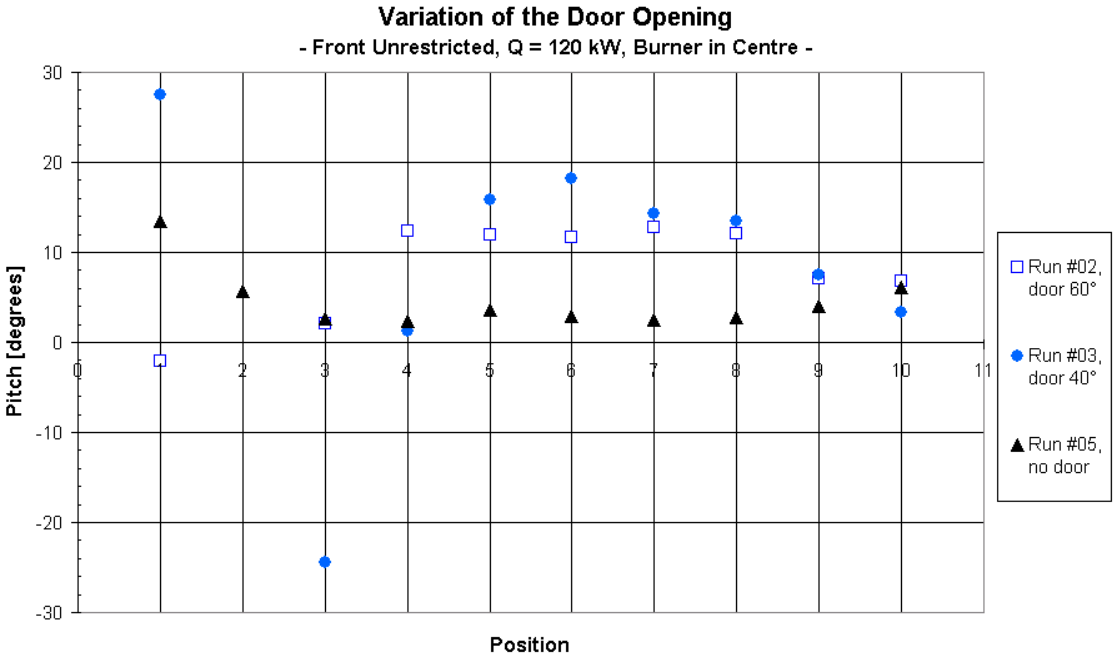

Figure 57: Influence of the door opening on the pitch angle

The flow direction in the horizontal plane is expected to be pushed towards positive pitch angles when the door is partly shut, as the hot air has to flow around the door and out through a much smaller door opening when compared with the fully open door.

The pitch angle in positions #2 and #3 in run #03 (door at 40 degrees) are close to or outside the calibration range, which could result from eddies or simply the fact that the flow is hitting the tip of the probe on an angle outside the calibration range. This explanation is confirmed when looking at the wide fluctuations in the unreduced data, attached Appendix G – Yaw, Pitch and Velocity Plots.

If the air would flow exactly along the door 60 degrees open, it would hit the tip of the probe at +30 degrees pitch; however it will more likely straighten itself slightly towards the centreline of the compartment.

The pitch is very steady at 12 degrees for run #02, positions #4 to #8 (300 mm – 500 mm BC), then straightening back to 7 degrees. This agrees with the idea that the hot air would follow the angle of the door, hit the sidewall of the adjacent compartment and curve back across the centreline of the compartment until it exits through the front opening.

The range from 150 mm to 600 mm below the ceiling in this series of experiments is not large enough to be able to confirm the later stages of this pattern.

Velocity

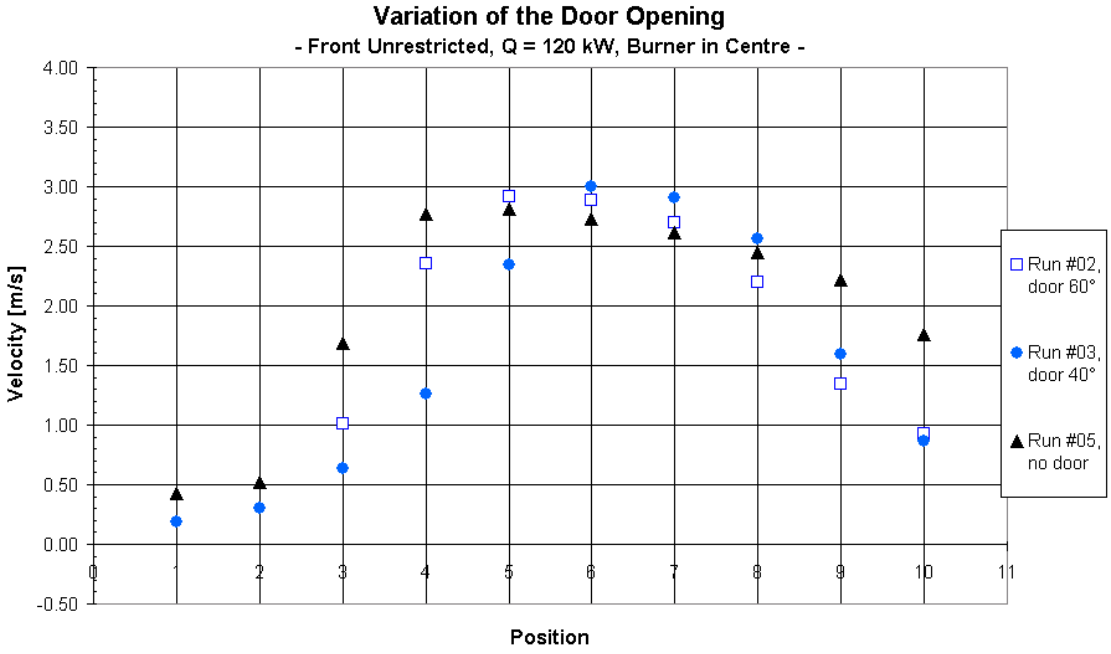

Figure 58: Influence of the door opening on the velocity

The velocity gradients become steeper and the position of maximum velocity along the centreline of the compartment is pushed further down and back the more the door angle is reduced.

This agrees with a spill plume that is directed to the left hand side by the door. The probe is no longer measuring perpendicular across the plume but slicing at an angle through it, reaching the area of maximum temperature and maximum velocity later.

The highest velocity of 3.00 m/s occurs at position #6 (400 mm BC) for the door at 40 degrees, followed by slightly lower peak of 2.91 m/s for the door 60 degrees in position #5 (350 mm BC). The highest velocity for the undisturbed flow through the door opening is 2.82 m/s at position #5.

The large reduction in velocity over positions #9 and #10 in runs #02 and #03 confirms the assumption that the probe is passing through the plume there.

6 Conclusions, Recommendations and Future Research

The adaptation and application of the five-hole probe in a series of full scale fire tests proved to be successful. The behaviour of a spill plume under a door soffit and the effects of fire size, burner location, front and door opening could be described qualitatively and quantitatively.

6.1 Flow Characteristics of the Spill Plume under a Door Soffit

Fire size

- The temperature at the tip and the steepness of the plume are directly proportional to the fire size.
- The plume generally flows along the centre line of the adjacent compartment in the horizontal plane.
- The velocity is directly proportional to the fire size and reaches a maximum of 3.31 m/s 400 mm to 450 mm below the ceiling for the 180 kW fire.

Location of the burner

- The temperature profile across the plume is more stepped the further the fire is away from the door opening.
- The flow in the vertical plane varies between 40 degrees and 45 degrees; a clear dependency on the location of the burner is not noticeable.
- The flow in the horizontal plane shows a sinusoidal pattern when the burner is in the corner or at the back wall with amplitude of 10 degrees and a wavelength of 600 mm for the burner location in the corner and at the back wall.
- The velocity reaches a distinct maximum of 2.98 m/s at position #4 (300 mm BC) when the burner is in the corner. Located at the rear wall or in the center, the maximum of approximately 2.83 m/s occurs at position #5 (350 mm BC).

Variation of the Front Opening

- The temperature profile across the plume loses its step character and temperatures increase as the front opening becomes smaller and the upper hot layer deepens.
- The yaw angle measurements become more negative as the hot layer depth increases, suggesting a steeper spill plume.
- The pitch angle measurements do not change significantly, however they lose some of the reproducibility of measurements at positions #4 and #5 (300 mm and 350 mm BC).
- The velocity profile across the plume loses its step character and becomes more uniform as the upper hot layer descends. The maxima of the velocity decrease and move further across the plume as the upper layer deepens.
- The submersion of the probe in the hot upper layer in run #18 causes large fluctuations of around 25 degrees for the entire duration of the experiment in the yaw and pitch readings.

Variation of the Door Opening

- The temperatures at the tip of the probe are generally higher and the spill plume is steeper the more the door is closed.
- The flow in the horizontal plane is directed by the angle of the door; the more the door is closed the more the plume is pushed outwards from the centreline of the compartment.
- The velocity gradients become steeper and the positions of maximum velocity along the centreline of the compartment are pushed further down and back because the probe is no longer moving perpendicularly through the plume as the door is closed.

6.2 Characteristics of the Five-Hole Probe

The application of a five-hole probe is rather costly, as it requires the use of a wind tunnel for the calibration and five pressure transducers during the experiment. There is obviously a trade-off between being able to measure the magnitude and direction of flow at one point with a five-hole probe or being able to measure the speed of the flow at five points with five bi-directional probes.

The data collected by the five-hole probe becomes increasingly difficult to interpret when it is fully submerged in the hot upper layer because the flow of spill plume is affected by the backflow of smoke in the upper layer, creating a more complex pressure field at the tip.

The angle of the flow towards the probe becomes too steep when the door in the doorway is 40 degrees open. Better results would require re-alignment with the flow.

6.3 Recommendations

The perpendicular pyramid probe (as defined by Dominy and Hodson, 1993) shown in Figure 59 is less sensitive to changes in Reynolds numbers (Cambridge University website: Pressure Probes, 2002), however due to the limited time available this probe could not be realised.

The perpendicular pyramid has sharper edges, which constrain separation of the flow to pre-defined regions. This reduces the sensitivity to changes in velocity and hence to changes in Reynolds numbers.

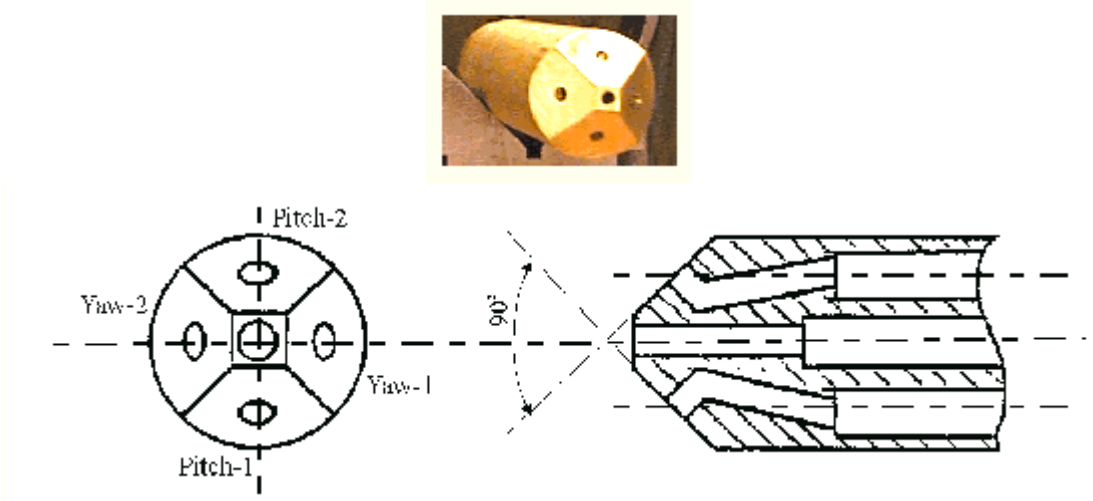

Figure 59: Perpendicular pyramid probe (Cambridge University website, Pressure probes, 2002)

It would be recommended to use this type of five-hole probe where a range of +/- 25 degrees is not sufficient or where the alignment of the probe with the direction of the gas flow is more difficult to achieve.

6.4 Future Research

Some questions that were left unanswered are:

- Analysis of the remaining 12 runs from the McLeans Island experiments and comparison with results from Fire Dynamic Simulator (FDS).
- Re-calibration and re-testing of the five-hole probe in the wind tunnel to assess the effect of heat and soot on its performance.
- Verification of the results of the probe submerged in the hot upper layer with flow visualisation or salt water modelling.

This is the first time a five-hole probe has been used successfully to measure the direction and speed of hot air flow in a fire compartment, hopefully encouraging others to adopt this technique and opening the door for many other applications i.e. the adaptation of the probe for measurements around smaller objects like smoke or heat detectors.

7 References and Bibliography

BAKER, R. C., An introductory guide to flow measurement, London: Mechanical Engineering, 1988

BRADSHAW, P., Experimental Fluid Mechanics, 2nd edition, Oxford: New York: Pergamon Press, 1970

BRYER, D. W., PANKHURST R. C., Pressure-probe methods for determining wind speed and flow direction, London : H.M.S.O, 1971

CHEREMISINOFF, N. P. AND P. N., Flow measurement for engineers and scientists, New York: M. Dekker, c1988

CLARK, L. R., 'The Effect of Door Angle on Fire Induced Flow Through A Doorway', Fire Engineering Project, School of Engineering, University of Canterbury, 2002

COX, G., Gas Velocity measurement in Fires by the Cross-Correlation of Random Thermal Fluctuations – A Comparison with Conventional Techniques, Combustion and Flame 28, pg. 155 – 163, 1977

DECARLO, J. P., Fundamentals of flow measurement, Research Triangle Park, N.C.: Instrument Society of America, c1984

DOMINY, R. G., & HODSON, H. P., An Investigation of Factors Influencing the Calibration of Five-Hole Probes for Three-Dimensional Flow Measurements, Journal of Turbomachinery, July 1993, Vol. 115, pp 513 –519

EMMONS, H.W., Vent Flows, SFPE Handbook of Fire Protection Engineering, Section 2 / Chapter 5, Quincy, MA, 1995

KARLSSON, B., QUINTIERE, J. G., Enclosure fire dynamics, Boca Raton, FL: CRC Press, 2000

MILLER, R. W., Flow measurement engineering handbook, 3rd edition, New York: McGraw-Hill, c1996.

OWER, E., PANKHURST, R. C., The measurement of air flow, Oxford, Pergamon Press, 1977.

RUTHERFORD, L., Experimental Results for Pre-Flashover Fire Experiments in Two Adjacent ISO Compartments, Fire Engineering Project, School of Engineering, University of Canterbury, 2002

Online References:

Cambridge University:
Hot Wire Anemometers, University of Cambridge, Department of Engineering, Whittle Laboratory, 14/01/02
http://www-g.eng.cam.ac.uk/whittle/current-research/hph/hot-wire/hot-wire.html,

Pressure Probes, University of Cambridge, Department of Engineering, Whittle Laboratory, 14/01/02
http://www-g.eng.cam.ac.uk/whittle/current-research/hph/pressure-probes/pressure-probes.html

Bibliography

COCKRELL, D. J. (Ed.), Conference on Fluid dynamic measurements in the industrial and medical environments, Proceedings, Leicester: Leicester University Press, 1972.

DOWDELL, R. B. (Ed.), Flow: its measurement and control in science and industry, Pittsburgh : Instrument Society of America, 1974

INCROPERA, F. P. & DEWITT, D. P., Fundamentals of Heat and Mass Transfer, New York: Wiley, 2001

TURNER, J. S., Buoyancy effects in fluids, Cambridge: C.U.P., 1973.

Online Bibliography

Cambridge University:
Least Squares Method of Data Reduction: n-Sensor Pressure Probes, University of Cambridge, Department of Engineering, Whittle Laboratory, 14/01/02
http://www-g.eng.cam.ac.uk/whittle/current-research/hph/leastsquares/leastsquares-2.html

GIRGIS, N., Full Scale Fire Experiments on Upholstered Furniture, Fire Engineering Project, School of Engineering, University of Canterbury, 2000
http://www.civil.canterbury.ac.nz/fire/pdfreports/NGirgis1.pdf

NIELSEN, CH., An Analysis of Pre-Flashover Experiments with Field Modelling Comparisons, Fire Engineering Project, School of Engineering, University of Canterbury, 2001
http://www.civil.canterbury.ac.nz/fire/pdfreports/CNielsen.pdf

United Sensor Corporation, 14/01/02, *http://www.unitedsensorcorp.com/*

8 Appendix A - Input File for p5hproc_Judith.exe

3 5min.txt

Number of measurements 15

Atmospheric pressure 101530.00

0.0002	0.0001	0.0005	0.0003	0.0004	297.87
-0.6419	-0.6196	-0.6168	-0.5279	-0.6096	411.2
-0.9678	-0.9289	-0.945	-0.8373	-0.9379	426.37
-1.0935	-1.0457	-1.1039	-0.9678	-1.0996	427.23
-0.8762	-0.9202	-0.9946	-0.7839	-1.0476	436.26
-0.3205	-0.8271	-0.5517	-0.7408	-0.6434	452.37
0.8867	-0.6549	0.5984	-0.5714	0.4673	462.05
2.1927	-0.1431	1.7005	-0.2559	1.7133	476.4
2.4056	0.1063	1.7075	0.0001	1.7399	473.06
1.9729	0.1987	1.2994	0.2105	1.2557	446.15
0.5955	-0.0519	0.2226	-0.0798	0.0905	384.25
-0.0347	-0.1112	-0.1731	-0.2451	-0.266	349.46
-0.046	-0.5256	-0.2795	-0.5773	-0.3052	443.08
0.9453	-0.6904	0.6219	-0.7203	0.5291	463.18
0.4477	-0.3337	0.1507	-0.7068	0.361	356.13

Units:

Atmospheric Pressure	Pa	
Pressure Readings	Pa	(columns 1 – 5)
Temperature	K	(column 6)

9 Appendix B – Calibration File Excerpt

Taken from *Jcal5.txt*

number yaw measurements = 13
number pitch measurements = 13
atmospheric pressure. Pa = 100342.0
temperature. K = 289.8
velocity. m/s = 2.24

yaw	pitch	press1	press2	press3	press4	press5	press6	press7
-30.0	30.0	1.3738	-1.2259	2.7350	-0.6791	2.0455	0.0875	3.0221
-25.0	30.0	1.7593	-0.6586	2.5659	-0.4929	2.4064	0.1167	2.9614
-20.0	30.0	2.0162	-0.2432	2.3869	-0.5257	2.6671	0.0584	2.9917
-15.0	30.0	2.2535	0.1824	2.1482	-0.5586	2.8476	0.0875	2.9917
-10.0	30.0	2.4017	0.6282	1.8797	-0.6791	2.9679	0.0875	2.9917
-5.0	30.0	2.4610	0.9929	1.5316	-0.7448	2.9980	0.0875	2.9614
0.0	30.0	2.4610	1.2867	1.2929	-0.7448	2.9679	0.1167	2.9614
5.0	30.0	2.4610	1.6211	0.9448	-0.6572	2.9980	0.1459	2.9917
10.0	30.0	2.4314	1.9149	0.6166	-0.4929	2.9379	0.2335	2.9917
15.0	30.0	2.2238	2.1885	0.1790	-0.4929	2.8476	0.2918	2.9614
20.0	30.0	2.0459	2.4519	-0.2984	-0.4929	2.7273	0.3210	3.0221
25.0	30.0	1.7000	2.5735	-0.7360	-0.5915	2.3764	0.2626	2.9311
30.0	30.0	1.2849	2.7254	-1.3526	-0.8434	2.0154	0.2335	2.9311
-30.0	25.0	1.6407	-1.2563	2.8245	-0.3614	1.8951	0.0875	2.9917
-25.0	25.0	2.0756	-0.5978	2.7350	-0.0986	2.3162	0.0875	3.0221
-20.0	25.0	2.3128	-0.0304	2.5062	0.0657	2.4866	0.1167	2.9311
-15.0	25.0	2.4907	0.3546	2.2675	-0.0657	2.6671	0.0875	2.9917
-10.0	25.0	2.5994	0.8105	2.0289	-0.0986	2.7574	0.1167	2.9311
-5.0	25.0	2.6883	1.1955	1.7404	-0.1643	2.8476	0.1167	2.9917
0.0	25.0	2.7180	1.4691	1.4719	-0.1972	2.8476	0.1459	2.9614
5.0	25.0	2.6587	1.7629	1.1238	-0.0657	2.8175	0.1751	2.9614
10.0	25.0	2.6290	2.1277	0.7061	0.0000	2.8476	0.2043	2.9917
15.0	25.0	2.4907	2.3404	0.3580	0.0986	2.6370	0.2043	2.9311
20.0	25.0	2.3128	2.6343	-0.1790	0.0329	2.5167	0.2043	3.0221
25.0	25.0	1.8976	2.7558	-0.8255	-0.2300	2.2259	0.1751	2.6986
30.0	25.0	1.5221	2.9382	-1.5018	-0.5586	1.8349	0.1751	2.6683
-30.0	20.0	1.8383	-1.2259	2.8543	0.0657	1.6644	0.1167	2.0113
-25.0	20.0	2.2535	-0.5978	2.7648	0.2848	2.0154	0.0875	2.9614
-20.0	20.0	2.5401	-0.0608	2.6455	0.4491	2.2861	0.0875	2.9614
-15.0	20.0	2.6587	0.5066	2.3869	0.5148	2.4365	0.1167	2.9614
-10.0	20.0	2.8366	0.9321	2.1482	0.4491	2.6070	0.1167	2.9917
-5.0	20.0	2.8366	1.2867	1.8299	0.3505	2.5769	0.1459	2.9614
0.0	20.0	2.7773	1.5907	1.5316	0.3176	2.5769	0.1459	2.9311
5.0	20.0	2.8366	1.9149	1.1736	0.4162	2.6070	0.1751	2.9614
10.0	20.0	2.8069	2.2493	0.8255	0.5148	2.6070	0.1751	3.0221
15.0	20.0	2.6587	2.4823	0.4177	0.5476	2.4566	0.1751	2.9614
20.0	20.0	2.4314	2.6951	-0.2387	0.3505	2.3162	0.1751	2.9917
25.0	20.0	2.1349	2.9078	-0.8255	0.1862	2.0154	0.1459	2.9917
30.0	20.0	1.8186	3.0294	-1.4421	-0.0986	1.6945	0.1167	3.0221
-30.0	15.0	2.0162	-1.2867	2.9140	0.4819	1.3937	0.1167	2.9614
-25.0	15.0	2.3424	-0.6586	2.7947	0.6791	1.7747	0.1167	2.9917
-20.0	15.0	2.5994	-0.0304	2.6455	0.8434	2.0455	0.1459	2.9614
-15.0	15.0	2.7773	0.4458	2.4466	0.9310	2.1959	0.1459	2.9917
-10.0	15.0	2.8959	0.9625	2.2079	0.9091	2.3162	0.1459	2.9917
-5.0	15.0	2.9552	1.3475	1.8797	0.8434	2.3764	0.1167	3.0221
0.0	15.0	2.9552	1.6819	1.5913	0.8105	2.3764	0.1459	2.9614

10 Appendix C – Test Combinations

The tables below show the angle combinations that were tested.

Varying locations with three different velocities with emphasis on the 25° combinations.

TEST # 1		Yaw										
		-25	-20	-15	-10	-5	0	5	10	15	20	25
Pitch	25	z			p		z					z
	20								p			
	15			z								p
	10	p										
	5									z		
	0	p		o			x o z					x
	-5							x				
	-10	x							x			o
	-15			o								
	-20						x			o		
	-25	x			o							x
x	V = 1.40 m/s			z	V = 1.32 m/s							
o	V = 2.18 m/s			p	V = 2.18 m/s							

Emphasis on large angle combinations and negative pitch at high velocity

TEST # 2		Yaw										
		-25	-20	-15	-10	-5	0	5	10	15	20	25
Pitch	25	x			x							
	20											x
	15											
	10	x										
	5						x					
	0	x					x					x
	-5											
	-10	x			x		x		x			x
	-15						x					
	-20											
	-25	x					x					x
x	V = 2.21 m/s											

Emphasis on medium and small angle combinations at lower velocity

TEST # 3		Yaw										
		-25	-20	-15	-10	-5	0	5	10	15	20	25
Pitch	25	x			x				X			
	20					X						X
	15		X					X		X		
	10	x										
	5				X		x				X	
	0	x	X				x		X			X
	-5											
	-10	x		X	x		x		x			X
	-15					X	x	X				
	-20		X							X		
	-25	x					x					X
X	V = 1.32 m/s						x	V = 2.21 m/s			from test # 2	

11 Appendix D – Triton Kaowool Ceramic Fibre Board Properties

12 Appendix E – Atmospheric Pressure for Christchurch Airport

Plot of the hourly pressures for the times of the experiments, derived from measurements made by the MetService at the Christchurch Airport. The data was provided by Elaine Fouhy, Climate Database expert at NIWA.

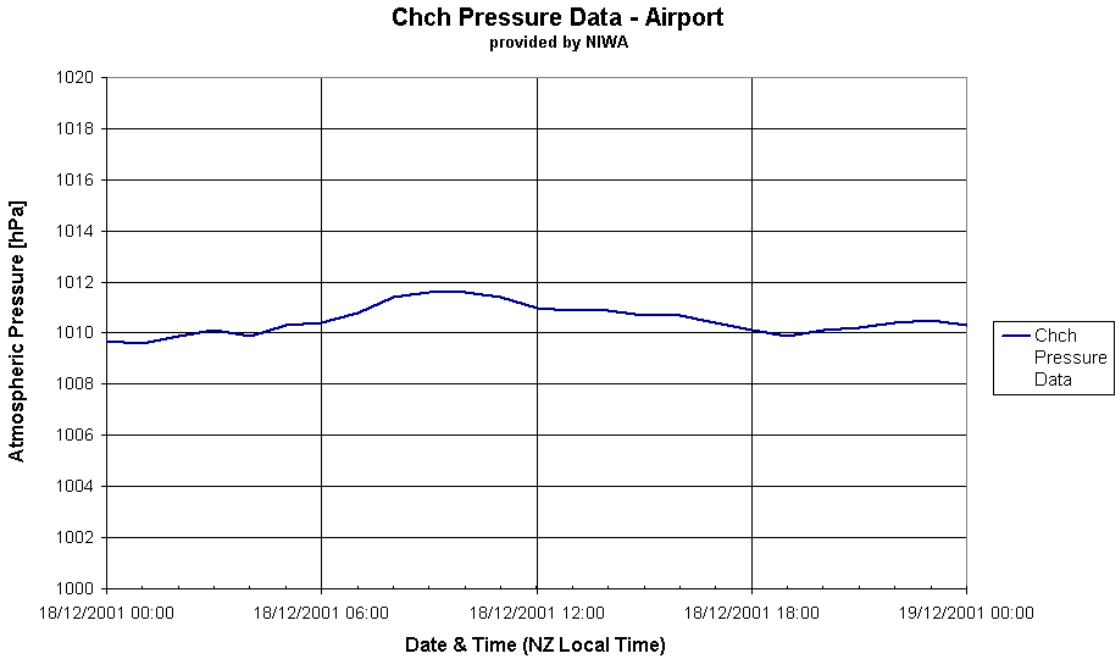

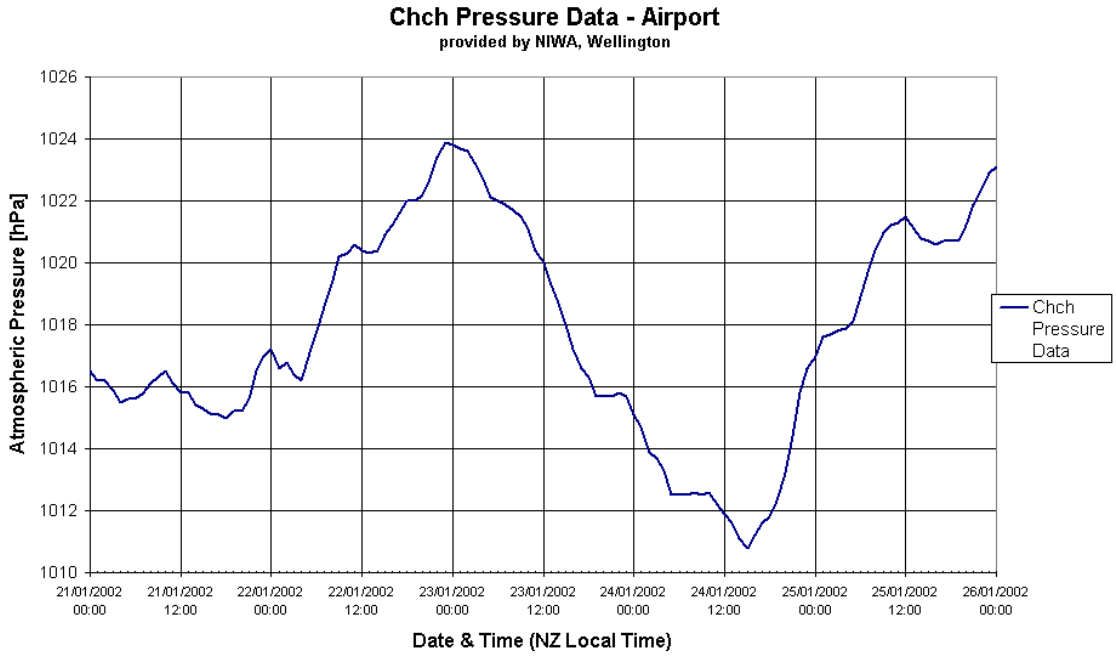

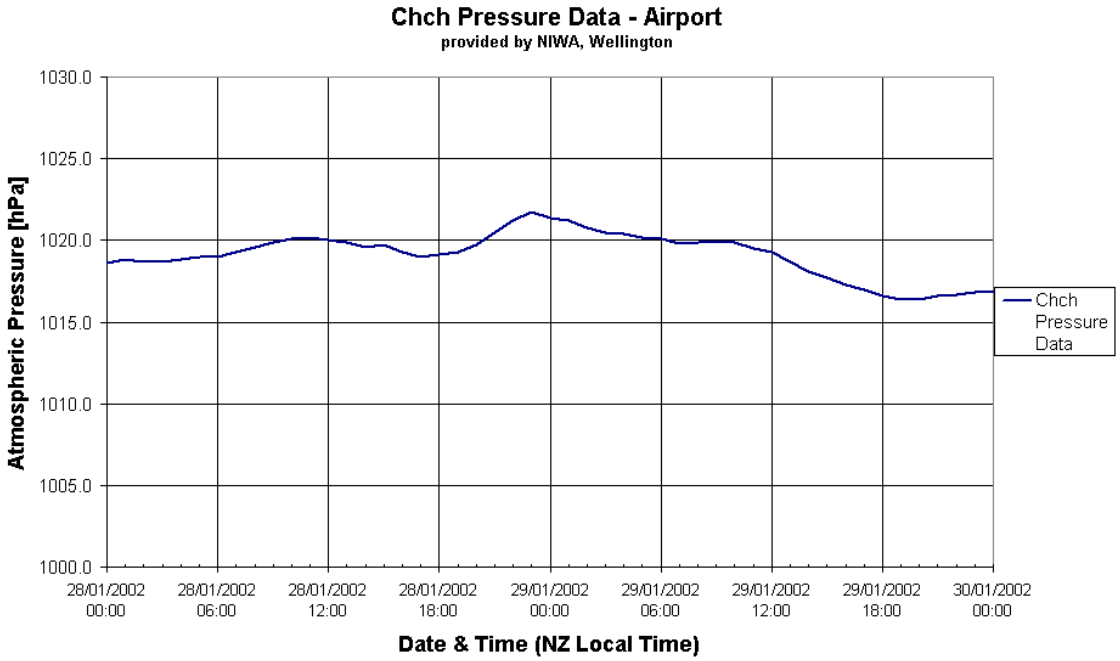
Chch Pressure Data - Airport
provided by NIWA, Wellington
Atmospheric Pressure [hPa]
1030.0
1025.0
1020.0
1015.0
1010.0
1005.0
1000.0
28/01/2002 00:00
28/01/2002 06:00
28/01/2002 12:00
28/01/2002 18:00
29/01/2002 00:00
29/01/2002 06:00
29/01/2002 12:00
29/01/2002 18:00
30/01/2002 00:00
Date & Time (NZ Local Time)
Chch Pressure Data

13 Appendix F – Speed Measurements of Bi-directional Probe

Run #	V_{min} [m/s]	V_{ave} [m/s]	V_{max} [m/s]	Run #	V_{min} [m/s]	V_{ave} [m/s]	V_{max} [m/s]
1	2.74	3.40	4.04	12	2.10	2.41	2.79
2	2.06	2.57	3.01	13	2.48	2.83	3.17
3	2.18	2.74	3.25	14	1.28	1.72	2.36
4	2.09	2.95	3.60	15	1.72	2.32	2.86
5	1.85	2.46	3.02	16	2.13	2.74	2.13
6	1.25	1.78	2.47	17	0.93	1.39	2.02
7	2.12	2.88	3.71	18	1.36	1.83	2.46
8	1.42	1.78	2.14	19	1.09	2.14	3.06
9	2.01	2.43	2.73	20	1.63	2.07	2.60
10	2.51	2.89	3.44	21	1.63	2.07	2.60
11	1.30	1.79	2.15	22	1.00	2.46	3.10

Speed measured 110 mm below the soffit with a bi-directional probe (from L. Clark, 2002)

14 Appendix G – Yaw, Pitch and Velocity Plots

Run #02, Front Unrestricted, Door at 60°, Q = 120 kW, Burner in the Centre

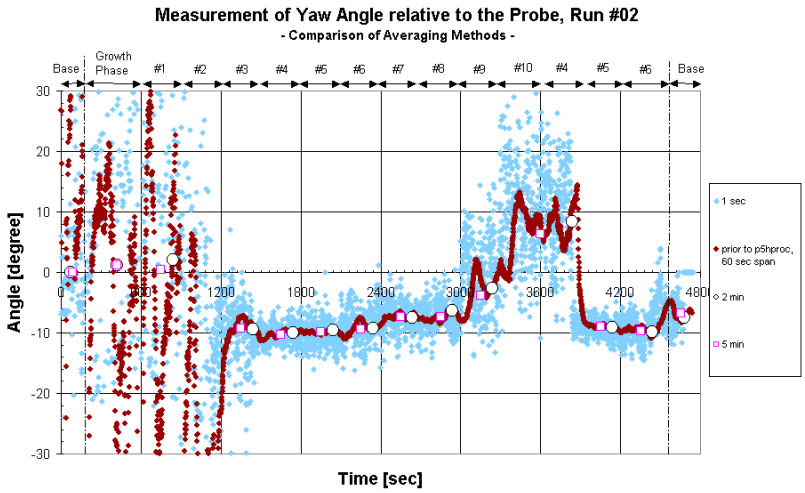

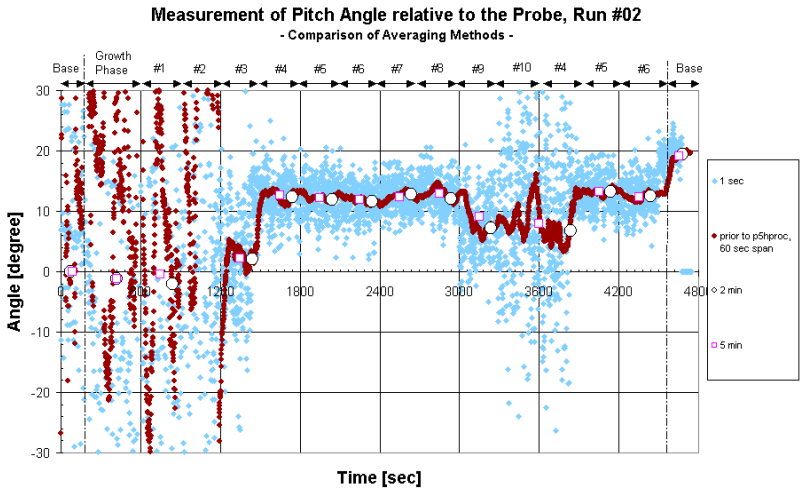

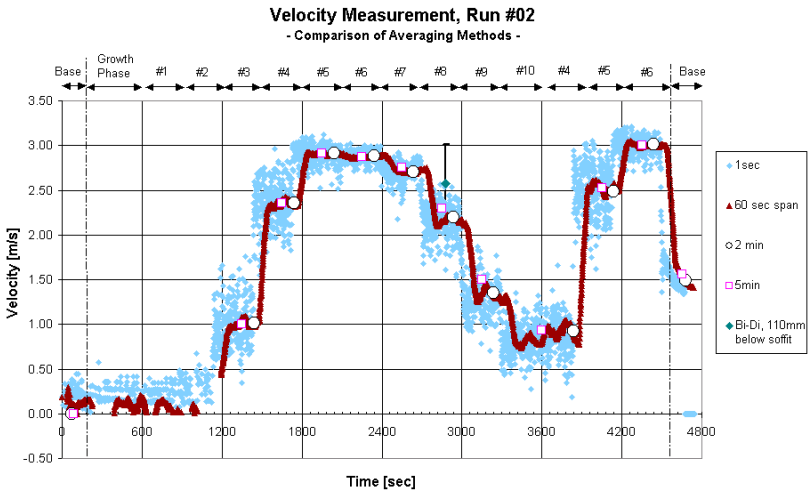

Run #03, Front Unrestricted, Door at 40°, Q = 120 kW, Burner in the Centre

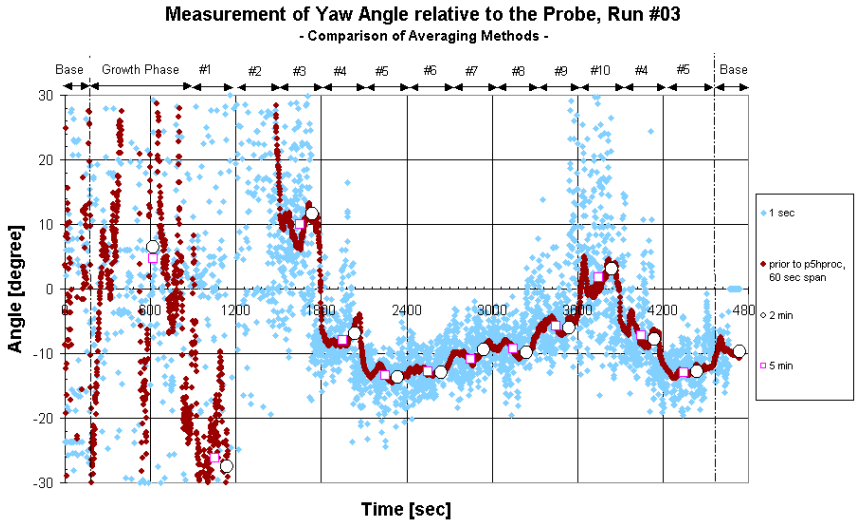

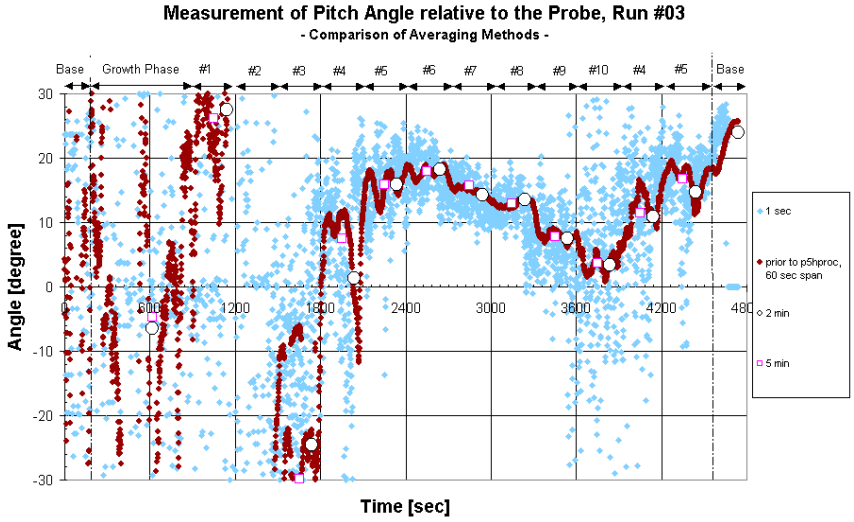

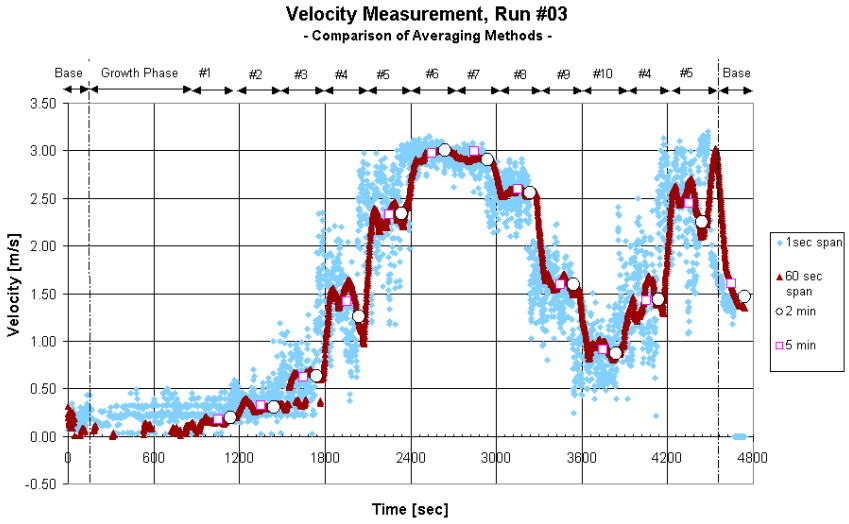

Run #05, Front Unrestricted, No Door, Q = 120 kW, Burner in the Centre

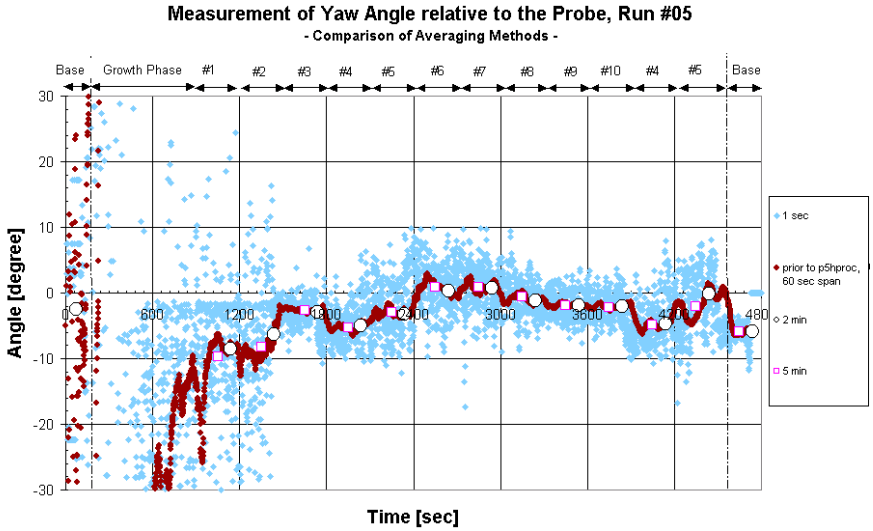

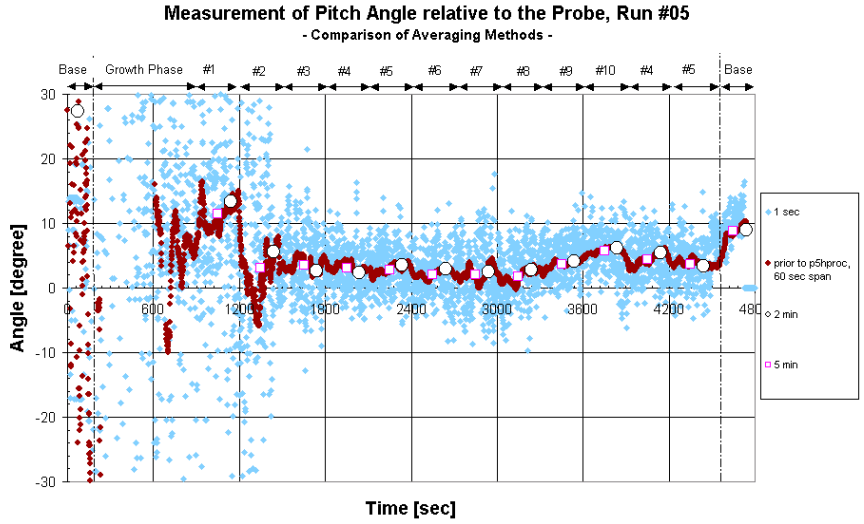

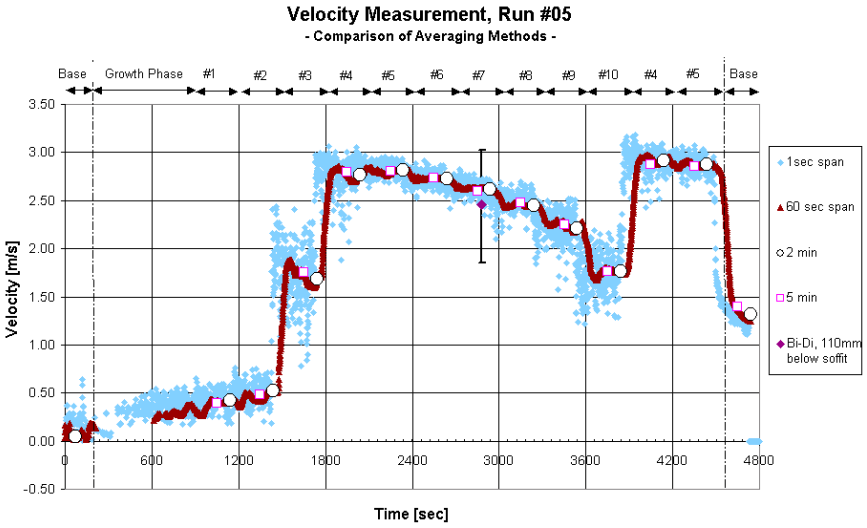

Run #06, Front Unrestricted, No Door, Q = 60 kW, Burner in the Centre

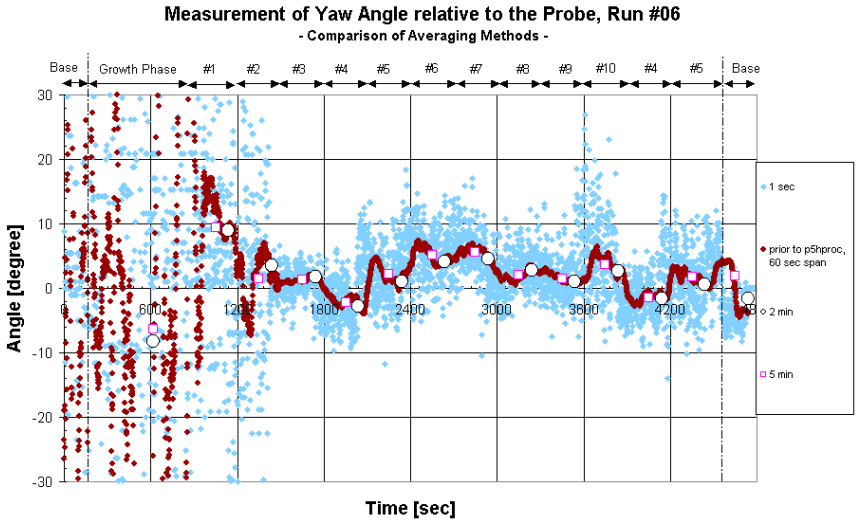

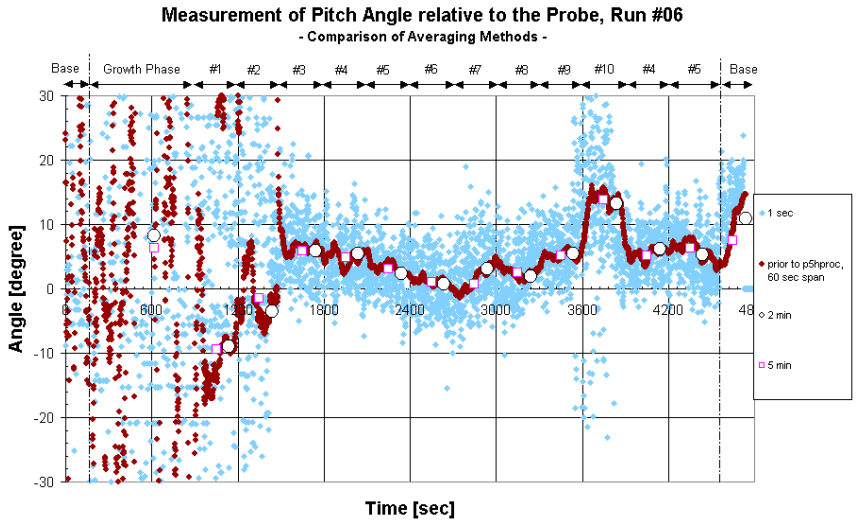

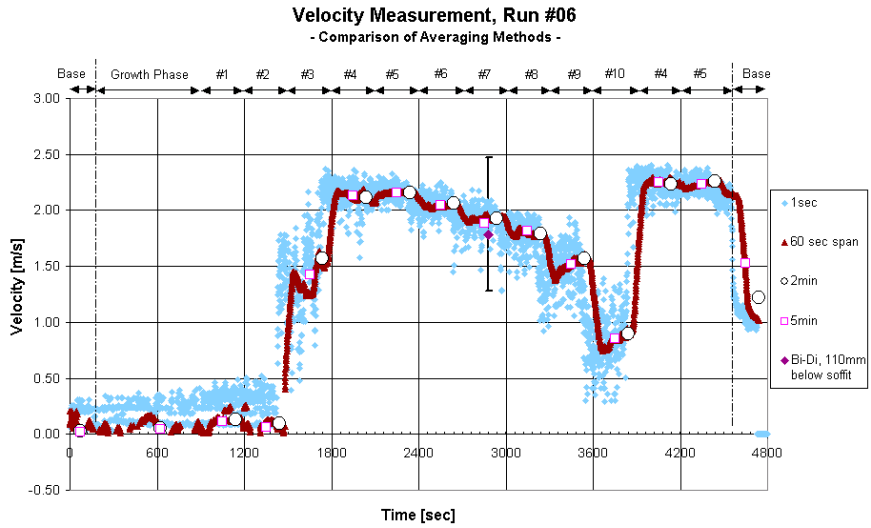

Run #07, Front Unrestricted, No Door, Q = 180 kW, Burner in the Centre

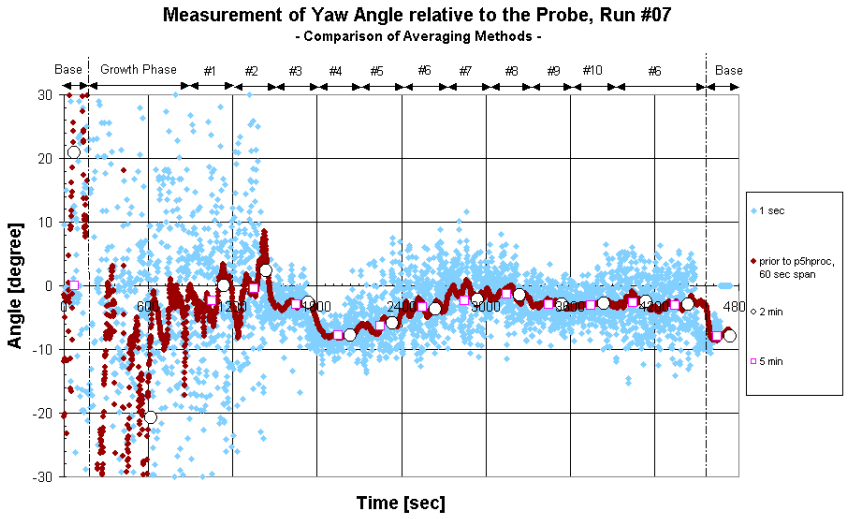

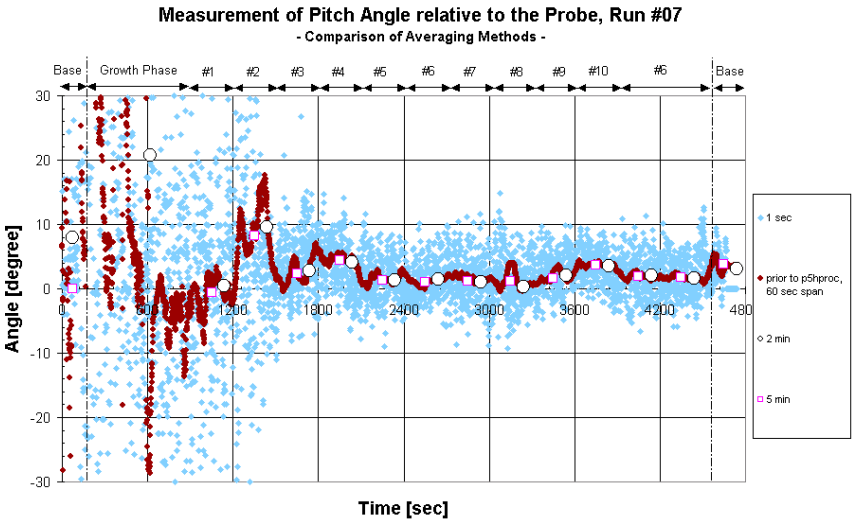

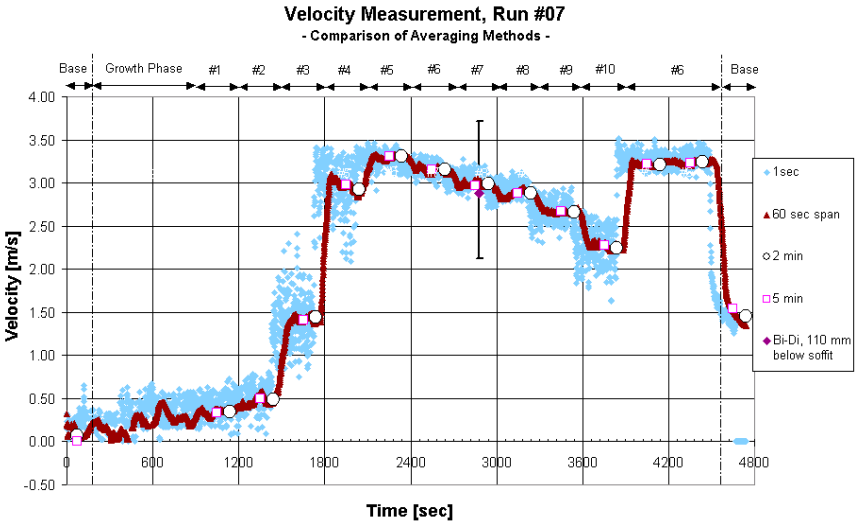

Run #09, Front Unrestricted, No Door, Q = 120 kW, Burner in the Corner

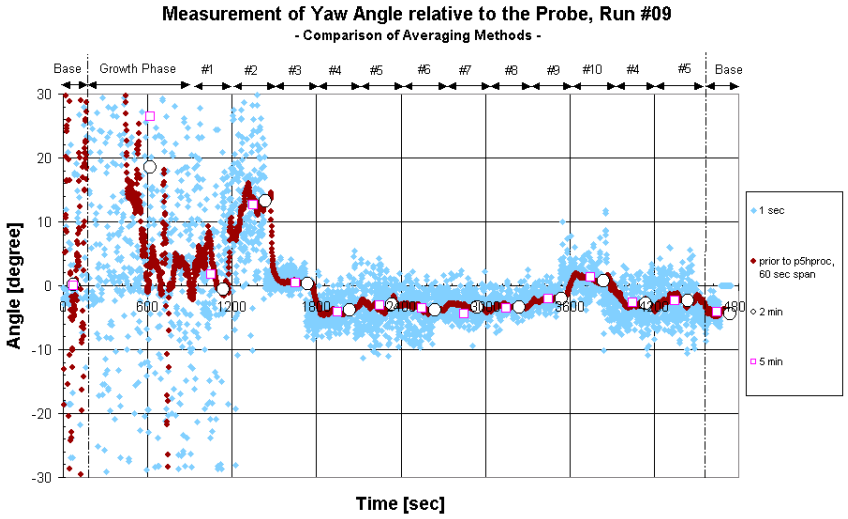

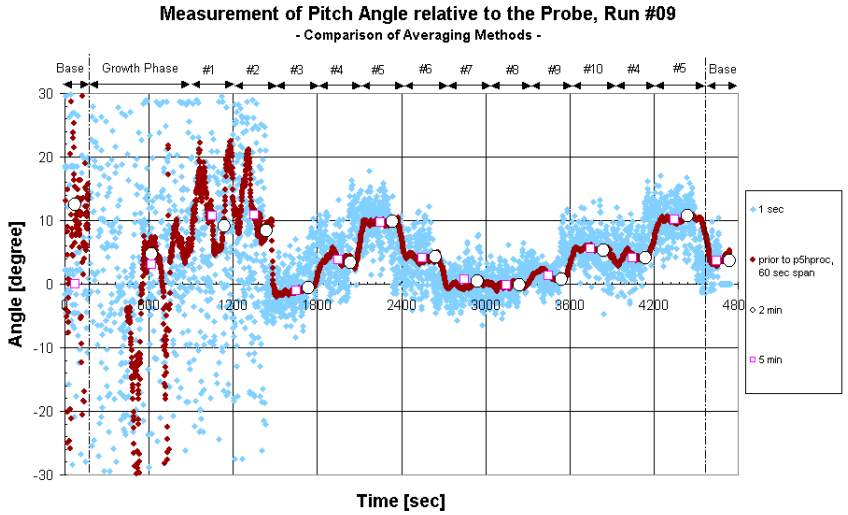

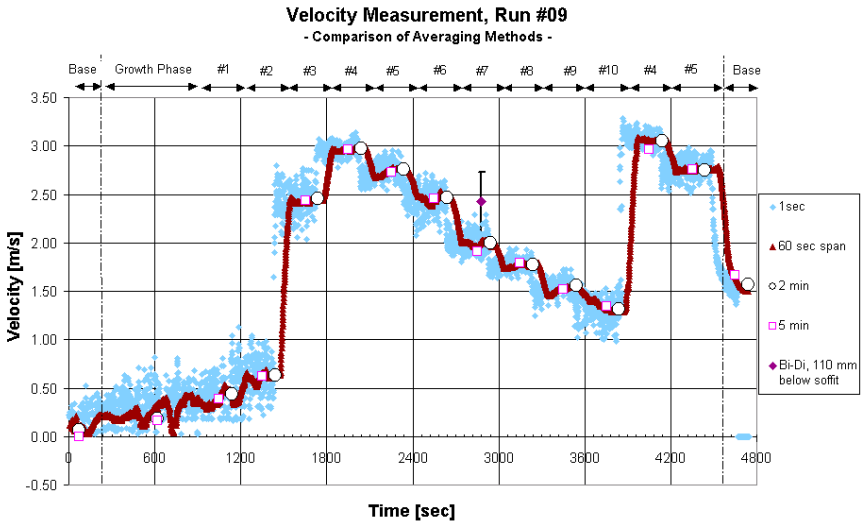

Run #10, Front Unrestricted, No Door, Q = 180 kW, Burner in the Corner

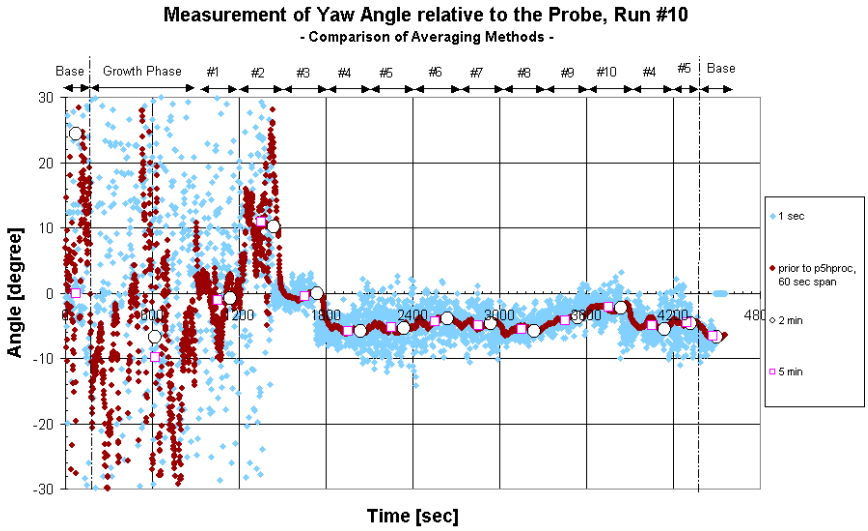

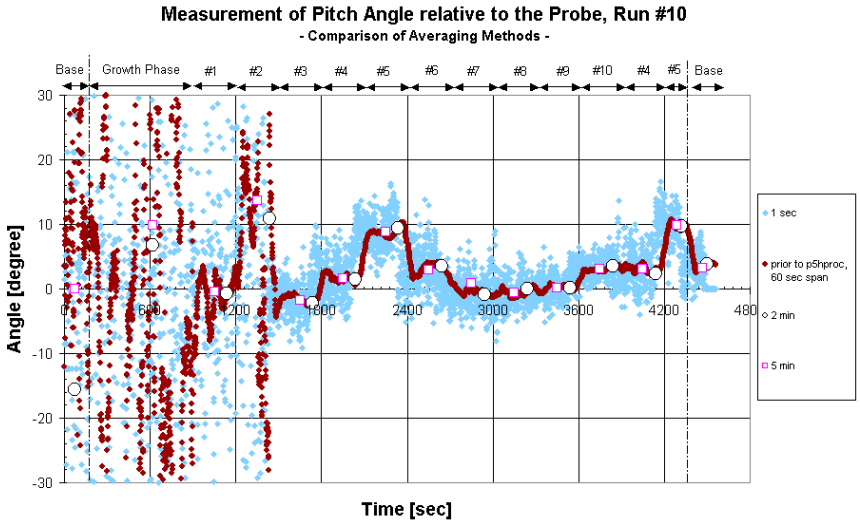

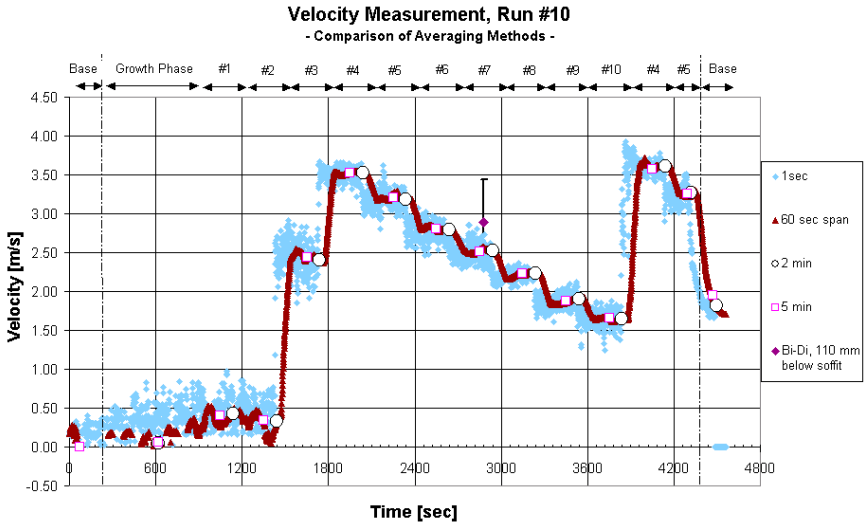

Run #12, Front Unrestricted, No Door, Q = 120 kW, Burner at the Rear Wall

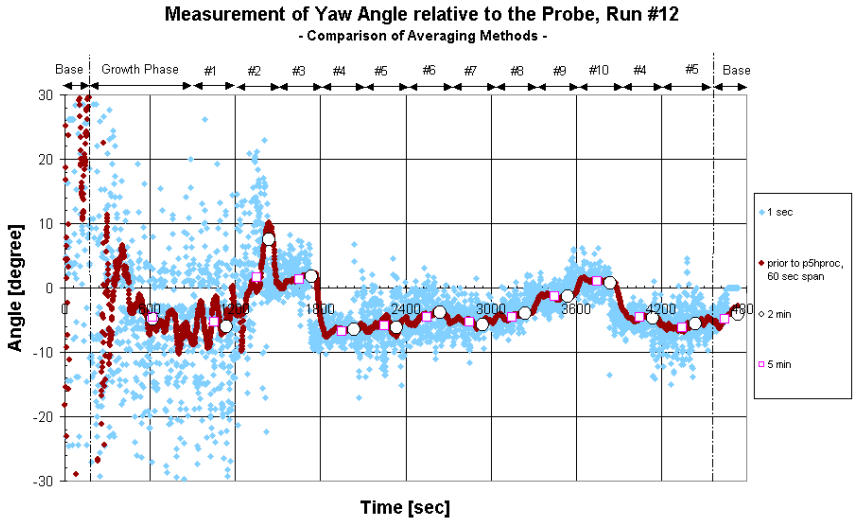

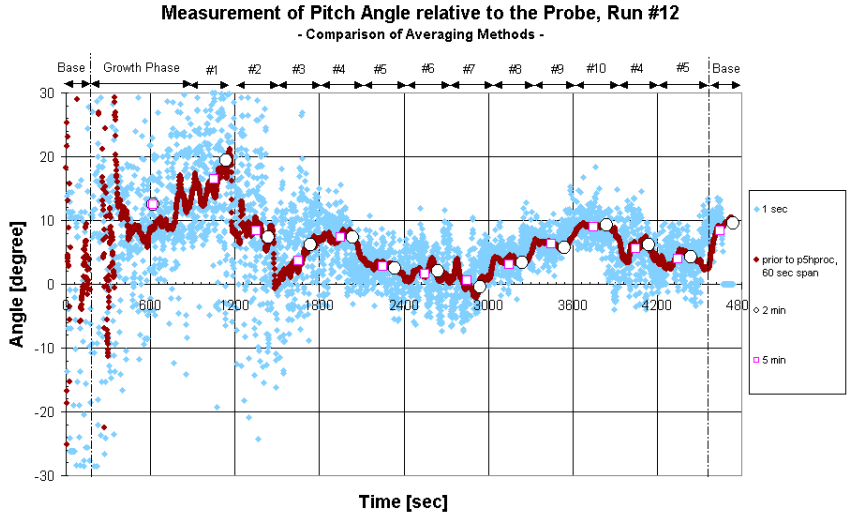

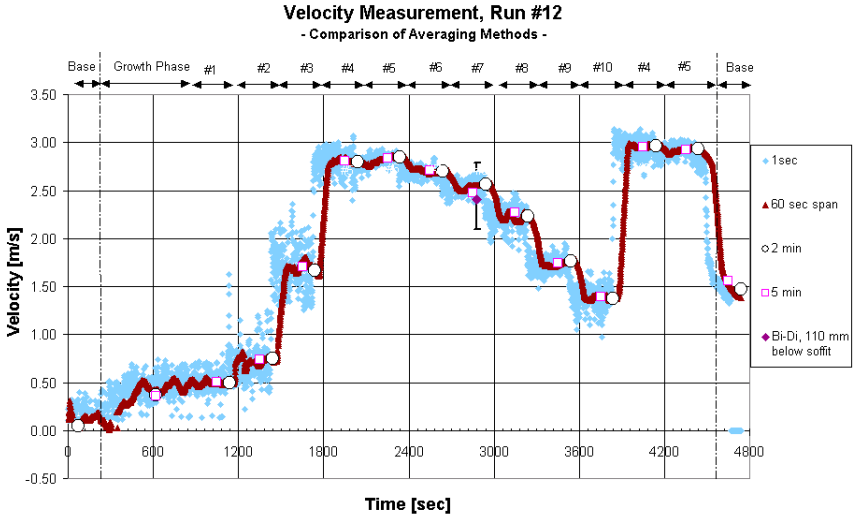

Run #15, Front Soffit, No Door, Q = 120 kW, Burner in the Centre

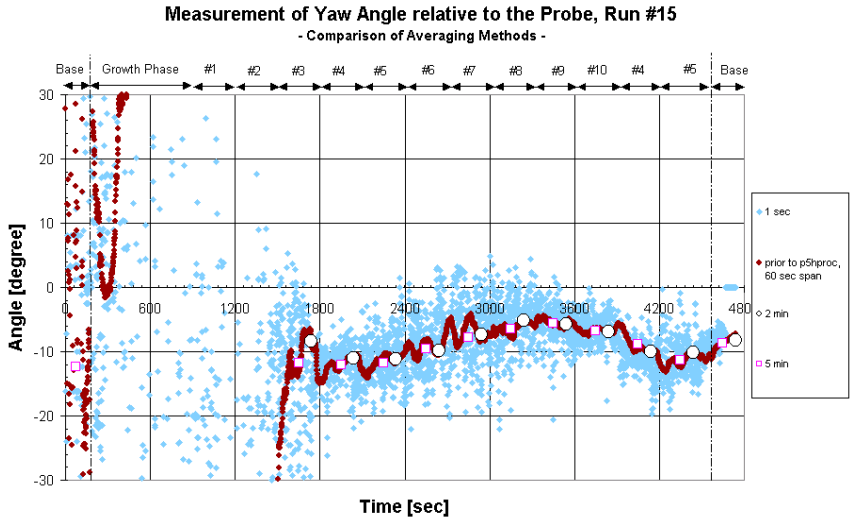

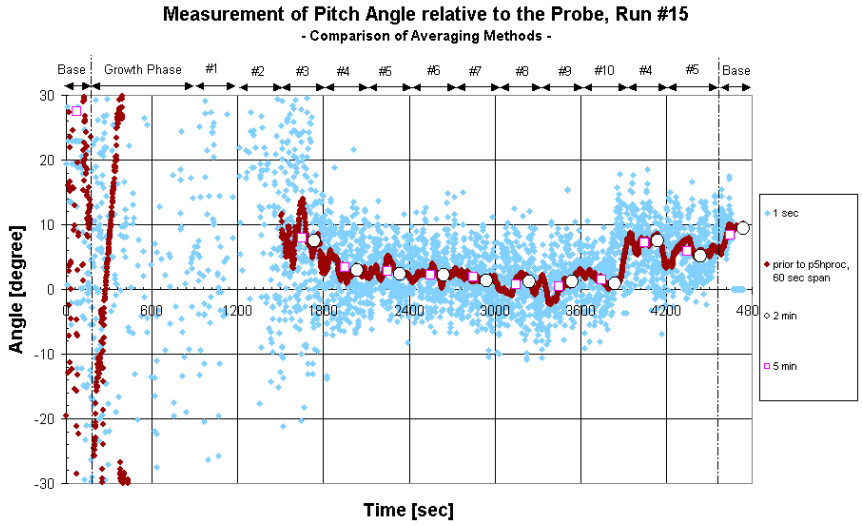

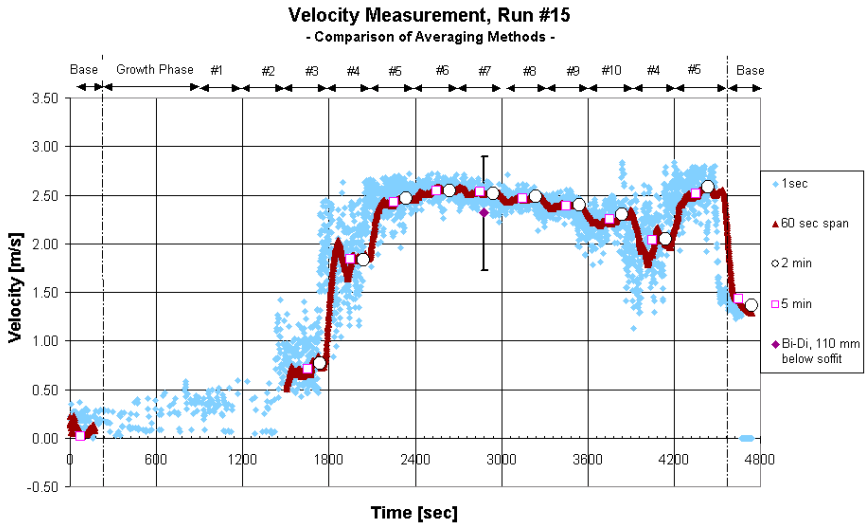

Run #18, Front Door Opening, No Door, Q = 120 kW, Burner in the Centre

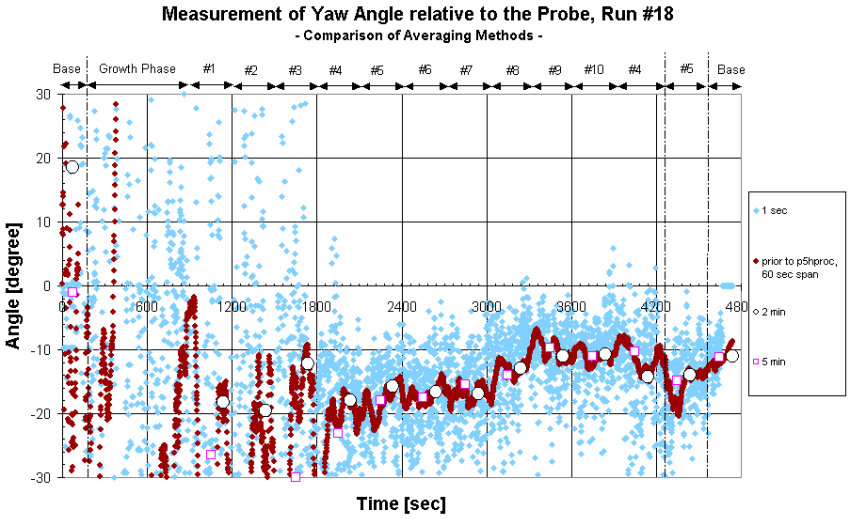

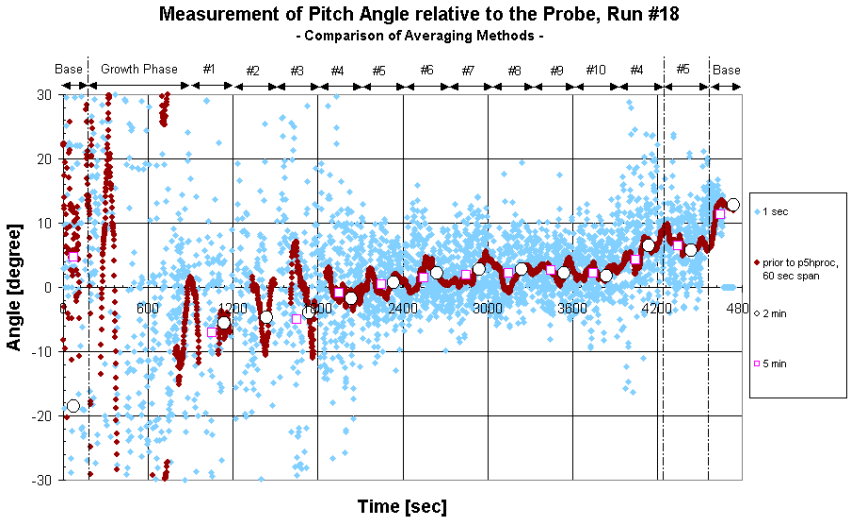

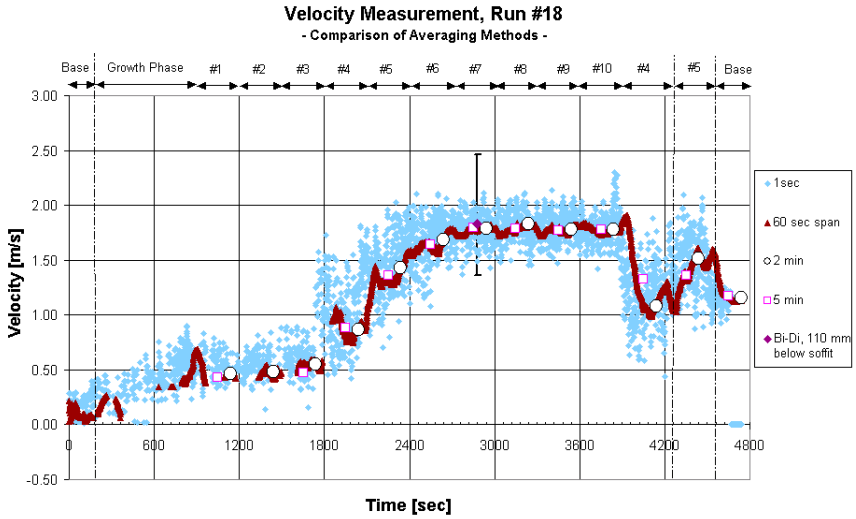

Run #20, Front Door Opening, Door at 40°, Q = 120 kW, Burner in Centre